

The Fragmentation vs. Functionalization Paths of Molecules during Atmospheric Chemical Aging

Heber J. Chacon-Madrid

April, 2012

Center for Atmospheric Particle Studies

Chemistry Department

Carnegie Mellon University

Pittsburgh, Pennsylvania

Thesis Committee:

Dr. Neil M. Donahue

Dr. Terrence J. Collins

Dr. Ryan C. Sullivan

Dr. Lynn M. Walker

Submitted in partial fulfillment of the requirements for the degree of Doctor of
Philosophy.

© Copyright by **Heber J. Chacon-Madrid**, 2012

All Rights Reserved

Abstract

Throughout this thesis we explore the two major mechanisms that organic carbon compounds experience in the atmosphere when reacting with major oxidizers: fragmentation and functionalization. We start by exploring the photo-oxidation of *n*-aldehydes – including their chemistry and organic aerosol formation – because they are known to fragment strongly in their first-generation chemistry with the OH radical. It is found that this strong fragmentation path suppresses their ability to form OA when compared to similar *n*-alkanes. *n*-Aldehydes with fewer than thirteen carbons do not produce OA under atmospheric concentrations. We also study two sequences of molecules with different saturation concentrations that systematically increase in oxygenation. Higher oxygenation was found to suppress the ability of a molecule to form OA. The position of a functional group in a carbon backbone was also found to affect OA formation. Functional groups located in the center of a large carbon backbone suppress OA formation when compared to functional groups on the end (e.g., 7- and 2-tridecanol, respectively). In the sequences mentioned, pinonaldehyde is a key molecule studied since it is an important oxidation product of alpha-pinene which is one of the most emitted molecules from biogenic sources. Production of OA from pinonaldehyde confirms the importance of biogenic aging.

As complement to the experimental work, two different computer simulations are used as prognostic tools of OA formation for the chemical species presented in this thesis. The first simulation is the two-dimensional volatility basis set (2D-VBS) developed by Donahue and co-workers at Carnegie Mellon University. This box model predicts OA evolution of bulk organic aerosol systems by knowing initial oxygenation and saturation concentrations. The second one is GECKO-A developed by Aumont and co-workers from the University of Paris. Its approach

consists of following every reaction and species involved in the chemistry of OA formation. Both simulations give reasonable results when compared to the experimental OA formation potential of different molecules presented in the first half of this thesis. This is despite their very two different approaches in predicting OA formation. We conclude that by properly considering fragmentation and functionalization paths, atmospheric OA formation can be reasonably predicted.

Acknowledgments

My life has been a great adventure, starting in a very humble family in Guatemala City and later moving to the United States to pursue a higher education. During this quest, I encountered wonderful people who have helped me greatly. Mentioning all of them would require a full-size library. I will start by thanking my parents and sister, Rigo Chacon, Silvia Madrid and Silvita Chacon-Madrid for their immense support and great desire to make the next generation better than the previous one. I want to also thank Dr. Eddie Olmstead for being my mentor at Fort Hays State University, where I was still adapting to a new country, language and culture; also I am thankful to Azarel Molina for being the best friend I have had. Additionally, the First Church of the Nazarene in Hays, Kansas was an immense support for me.

My wife, Kelly (Zewe) Chacon-Madrid has been the most incredible person in my life. I am extremely lucky to have found her and made her the partner of my life. I want to thank my mentors in the journey as a graduate student, including my advisor Neil Donahue who is an incredible researcher, thinker and writer. Albert Presto was very kind to guide me into the details of environmental research; his help was priceless.

Through my time at Carnegie Mellon, Pittsburgh, and Hays, Kansas I made many friends to whom I am extremely thankful. The next list is not an all inclusive one: Marcos Battistel, Sabrina Lusvarghi, Scott Epstein, Ellis Robinson, William Burroughs, Kaytlin Henry, Ben Murphy, Gabi Engelhart, Jeff Pierce, Daniel Tkacik, Melissa Day, the Zewe family, the Stump family, the Pimpkin family, the Molina family, the von Ahn group in computer science, The Church of the Nazarene in Lincoln Place, Pittsburgh, and many more.

Table of Contents

Abstract.....	ii
Acknowledgments.....	iv
List of Figures	x
List of Tables	xvii
1 Chapter 1 – Introduction.....	18
1.1 Emissions and their atmospheric evolution.....	18
1.2 Importance of studying Particulate Matter	19
1.3 Chemistry of Organics in the Atmosphere.....	19
1.4 Thesis Outline.....	20
1.4.1 Use of Structure Activity Relationships throughout this Thesis	22
2 Chapter 2 – Functionalization <i>vs.</i> Fragmentation: <i>n</i> -Aldehyde Oxidation Mechanisms and Secondary Organic Aerosol Formation	24
Abstract.....	24
2.1 Introduction	25
2.2 Experimental Section	29
2.2.1 Molar Yield Calculations.....	30
2.2.2 SOA Mass Yield and Wall Loss Calculations	31
2.3 Results.....	32
Experimental Data	32

Calculation of Branching Ratios.....	34
SOA mass yields.....	37
2.4 Discussion.....	38
Gas-phase reactions and SOA mass yields.....	38
Gas-phase reaction mechanism details.....	41
2.5 Environmental Significance.....	43
Acknowledgments.....	44
3 Chapter 3 – Fragmentation vs. Functionalization: Chemical Aging and Organic Aerosol Formation.....	45
Abstract.....	45
3.1 Introduction	46
3.2 Experimental	52
3.2.1 Injection of molecules into the chamber	53
3.2.2 SOA Mass Yield and Wall Loss Calculations	54
3.2.3 Measurement of reactants	55
3.2.4 Synthesis of Organic Species.....	56
3.3 Results.....	57
3.4 Discussion.....	60
3.4.1 <i>n</i> -Tridecanal and Pinonaldehyde vs. <i>n</i> -Pentadecane.....	60
3.4.2 <i>n</i> -Tridecanal <i>versus</i> Pinonaldehyde	61
3.4.3 2- <i>versus</i> 7-Tridecanone SOA mass yields.....	63

3.4.4	<i>n</i> -Nonadecane, <i>n</i> -Heptadecanal and <i>cis</i> -Pinonic Acid	65
3.5	Environmental Significance.....	66
	Acknowledgments.....	67
4	Chapter 4 – Photo-oxidation of pinonaldehyde at low NO _x : from chemistry to organic aerosol formation	68
	Abstract.....	68
4.1	Introduction	69
4.1.1	Pinonaldehyde as a key molecule	69
4.1.2	Chemistry of aldehydes under low-NO _x conditions	71
4.1.3	Objectives.....	72
4.2	Experimental	73
4.2.1	SOA Mass Yields and Wall Loss Calculations.....	74
4.2.2	Measurement of reactants	75
4.2.3	Synthesis of Pinonaldehyde	76
4.3	Results.....	76
4.4	Discussion.....	79
4.4.1	Pinonaldehyde vs. <i>n</i> -tridecanal.....	79
4.4.2	Pinonaldehyde vs. <i>n</i> -pentadecane.....	79
4.4.3	Pinonaldehyde: low and high NO _x	80
4.4.4	α-Pinene and Pinonaldehyde.....	83
4.5	Environmental Significance and Conclusions.....	84

Acknowledgments.....	85
5 Chapter 5 – Simulations of smog-chamber experiments using the two-dimensional volatility basis set and GECKO-A: linear oxygenated precursors.....	86
Abstract.....	86
5.1 Introduction	86
5.1.1 The Two-Dimensional-Volatility Basis Set (2D-VBS) framework as a prognostic tool.....	89
5.1.2 Generator for Explicit Chemistry and Kinetics of Organics in the Atmosphere (GECKO-A).	91
5.2 Methods and Simulations	92
5.2.1 The 2D-VBS.....	92
5.3 The 2D-VBS: Results and Discussion	95
5.3.1 <i>n</i> -Pentadecane.....	98
5.3.2 <i>n</i> -Tridecanal.	98
5.3.3 Other Precursors: Position of functional groups.	99
5.4 GECKO-A: Results and Discussions.....	100
5.5 Environmental Significance.....	104
Acknowledgments.....	106
6 Chapter 6 – Conclusions and Future Work	107
6.1 Future Work.....	110
6.1.1 Functional groups.	110

Chemistry of species with multiple functional groups.	111
6.1.2 GECKO-A and the 2D-VBS.	112
Appendices.....	113
7 References	135

List of Figures

Figure 2.1. Reaction mechanism of *n*-aldehyde + OH radical in the presence of high NO_x. The first branching point (shown in blue) in the reaction mechanism is the peroxyacyl radical (PAR) becoming either a peroxyacyl nitrate (PAN) or an alkoxyacyl radical (AAR). The Alkoxyacyl radical will fragment and form a C_{n-1} peroxy radical that will eventually branch between a C_{n-1} alkyl nitrate and a C_{n-1} alkoxy radical. This alkoxy radical branches (arrows in green) between the C_{n-1} aldehyde and an isomerization structure. Long straight-chain aldehydes have a preference towards isomerization on this last step..... 26

Figure 2.2. *n*-Undecanal decay. Loss of parent aldehyde (*n*-undecanal) and formation of C_{n-1} aldehyde (*n*-decanal) products vs. time in an OH oxidation experiment, observed with a PTRMS. The molar yield of *n*-decanal is 9 ± 5%; however, when assuming a nitric oxide only path, this yield becomes 16 ± 5%. The *m/z* = 171 signal follows *n*-undecanal initially. Later on, other products with *m/z* = 171 are formed..... 34

Figure 2.3. Yields and ultimate fate of peroxy acyl radicals (PAR) from *n*-aldehyde + OH reactions. The height of each bar is the aldehydic hydrogen abstraction molar yield, based on site-specific SAR OH reactivity calculations. The bar filling indicates the relative importance of C_{n-1} aldehyde formation vs isomerization and C_{n-1} alkyl nitrate. This reveals how the branching between the C_{n-1} aldehyde and an isomerization path varies with respect to molecule size. Branching ratios including PAN formation (which varies with the experimental NO₂:NO) can be found in Figure F, in the Appendices..... 36

Figure 2.4. Comparison of SOA mass yields from *n*-tridecanal, *n*-pentadecane and *n*-dodecane. *n*-Tridecanal clearly forms less SOA than similar vapor pressure *n*-alkanes such as *n*-pentadecane because of its ability to fragment, forming alkyl nitrates, a C_{n-1} aldehyde and isomerization species. Even when the *n*-tridecanal backbone has been attacked by OH, its aldehyde functional group can fragment to give a CO₂ or form the PAN; *n*-pentadecane cannot fragment easily in the first generations of oxidation. *n*-Dodecane and *n*-tridecanal SOA mass yields are very similar, that is because both molecules form the C_{12} alkoxy radical in significant amounts. The *n*-alkanes SOA mass yields are fits from the work of Presto et al., 2010. Smaller *n*-aldehydes (C_5 , C_8 and C_{11}) SOA mass yields are significantly smaller than that of *n*-tridecanal..... 37

Figure 2.5. A continuation of the reaction mechanism shown in Figure 2.1, following the 'isomerization' pathway. This becomes important for larger *n*-aldehydes. The red arrows represent the branching point between cyclization and δ -dicarbonyl formation, and it is dependent on relative humidity. Holt et al., 2005 shows that low relative humidity and long straight chain molecules favor cyclization. Figure 2.2 shows a decoupling from the inferred *n*-undecanal and the *m/z* 171. This decoupling might be related to the creation of δ -dicarbonyl, since it has the same molecular weight as the C_n *n*-aldehyde. This decoupling happens to all the aldehydes studied (Refer to the Appendices, Figures A, B, C)..... 42

Figure 3.1. Major mechanisms in gas and aerosol-phase oxidation. The three major chemical mechanisms that a carbon backbone undergoes in the atmosphere are represented along with their interaction with aerosols. They are described and revised in Kroll and Seinfeld, 2008 and Rudich et al., 2007. Both, functionalization and accretion tend to decrease the vapor pressure of species by either adding polarity to the molecule or by accreting with other molecules. Fragmentation cleaves carbon-carbon bonds of molecules, generally increasing the vapor

pressure of products; however, a good exception is the ozonolysis of monoterpenes, where both fragmentation and functionalization happen simultaneously, adding polarity and decreasing the overall vapor pressure of the products. The competition of these three mechanisms define the fate of molecules in the atmosphere, but it is not clear how this competition plays out while molecules and particles age..... 48

Figure 3.2. Two sequences of molecules with progressively increasing oxidation state but similar vapor pressures ($\sim 10^5$ and $\sim 10^3 \mu\text{g m}^{-3}$), shown in a two-dimensional volatility-oxidation state space. The $10^5 \mu\text{g m}^{-3}$ sequence is: *n*-pentadecane, *n*-tridecanal, pinonaldehyde, and 2- and 7-tridecanone (co-located with *n*-tridecanal). The $10^3 \mu\text{g m}^{-3}$ sequence is: *n*-nonadecane, *n*-heptadecanal and *cis*-pinonic acid. The species lie in the intermediate volatile organic carbon (IVOC) range occupied by many first-generation oxidation products associated with secondary organic aerosol (SOA) formation. Pinonaldehyde and *cis*-pinonic acid are first-generation products of α -pinene oxidation. Ambient oxidized organic aerosol (OOA) lies in the ranges indicated, with SV-OOA being fresher, less oxidized and more volatile and LV-OOA being more aged and less volatile..... 51

Figure 3.3. SOA mass yields of organic species with vapor pressures of $10^5 \mu\text{g m}^{-3}$. *n*-Tridecanal, pinonaldehyde and *n*-pentadecane SOA mass yields after the OH radical reaction at high NO_x are presented here. *n*-Pentadecane yields are a fit that comes from Presto et al., 2010. The suppression of SOA yields for *n*-tridecanal and pinonaldehyde vs. *n*-pentadecane are related to the tendency of the aldehydic moiety to fragment relatively quickly as detailed in Chacon-Madrid et al., 2010. At this point, it is not clear how the ketone and cyclobutane moieties influence the SOA formation from pinonaldehyde, if at all..... 58

Figure 3.4. SOA mass yields of ketones with vapor pressures of $10^5 \mu\text{g m}^{-3}$. 2- and 7-tridecanone SOA mass yields are slightly different. The lower efficiency of 7-tridecanone to form SOA might be related to higher fragmentation paths when it reacts with the OH radical as compared to 2-tridecanone. Additionally, splitting the molecule in the middle might have bigger consequences on SOA production versus splitting it on the side (e.g. 2-tridecanone). However, the differences in SOA yields are not as pronounced as the mechanisms would suggest. Photolysis might play a more important role on the oxidation products of 2-tridecanone..... 58

Figure 3.5. SOA mass yields of organic species with vapor pressure of $\sim 10^3 \mu\text{g m}^{-3}$. *n*-Pentadecane (from the $10^5 \mu\text{g m}^{-3}$ sequence) is shown as a reference. The differences in SOA mass yields between *n*-nonadecane and *n*-heptadecanal are not surprising. The aldehydic moiety is very reactive and causes fragmentation at high NO_x , while the *n*-nonadecane does not have relevant first-generation fragmentation paths..... 60

Figure 3.6. Pinonaldehyde + OH radical in the presence of NO_x . Consumption of *m/z* 169 (molecular weight of pinonaldehyde + 1 in a PTR-MS), and the formation of *m/z* 155 (molecular weight of *nor*-pinonaldehyde +1). *nor*-Pinonaldehyde molar yield from the OH radical oxidation of pinonaldehyde in the presence of NO_x is about ~50%. 62

Figure 3.7. A partial high- NO_x OH-radical oxidation mechanism of 7-tridecanone, emphasizing the OH radical attack of the β -hydrogens. Figure N in the Appendices shows evidence of *n*-hexanal formation from the OH radical oxidation of 7-tridecanone at high NO_x 64

Figure 4.1. Pinonaldehyde ($\text{C}_{10}\text{H}_{16}\text{O}_2$) is a C_{10} -keto-aldehyde structure with a characteristic cyclobutane. Similar structures can be found in other products of photo-oxidation from different monoterpenes. It is a highly reactive molecule, with an OH-radical lifetime in the order of hours..... 70

Figure 4.2. A simplified aldehyde + OH radical chemical-path in the absence of NO_x . After the aldehyde (red structure) is attacked, an acyl-peroxy radical is formed. In the absence of NO_x , the acyl-peroxy radical forms a peroxyacid (blue structure) or an acyl-oxy radical (green structure) when reacting with HO_2 or RO_2 , respectively. The acyl-oxy radical decomposes quickly, losing one carbon..... 72

Figure 4.3. Pinonaldehyde and *n*-tridecanal SOA mass yields at high and low NO_x . The potential to form organic aerosol from pinonaldehyde + OH – and *n*-tridecanal – is less than that from *n*-pentadecane + OH under high and low NO_x . *n*-Pentadecane yields come from Presto et al. Pinonaldehyde (triangles) and *n*-tridecanal (squares), independent from NO_x concentration, suffer fragmentation paths in its first-generation chemistry that limits its SOA formation potential. *n*-Alkanes such as *n*-pentadecane do not experience significant fragmentation in their first-generation chemistry 77

Figure 4.4. Comparison between SOA mass yields of pinonaldehyde in the absence (brown) and presence (blue) of UV light, under low NO_x . In order to understand if the difference in pinonaldehyde SOA yields between low and high NO_x is due to photolysis of hydroperoxides and subsequent fragmentation, an experiment in the dark is performed. The dark experiment (no UV light) produces more SOA than the one where the oxidation reaction is exposed to UV lights. We can infer that UV light is responsible for fragmentation paths, and it is likely that the fragmentation happens on hydroperoxide moieties since the experiments are performed under low NO_x 82

Figure 4.5. Pinonaldehyde SOA yields in the context of α -pinene SOA yields. As a first-generation product from α -pinene + OH, pinonaldehyde can form SOA at lower yields than α -pinene itself. Nonetheless, the yields of pinonaldehyde, including low NO_x , are significant and

higher than zero. This figure shows how later-generation species from α -pinene photo-oxidation are capable of forming SOA, making atmospheric chemical aging an important source of SOA..... 83

Figure 5.1. Product volatility distribution of generic 2D-VBS (gray) vs. explicit 1st-generation treatments (red) for different precursors (volatility indicated with a green circle). The red bars are slightly offset to reveal gray bars behind. These panels show the product distribution volatility of the expected first-generation products of OH oxidation for two different cases. The first case is the 2D-VBS Simulation; this distribution is obtained from the average chemistry implied by the box model for bulk organic material. The second case – explicit 1st-gen. – presents a distribution that is obtained from the literature hydrocarbon + OH chemistry for individual molecules. The main reason for the differences between both cases is that the 2D-VBS considers average chemistry of bulk organic material which is quite different from that of linear mono-oxygenated molecules. However, we believe that after establishing only the first-generation, the 2D-VBS box model can acceptably predict experimental SOA mass yields. *n*-Pentadecane does not suffer strong fragmentation paths in its first-generation chemistry, this is why we only present its product-distribution from the 2D-VBS..... 94

Figure 5.2. Simulations vs. Experimental Results. Each panel presents SOA mass yields for three sets of results; (i) 2D-VBS Simulation (solid black), (ii) Explicit 1st-gen. Simulation (solid violet) and (iii) experimental results. For all oxygenated species we encounter an acceptable agreement between the experimental data and the Explicit 1st-gen. Simulation. This means that establishing only the first-generation chemistry and then use the 2D-VBS box model is sufficient to present acceptable agreements between simulations and experimental data. *n*-Pentadecane

does not need first-generation products to be establish; the 2D-VBS Simulation predicts SOA mass yields adequately.....	97
---	----

Figure 5.3. GECKO-A simulations of SOA mass yields for three different carbonyls – all with thirteen carbons – present an over-prediction when compared to experiments. However, when considering experimental uncertainty in the order of ~20%, the comparisons are very encouraging. Also, the agreement between GECKO-A and experiments are similar – if not better – in here than with α -pinene oxidation experiments.....	101
---	-----

Figure 5.4. The species presented in this panel are of lower volatility than those in Fig. 5.3. The agreements between GECKO-A and most experimental yields are also very acceptable in this Figure. <i>n</i> -Heptadecanal is the only species for which the differences are much larger than the ~20% of experimental uncertainty. Considering that GECKO-A has to rely on different structure activity relationships that possess a high degree of uncertainty, these results are very encouraging. Other aspects, such as vapor losses to walls of later-generation products, have to be approached in future experiments.....	103
---	-----

List of Tables

Appendices:

Table A. Most of the information presented in this table is for initial conditions. The NO₂:NO kept relatively constant for the first 30 minutes of the oxidation. The Structure Activity (SAR) rate constants were calculated from Kwok et al., 1995 and used for “inferred *n*-aldehyde” concentrations..... 114

Table B. Conditions for the different experiments presented on **Chapter 3** are shown on this table..... 123

Table C. Conditions of all experiments performed and presented in **Chapter 4**..... 130

Table D. Conditions of all experiments performed and presented in **Chapter 5**..... 132

Chapter 1 – Introduction

1.1 Emissions and their atmospheric evolution

Different types of chemical species are emitted into the Earth's atmosphere constantly, either from man-made activities (anthropogenic) or from natural sources (biogenic), such as vegetation. They can also be of inorganic or organic nature, starting their journey as gases or particles. Inorganic material oxidizes rapidly, forming particulate matter (PM) that remains relatively inert during its travel in the troposphere (e.g. sulfates, nitrates, and ammonium salts) [1]; such chemistry is better understood than that of organics [2]. The oxidation of organic material in the atmosphere is much more dynamic due to constant photo-oxidation and changes in thermodynamic properties [3, 4].

Fine particulate matter – with sizes of $2.5 \mu\text{m}$ in diameter or less – in the atmosphere can be composed of up to ninety percent organic species by mass [5, 6], averaging about half of all mass [6], representing tens of thousands of different compounds [7]. For this reason, and due to its tremendous complexity, the study of the evolution of organic aerosols and gases in the atmosphere requires deep understanding.

Organic species are emitted either as gases or particles. The ones emitted as particles are known as primary organic aerosol (POA), and can have semi-volatile constituents that can “partition” into the gas-phase with dilution or higher temperature [8]. Species that partition from POA to the gas phase, in addition to those directly emitted as gases, can experience direct chemical transformation by three major oxidizers: the OH radical, ozone, and the nitrate radical [9]. After experiencing chemical oxidation, material can condense – or re-condense – partitioning into new or existing particulate matter, forming secondary organic aerosol (SOA).

Such partitioning is dominated by the amount of existing organic aerosol [10-12]. The aforementioned oxidants can also react heterogeneously with POA and SOA, potentially affecting particulate matter characteristics; however, this mechanism is believed to be slower than gas-phase oxidation [13].

1.2 Importance of studying Particulate Matter

Particulate matter smaller than $2.5 \mu\text{m}$ in diameter, or $\text{PM}_{2.5}$, is of great significance and importance to the scientific community. There are multiple reasons for its importance, among them detrimental effects on human health [14, 15] and an increase in human-mortality [16, 17]. It is believed that $\text{PM}_{2.5}$ is responsible for the premature death of up to eight-hundred-thousand people worldwide every year [18]. Furthermore, particles can absorb water, changing cloud properties that can have an effect on the radiative balance between the Earth and the Sun [19]. Other effects from particulates include changes in climate [20] and poor visibility [21]. Forest ecosystems can also be negatively affected by deposition of particulate pollutants [22].

1.3 Chemistry of Organics in the Atmosphere

The major oxidizers in the atmosphere, as mentioned before, are the OH radical, ozone and the nitrate radical. We concentrate on the OH radical throughout this thesis due to its high reactivity with virtually all organic material [23]. Photo-oxidation mechanisms of organic material with OH can be thought of a competition between three major paths: fragmentation, functionalization and accretion. Functionalization refers to the addition of functional groups to carbon backbones (increasing oxygen to carbon ratios) with no change in the number of carbons. This mechanism decreases vapor pressures [24], making it more likely for species to partition into existing aerosols. Fragmentation mechanisms consist of carbon–carbon bond

cleavage resulting in two separate organic products [25] (cleavage of a carbon-ring is an exception). In most cases, fragmentation also involves addition of functional groups. The third mechanism, accretion or oligomerization, involves association reactions – typically in the aerosol-phase – that increases carbon number without change in O:C [26, 27]. Throughout this thesis we concentrate mainly on the first two paths – fragmentation and functionalization – because they are the ones that can have a more profound effect on SOA mass. Accretion creates larger molecules in the condensed-phase, changing the properties of aerosol, but it is not a focus of this thesis.

1.4 Thesis Outline

In this doctoral work, we examine different aspects of the atmospheric chemistry of organic species. Specifically, we concentrate on understanding how the competition between fragmentation and functionalization of molecules changes as they experience photo-oxidization with the OH radical. Due to the complexity of the system, we decide to start the study of fragmentation and functionalization by examining *n*-aldehydes. They are known to fragment with the OH radical [23, 28] in the first-generation of chemical reaction. However, previous studies of *n*-aldehydes concentrated on small carbon-number species, and there have not been many publications on the ability of these species to produce organic aerosol. Consequently, we analyze the *n*-aldehyde chemistry of larger carbon-number (C₅ to C₁₃) species with the goal of understanding their ability to form organic aerosol even when they experience a strong fragmentation path.

The chemistry of aldehydes allows us to understand how a strong fragmentation-path suppresses organic aerosol (Chapter 2); however, a more important question was how organic aerosol formation is suppressed – or not – as molecules become more oxidized. Concentrating

on systematically more oxidized molecules was critical, since it is well known that atmospheric organic aerosol becomes steadily more oxidized through its atmospheric life-time [29]. The next step consisted of studying chemical species with similar vapor pressures (saturation concentration in $\mu\text{g m}^{-3}$) and higher oxidation states. By researching species with similar vapor pressures, comparisons of SOA mass yields allow us to make conclusions regarding the competition of fragmentation and functionalization paths (Chapter 3).

The experiments performed and reviewed in Chapters 2 and 3, including the *n*-aldehydes and sequences of higher oxidation species, were conducted under high- NO_x conditions. High- NO_x conditions are representative of polluted and/or urban settings [30]. However, some chemical species, such as pinonaldehyde (major product of α -pinene photo-oxidation [31, 32]), are more abundant in non-urban settings with plenty of vegetation [33]. Consequently, it was important to determine SOA mass yields of pinonaldehyde (and *n*-tridecanal for comparison) under low- NO_x conditions (Chapter 4). The chemistry under low- NO_x conditions is very different to that of high NO_x , due to the absence of organic nitrates and abundance of hydroperoxides as products [34]. Presenting the SOA yields of pinonaldehyde under low- NO_x tells us how important monoterpene-like first-generation products are with respect to organic aerosol formation. This is especially true because of chemical-structure similarities between pinonaldehyde and other first-generation products from monoterpene oxidation [35, 36].

The last part of this thesis (chapters 5 and 6) concentrates on computer simulations of SOA mass yields for the chemical species investigated in the initial chapters (2 through 4). We work on simulations with two different approaches. One that concentrates on chemistry averages of bulk organic aerosol, and another that uses explicit chemistry that follows every species involved. With the first approach, we use the two-dimensional volatility basis set (2D-

VBS) box model, developed by Donahue and co-workers, first introduced by Jimenez et al., 2009 [3], and expanded by Donahue et al., 2011 and 2012 [37, 38]. In the second approach, the Generator for Explicit Chemistry and Kinetics of Organics in the Atmosphere (GECKO-A) is utilized. GECKO-A was developed in the University of Paris by Aumont and co-workers and explained in detail by Aumont et al., 2005 [39, 40] and Valorso et al., 2010 [41]. By using the 2D-VBS and GECKO-A as prognostic tools of SOA formation, we test our understanding of organic aerosol chemistry.

1.4.1 Use of Structure Activity Relationships throughout this Thesis

Throughout the different chapters presented in this thesis two different types of structure activity relationships are used to aid our conclusions regarding chemical mechanisms and vapor pressures. The first one is the structure-activity relationship (SAR) – or structure-reactivity relationship – from Kwok and Atkinson, 1995 [42]. SARs from Kwok and Atkinson can predict gas-phase kinetic rate constants for different organic species reacting with the OH radical. The way the calculations of these rate constants are determined is by assigning a local rate constant to each carbon in a molecule. However, this local rate constant is affected by the type of carbon (e.g. primary, secondary or tertiary) and by the functional groups in proximity. Certain functional groups enhance reactivity, while others suppress a local rate constant. By adding all local rate constants for all carbons with extractable hydrogens in a molecule, we can obtain the overall rate constant. The data given by the SARs to calculate rate constants was obtained from experimental rate constants of a large number of experiments. However, most molecules were of simple structures. This makes the SARs highly uncertain for more complex, multi-functional molecules.

We also utilize structure activity relationships to calculate vapor pressures of species throughout this thesis. The one that is utilized the most is that from Pankow and Asher, 2008 [43]. The idea of these SARs is very similar to that of Kwok and Atkinson SARs. Vapor pressure is very much dependent on the amount of carbons in a molecule, as well as the number of functional groups.

Chapter 2 – Functionalization vs. Fragmentation: *n*-Aldehyde Oxidation Mechanisms and Secondary Organic Aerosol Formation

Abstract

Because of their relatively well-understood chemistry and atmospheric relevance, aldehydes represent a good model system for carbon-carbon fragmentation reactions in organic-aerosol aging mechanisms. Small aldehydes such as ethanal and propanal react with OH radicals under high NO_x conditions to form formaldehyde and ethanal, respectively, with nearly unit yield. CO₂ is formed as a coproduct. This path implies the formation of the C_{n-1} aldehyde, or an aldehyde with one less methylene group than the parent. However, as the carbon number of the *n*-aldehyde increases, reaction with the carbon backbone becomes more likely and the C_{n-1} formation path becomes less important. In this work we oxidized *n*-pentanal, *n*-octanal, *n*-undecanal and *n*-tridecanal with OH radical at high NO_x. The C_{n-1} aldehyde molar yields after the peroxy radical + NO reaction were 69 ± 15, 36 ± 10, 16 ± 5 and 4 ± 1%, respectively. Complementary structure-activity relationship calculations of important rate constants enable estimates of branching ratios between several intermediates of the C_n *n*-aldehyde reaction with OH: C_n peroxyacetyl nitrate versus C_n alkoxyacetyl radical formation, C_{n-1} alkyl nitrate versus C_{n-1} alkoxy radical, and C_{n-1} aldehyde formation versus isomerization products. We also measured SOA mass yields, which we compare with analogous *n*-alkanes to understand the effect of fragmentation on organic-aerosol formation.

2.1 Introduction

Aldehydes are either formed or emitted from biogenic and anthropogenic sources and play an important role in the photochemistry of the atmosphere [44]. Anthropogenic emissions of many straight-chain aldehydes are higher than emissions of *n*-alkanes with the same carbon numbers [45, 46]. Aldehydes are especially common in natural environments because they are both directly emitted and formed in the first photo-oxidation stage of many organic compounds [47, 48]. They are intermediates in environmental oxidation processes, especially in the reactions of terpenes with ozone [49]. They are toxic, cause eye irritation, and cause odor problems [50]. However, the chemistry of long, straight-chain aldehydes has not been explored thoroughly, though reactions involving aldehydes are known to influence the production of radical species such as HO₂, OH and RO₂ [50]. Aldehydes also react to form peroxyacetyl nitrates (PANs). PANs are reservoirs for long-range transport of NO_x in the free troposphere, where they are more stable because of the low temperature [51]. Finally, aldehydes are potential precursors for secondary organic aerosol (SOA), which has been linked to an increase in human mortality [17].

There is a growing realization that we must understand multiple generations of oxidation chemistry to properly describe organic-aerosol behavior in the atmosphere [3, 52, 53]. An especially important question is the extent to which later generation products become more vulnerable to carbon-carbon bond cleavage (fragmentation) [3, 54] rather than yielding progressively more functionalized oxidation products with the same carbon number as the parent hydrocarbon. The emerging short hand for this competition is 'fragmentation vs. functionalization'. Because they are an important first-generation product in many hydrocarbon oxidation sequences [23], aldehydes make an excellent model system to explore this chemistry.

Specifically, *n*-aldehydes make a fascinating sequence because small *n*-aldehydes have unique radical oxidation chemistry, but as the carbon number of an *n*-aldehyde is systematically increased, eventually the alkyl carbon backbone should overwhelm the aldehydic moiety and the aldehyde chemistry should come to resemble that of an *n*-alkane.

The OH-induced oxidation of small aldehydes in the presence of NO and NO₂ is well understood, following the mechanism in Figure 2.1 [23]. Small aldehydes such as ethanal and propanal react with OH radicals under high-NO_x conditions to form formaldehyde and ethanal, respectively [23]. These are fragmentation reactions, with what amounts to loss of a methylene and production of the C_{n-1} aldehyde and CO₂.

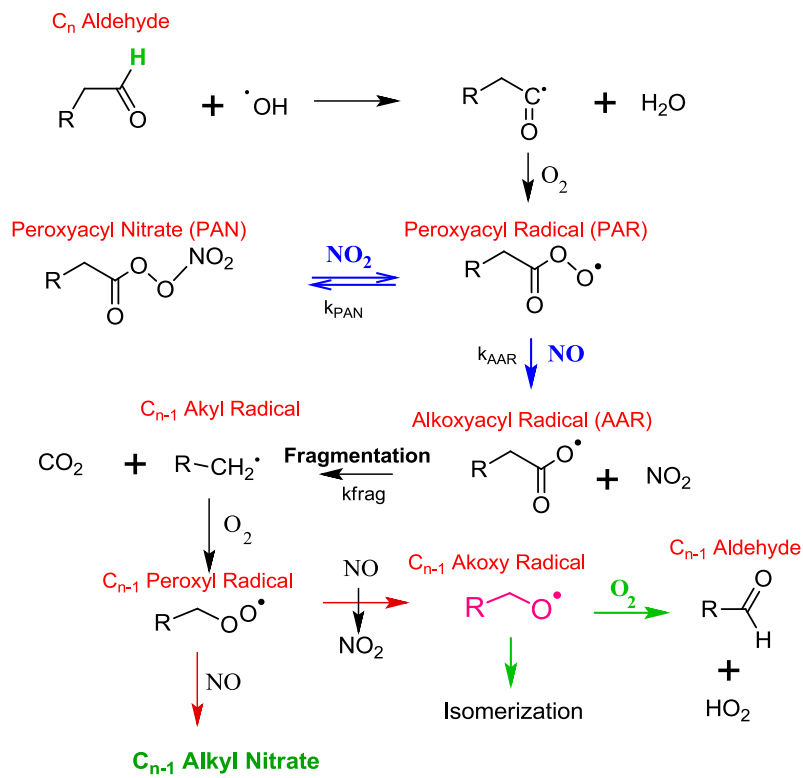


Figure 2.1. Reaction mechanism of *n*-aldehyde + OH radical in the presence of high NO_x. The first branching point (shown in blue) in the reaction mechanism is the peroxyacetyl radical (PAR) becoming either a peroxyacetyl nitrate (PAN) or an alkoxyacetyl radical (AAR). The Alkoxyacetyl radical will fragment and form a C_{n-1} peroxy radical that will eventually branch between a C_{n-1} alkyl nitrate and a C_{n-1} alkoxy radical. This alkoxy radical branches (arrows in green) between the C_{n-1} aldehyde and an isomerization structure. Long straight-chain aldehydes have a preference towards isomerization on this last step.

The reaction is initiated by abstraction of the aldehydic hydrogen (green hydrogen in Figure 2.1) and subsequent formation of the peroxyacyl radical (PAR). Reaction of the PAR is an important branching point (blue arrows in Figure 2.1) including reactions with both NO and NO_2 . The NO path involves the formation of an alkoxyacyl radical (AAR) that subsequently fragments and forms a C_{n-1} peroxy radical, which in turn branches (red arrows in Figure 2.1) between a C_{n-1} alkyl nitrate and a terminal C_{n-1} alkoxy radical (pink structure, Figure 2.1). Unlike “normal” peroxy radicals (without the carbonyl), the peroxyacyl radical + NO reaction does not produce nitrates [55]. The NO_2 path forms a peroxyacyl nitrate (PAN).

The PAR branching (blue arrows in Figure 2.1) is controlled by the rates of PAN and AAR production, which depend on the NO_2 and NO concentrations as shown in equations 1 and 2:

$$\frac{d[\text{PAN}]}{dt} = k_{\text{PAN}}[\text{PAR}][\text{NO}_2] \quad (2.1)$$

$$\frac{d[\text{AAR}]}{dt} = k_{\text{AAR}}[\text{PAR}][\text{NO}] \quad (2.2)$$

The branching ratio of PAN and AAR production is thus given by

$$\frac{[\text{PAN}]}{[\text{AAR}]} \approx \frac{k_{\text{PAN}}[\text{NO}_2]}{k_{\text{AAR}}[\text{NO}]} \quad (2.3)$$

For propanal, k_{PAN} and k_{AAR} are 9.3×10^{-12} and $20 \times 10^{-12} \text{ cm}^3 \text{ s}^{-1}$ molecule $^{-1}$ at 298 K [56]. We shall use these rate constants for all larger alkoxyacyl radical reactions along with the measured $\text{NO}_2:\text{NO}$ ratio to estimate the branching between PAN and AAR formation for higher carbon-number systems. Though PAN formation is reversible, in this study we shall focus on initial rates to constrain yields, and the PAN lifetime is long enough ($\sim 1 \text{ hr}$) for us to neglect PAN decomposition [56]. We are not interested in the consumption of AAR either, because every AAR molecule will quickly become a C_{n-1} peroxy radical.

The second branching point is the creation of a C_{n-1} alkyl nitrate versus the C_{n-1} alkoxy radical (red arrows in Figure 2.1). This branching is dependent upon size as shown by Arey et al., 2001 [57], and the nitrate formation is favored less for primary peroxy radicals as shown by Cassanelli et al., 2007 [58].

The last major branching point (green arrows in Figure 2.1) occurs at the C_{n-1} alkoxy radical (pink structure, Figure 2.1), which can isomerize via a 1,5-hydrogen shift, react with oxygen, or decompose (Figure 2.1 does not show the decomposition pathway). This branching has been studied in detail for *n*-alkanes [59-62], but not for terminal alkoxy radicals formed from aldehydes (pink structure in Figure 2.1). Long straight-chain alkanes ($\geq C_7$) strongly favor the isomerization path over oxygen reaction or decomposition [23]. For example, according to Kwok et al., 1996 [61], the ratio of isomerization to reaction with oxygen is 14 for *n*-heptane, and 50 for *n*-octane. Thus, for *n*-alkanes the isomerization reaction is regarded as completely dominant above C_7 [59]. However, *n*-aldehydes preferentially form the terminal (primary) C_{n-1} alkoxy radical, whereas *n*-alkanes form secondary alkoxy radicals. Consequently, the chemistry of the alkoxy radical is potentially different for *n*-aldehydes and *n*-alkanes.

In general, after abstraction of the aldehydic hydrogen we expect four major reaction products: the PAN, the C_{n-1} alkyl nitrate, the C_{n-1} aldehyde, and the products of alkoxy isomerization. Because the PAN is a reversible reservoir and its relative importance depends strongly on experimental (and ambient) $NO_2:NO$, the ratio of C_{n-1} alkyl nitrate to isomerization to C_{n-1} aldehyde formation is the major feature we shall seek to constrain and understand.

A final reaction pathway for aldehydes and OH is H-atom abstraction on the carbon backbone distant from the aldehydic moiety. To first order we expect the rate constants and first-generation reaction products from this pathway to resemble *n*-alkane reaction mechanisms

[59]. Consequently, we shall use published structure activity relations (SAR's) [42] to calculate the ratio of aldehydic hydrogen to backbone hydrogen abstraction by OH, and we shall use SOA formation experiments to constrain the overall yields of low-volatility reaction products and compare those results to SOA mass yields from corresponding *n*-alkanes.

When OH reacts along the carbon backbone, there is a possibility that the alkoxy radical formed on the fourth carbon from the aldehydic moiety can none-the-less react with this moiety. The fourth carbon from the aldehydic functional group has been shown to be highly reactive [42]. This reaction can potentially form a C_{n-1} hydroxycarbonyl structure. This has been proposed by Jenkin et al., 2000 [63], where an acyl-oxy radical attacks an internal aldehydic moiety after α -pinene reacted with ozone. However, this is a small path compared to all the reactive sites on the molecule. Other alkoxy radicals formed on the carbon-backbone will not isomerizes with the aldehydic moiety due to huge entropy penalties (longer shifts) or large activation barriers (shorter shifts) [64].

Here we shall present measurements of C_{n-1} aldehyde formation and SOA yield for several *n*-aldehydes. There are two major goals of this work: (1) to determine the importance of C-C backbone reaction for these large aldehydes in order to explore fragmentation in atmospheric oxidation schemes, and, (2) to quantify SOA formation in order to asses the importance of these species (and by extension, other oxygenated IVOCs) as SOA precursors. The SOA results also inform the gas-phase mechanism.

2.2 Experimental Section

We conducted experiments in the Carnegie Mellon University smog chamber. Many details of our experimental procedures are described elsewhere [65]. The chamber consists of a 12 m³

Teflon bag (Welch Fluorocarbon) suspended inside a temperature controlled room held at 295 K for these experiments. The experiments were conducted under high- NO_x conditions (maximum of 4 ppbC/ppb NO_x). Table A in the Appendices contains the specific concentrations and related ratios for all the experiments. Particle-number size distributions were monitored using a scanning mobility particle sizer (SMPS, TSI 3936, 15 - 700 nm D_p). The concentration of the *n*-aldehydes was monitored with a unit mass-resolution proton-transfer reaction mass spectrometer (PTR-MS, Ionicon GmbH). For each experiment, HONO photolysis was used to create OH radicals. Additional Nitric Oxide (NO) was added to achieve the desired VOC: NO_x ratio. Ammonium sulfate particles (Sigma Aldrich, 99.99%) were used as inert condensation seeds, which we formed from an aqueous solution with a nebulizer (TSI 3075) then dried and neutralized. The organic species used were *n*-pentanal (Sigma-Aldrich, 97%), *n*-octanal (Sigma-Aldrich, 99%), *n*-undecanal (Sigma-Aldrich, 97%) and *n*-tridecanal (Alfa Aesar, 94%). The aldehydes were all used without further purification. UV lights (General Electric 10526 black lights) with a $J_{\text{NO}_2} = 0.06 \text{ min}^{-1}$ were used to initiate photo-oxidation after all the components were mixed in the chamber.

2.2.1 Molar Yield Calculations

We evaluated PTR-MS signal ratios to obtain the molar yield of the C_{n-1} *n*-aldehydes. We make three key assumptions with the PTR-MS data: (1) the parent ion ($m/z = \text{MW} + 1$) makes up the same fraction of the total ion signal for both the C_n and C_{n-1} *n*-aldehydes, (2) *n*-aldehydes dominate the signal at $m/z = \text{MW} + 1$, at least at the beginning of each experiment, and (3) sensitivities (e.g., parent ion counts/ppb *n*-aldehyde) for these ions are identical. The absolute sensitivities for the individual C_{n-1} aldehydes were not calibrated. For example, the molar yield of *n*-dodecanal formed from oxidation of *n*-tridecanal was calculated by dividing the signal of

m/z 185 (corresponding to the *n*-dodecanal molecular weight plus one) by the net reduction of *m/z* 199 from its initial value (corresponding to *n*-tridecanal molecular weight plus one) during the first hour of oxidation. We followed the same procedure to determine the molar yields of *n*-decanal, *n*-heptanal and *n*-butanal. We feel comfortable using the PTR-MS as our gas-phase monitor since it has shown to be accurate within experimental uncertainty [66]. PTR-MS calibrations were performed similarly to de Gouw et al., 2003 [66].

2.2.2 SOA Mass Yield and Wall Loss Calculations

The SOA mass yield from a reaction is defined as the mass of organic aerosol formed divided by the mass of precursor consumed [12].

$$Y = \frac{C_{OA}}{\Delta C_{precursor}} \quad (2.4)$$

Where C_{OA} is the mass of organic aerosol created, and $\Delta C_{precursor}$ is the mass of the precursor organic species consumed to form the organic aerosol (C_{OA}) and other products.

We determined SOA mass yields for the *n*-aldehydes with the aid of inorganic seeds, which promote condensation and allow an independent measurement of particle wall losses. We injected dried ammonium sulfate particles up to $\sim 10^4$ particles cm^{-3} or ~ 10 to $15 \mu\text{g}/\text{m}^3$. The ammonium sulfate concentration is very much inside the range of a typical ambient aerosol mass concentration of between 5 and $30 \mu\text{g}/\text{m}^3$ [5].

Total SOA production (C_{OA}) is determined by using the ratio of suspended organic aerosol (C_{OA}^{sus}) to suspended ammonium sulfate (C_{seed}^{sus}) and the initial concentration of ammonium sulfate $C_{seed}^{sus}(t = 0)$, as described by Hildebrandt et al., 2009 [65]:

$$C_{OA}(t) = \frac{C_{OA}^{sus}(t)}{C_{seed}^{sus}(t)} C_{seed}^{sus}(t = 0) \quad (2.5)$$

$C_{seed}^{sus}(t)$ is obtained by fitting an exponential decay to the ammonium sulfate volume concentration (measured with the SMPS) over the interval between seed injection (and mixing) in the chamber and the onset of photo oxidation. Extrapolation of this signal after the photo-oxidation process starts defines the seed mass concentration as a function of time.

At time 0 (onset of photo oxidation) and later, the difference between the total aerosol mass concentration in the chamber (measured with an SMPS) and the extrapolated ammonium-sulfate mass concentration is considered the $C_{OA}^{sus}(t)$. To obtain the total $C_{OA}(t)$ from the suspended mass concentration we correct for wall losses, assuming that organic particles lost to the wall are in equilibrium with the suspended particles and vapor-phase species as. This is the upper-limit estimate for SOA production explained in Weitkamp et al., 2007 [67]. The difference in SOA yields for *n*-tridecanal when assuming particles lost to the wall are in equilibrium with the suspended particles (upper limit) versus not in equilibrium (lower limit) is approximately 20%.

2.3 Results

Experimental Data. Figure 2.2 shows a time series of C_n *n*-aldehyde decay (C_{11} , *n*-undecanal) and C_{n-1} *n*-aldehyde formation (C_{10} , *n*-decanal) for a typical experiment. Isobaric ions (especially at unit mass resolution) can interfere with the target PTRMS signal, but for the first hour of the experiment shown in Figure 2.2, the $m/z = 171$ signal follows a decay in the form of $[A]_0 e^{-kt[OH]}$, where $[OH]$ is not constant and decreases exponentially most of the time. $[A]_0$ is the initial concentration of the aldehyde, k is its rate constant and t is time. The concentration of OH is obtained by using methanol as a tracer. This is done in a similar way presented by Miracolo et al., 2008 [68] where they use *n*-pentane as the OH tracer.

Later in the experiment (Figure 2.2) other species, presumably later-generation reaction products, contribute to the signal at $m/z = 171$. Consequently, we base our yield estimates on the ratio of the initial (~30 - 60 minutes) decay and growth rates of the aldehyde signals. The inferred *n*-undecanal from Figure 2.2 is obtained by assuming a structure activity relationship rate constant of $3.6 \times 10^{-12} \text{ cm}^3 \text{ s}^{-1} \text{ molecule}^{-1}$, and an OH concentration obtained from a tracer of known rate constant (in this case methanol). We repeated these measurements for *n*-pentanal, *n*-octanal and *n*-tridecanal. The observed molar yields for the formation of *n*-butanal, *n*-heptanal, *n*-decanal and *n*-dodecanal from the parent aldehyde are 29 ± 10 , 16 ± 5 , 9 ± 5 and $4 \pm 1\%$, respectively. The most obvious feature of these data is that the C_{n-1} aldehyde yields decrease dramatically as carbon number increases, but they remain well above zero out to C_{13} . The raw yields are sensitive to $\text{NO}_2:\text{NO}$ ratio, which can be found in Table A in the Appendices. However, by correcting for PAN formation we can calculate the C_{n-1} aldehyde yields in absence of NO_2 ; these yields are 69 ± 15 , 36 ± 10 , 16 ± 5 and $4 \pm 1\%$, respectively. We assume that the ratios of C_{n-1} alkyl nitrate: C_{n-1} aldehyde : Isomerization products are the same in a NO-path-only vs. NO and NO_2 . For example, *n*-pentanal forms about 0.76 of peroxyacetyl radical, from which there is no PAN formation. Then, 5% becomes C_{n-1} alkyl nitrate ($0.05 \times 0.76 = 0.038$) according to Arey et al., 2001 [57] and Cassanelli et al., 2007 [58]. Since the ratio of C_{n-1} alkyl nitrate to C_{n-1} aldehyde to isomerization should be the same as the measured NO and NO_2 case (refer to Figure F, Appendices), their total yields should be 0.69 and 0.03 respectively.

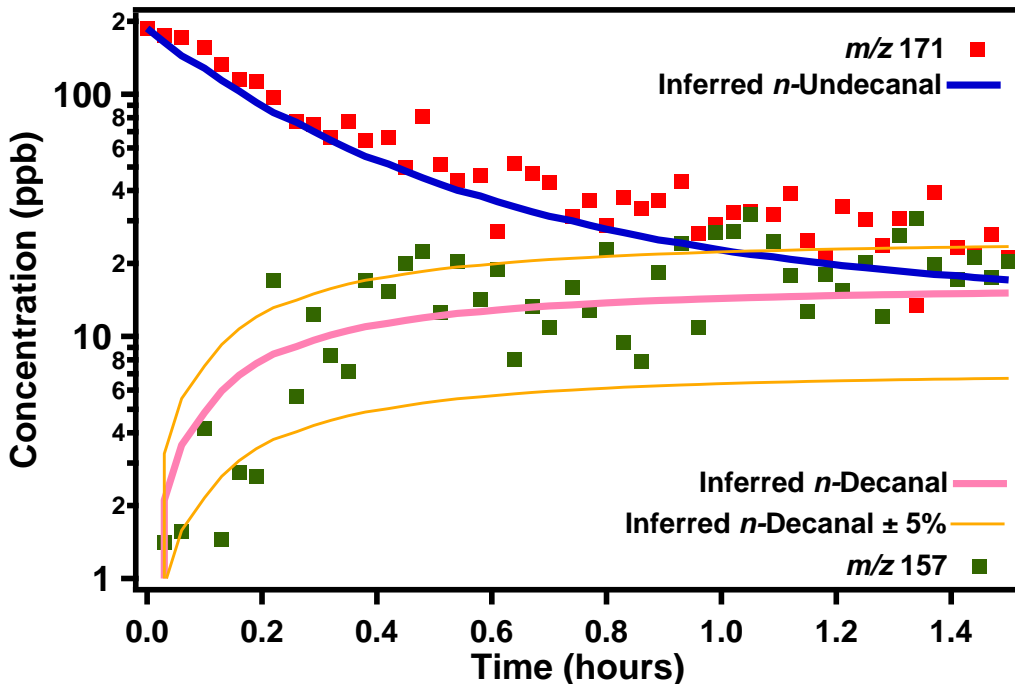


Figure 2.2. *n*-Undecanal decay. Loss of parent aldehyde (*n*-undecanal) and formation of C_{n-1} aldehyde (*n*-decanal) products vs. time in an OH oxidation experiment, observed with a PTRMS. The molar yield of *n*-decanal is $\sim 9 \pm 5\%$; however, when assuming a nitric oxide only path, this yield becomes $16 \pm 5\%$. The pink line represents exactly the 9% molar formation of *n*-decanal. The $m/z = 171$ signal follows *n*-undecanal initially. Later on, other isobaric product(s) with $m/z = 171$ are formed.

Calculation of Branching Ratios. We calculated the molar yield for formation of the C_n peroxyacetyl radical (PAR) using published SARs [42]. This is the ratio of the OH attack on the aldehydic hydrogen (green hydrogen in Figure 2.1) to all sites in the molecule. These yields are the full heights of the bars in Figure 2.3. Using the measured formation of C_{n-1} aldehyde, the inferred total PAR formation, the calculated ratio of PAN formation to PAR + NO reaction, and the calculated C_{n-1} alkyl nitrate (green species, Figure 2.1) we can apportion the various PAR reaction pathways (blue, red and green arrows in Figure 2.1).

The C_{n-1} alkyl nitrate is calculated by assuming that 5, 12, 20 and 30% of the C_{n-1} peroxy radical will form the C_{n-1} alkyl nitrate for $n = 5, 8, 11$ and 13 , respectively. This comes from

experimental data from Arey et al., 2001 and Cassanelli et al., 2007 [57, 58]. Note that the C_{n-1} alkyl nitrate yield formation is about 65% of those given by Arey et al., 2001 [57] because terminal peroxy radicals have lower alkyl-nitrate yields than secondary peroxy radicals [58].

We can illustrate this calculation for *n*-tridecanal. The branching ratio for aldehydic hydrogen abstraction is 0.54 according to the SAR. With a $NO_2:NO \sim 0.2$ (Table A and Figure F in the Appendices), the PAN molar yield is 0.05, and so the AAR yield is 0.49 ($0.05 + 0.49 = 0.54$). Approximately 30% of the AAR becomes a C_{12} alkyl nitrate ($0.30 \times 0.49 = 0.15$). The rest becomes a C_{n-1} alkoxy ($0.49 - 0.15 = 0.34$), which then splits between a C_{n-1} aldehyde and isomerization products. The measured C_{n-1} aldehyde molar yield is 0.04. We therefore conclude that the isomerization product yield is $0.34 - 0.04 = 0.30$.

The results of these branching calculations are shown in Figure 2.3. All of the necessary information for these calculations is presented in the Appendices, Figure F. The branching among C_{n-1} alkyl nitrate, isomerization products, and the C_{n-1} *n*-aldehyde is indicated in Figure 2.3 by the green, hatched red, and solid red regions. The calculated branching ratios between the C_{n-1} *n*-aldehyde and the isomerization products (green arrows Figure 2.1) are 20:1, 1.7:1, 0.54:1 and 0.13:1 for C_5 , C_8 , C_{11} and C_{13} *n*-aldehydes. Aldehyde formation dominates for the smallest molecules studied, while isomerization dominates for the largest molecules, but aldehyde formation is non-negligible in all cases.

The branching ratios of the C_{n-1} *n*-aldehyde versus isomerization products at the C_{n-1} alkoxy-radical stage are somewhat surprising (Figure 2.1, green arrows). Secondary alkoxy radicals produced from *n*-alkanes larger than C_7 do not react with O_2 in significant amounts; the isomerization path overwhelms this step [61]. However, in the case of primary alkoxy radicals produced from *n*-aldehydes, the oxygen reaction path is very significant, even for a C_{12} . This can

be due to the fact that terminal (primary) alkoxy radicals are potentially worse at H-atom abstraction. A potential reason is their higher energy of activation compared to a secondary alkoxy radical when abstracting a hydrogen [69].

Ferenac et al., 2003 [70] and Hein et al., 1999 [71] have mentioned that secondary alkoxy radicals are slightly more reactive than primary with O_2 at 298 K. All else being equal, this implies that $n\text{-}C_{12}$ (coming from a $n\text{-}C_{13}$ aldehyde) primary alkoxy radical formation would be negligible. Since that is not the case, we favor the hypothesis that terminal alkoxy radicals are slower at hydrogen abstraction than secondary ones.

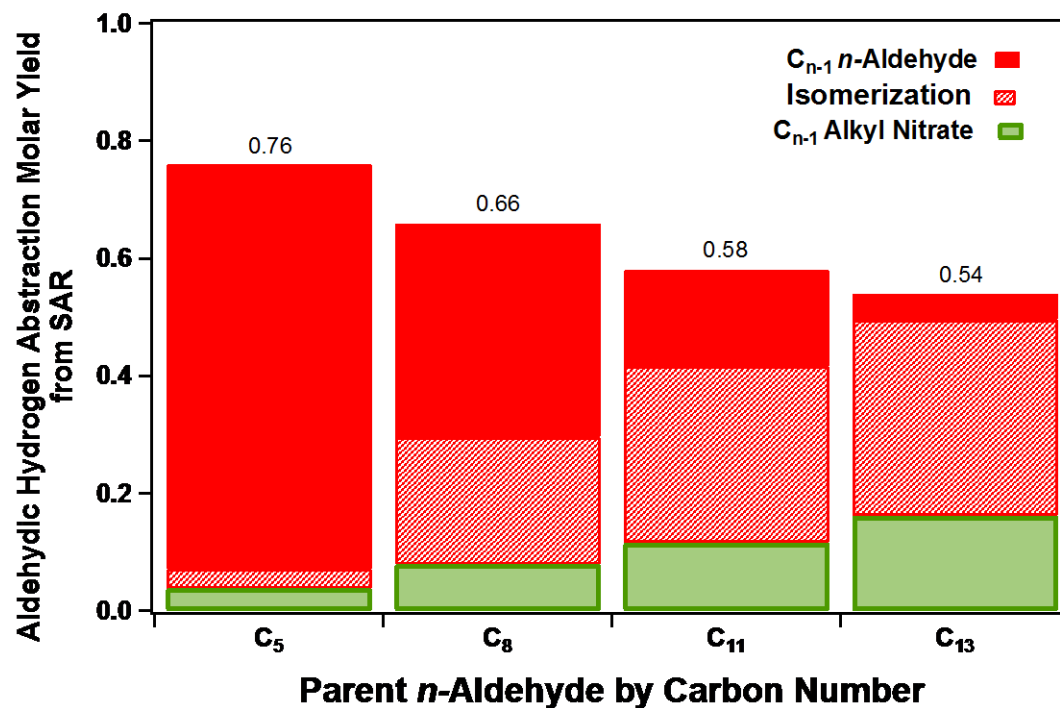


Figure 2.3. Yields and ultimate fate of peroxy acyl radicals (PAR) from *n*-aldehyde + OH reactions. The height of each bar is the aldehydic hydrogen abstraction molar yield, based on site-specific SAR OH reactivity calculations. The bar filling indicates the relative importance of C_{n-1} aldehyde formation vs isomerization and C_{n-1} alkyl nitrate. This reveals how the branching between the C_{n-1} aldehyde and an isomerization path varies with respect to molecule size. Branching ratios including PAN formation (which varies with the experimental $NO_2:NO$) can be found in Figure F, in the Appendices.

SOA mass yields. We measured SOA mass yields individually for *n*-C₅, *n*-C₈, *n*-C₁₁, and *n*-C₁₃ aldehydes + OH under high NO_x. The OH radical was always in excess than the aldehydes concentration. SOA mass yields for *n*-aldehydes smaller than C₁₁ were extremely small (< 0.02 with a maximum C_{OA} ~ 10 µg/m³). The mass yields for *n*-C₅, *n*-C₈, *n*-C₁₁ were also not significantly different for C_{OA} < 10 µg/m³. We cannot rule out impurities as a major source of the very low levels of SOA formed during those experiments; consequently, the data imply that *n*-aldehydes smaller than C₁₁ are insignificant sources of SOA. Such impurities could not be identified using the PTR-MS or a gas chromatograph. *n*-Tridecanal, however, did form significant SOA. The mass yields for *n*-tridecanal are shown in Figure 2.4 as a function of the SOA mass concentration, which is the conventional format for graphing SOA mass yield data.

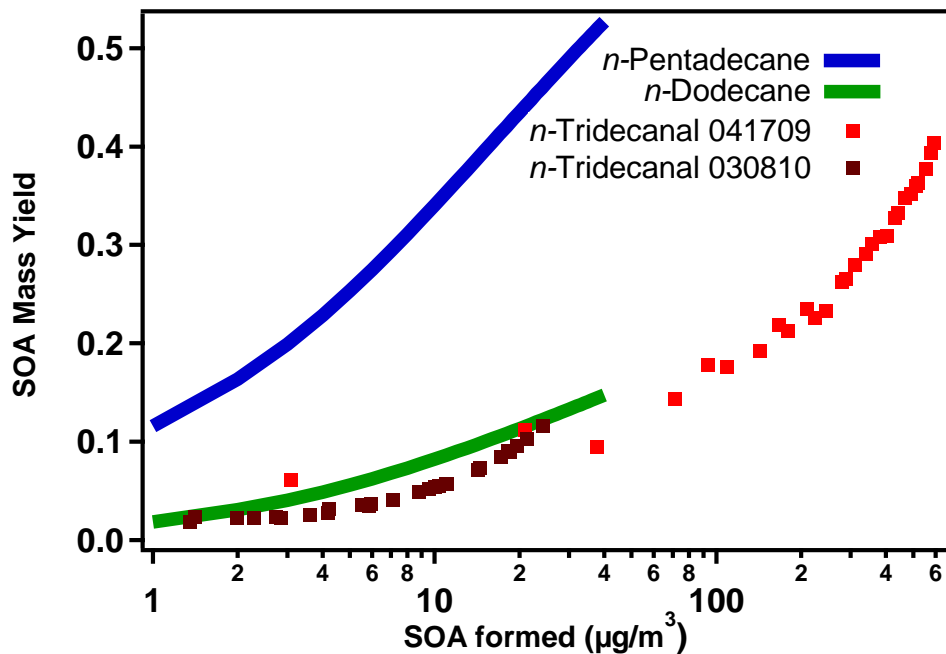


Figure 2.4. Comparison of SOA mass yields from *n*-tridecanal, *n*-pentadecane and *n*-dodecane. *n*-Tridecanal clearly forms less SOA than similar vapor pressure *n*-alkanes such as *n*-pentadecane because of its ability to fragment, forming alkyl nitrates, a C_{n-1} aldehyde and isomerization species. Even when the *n*-tridecanal backbone has been attacked by OH, its aldehyde functional group can fragment to give a CO₂ or form the PAN; *n*-pentadecane cannot fragment easily in the first generations of oxidation. *n*-Dodecane and *n*-tridecanal SOA mass yields are very similar, that is because both molecules form the C₁₂ alkoxy radical in significant amounts. The *n*-alkanes SOA mass yields are fits from the work of Presto et al., 2010 [72]. Smaller *n*-aldehydes (C₅, C₈ and C₁₁) SOA mass yields are significantly smaller than that of *n*-tridecanal.

2.4 Discussion

Gas-phase reactions and SOA mass yields. The C₁₃ *n*-aldehyde clearly forms SOA when it reacts with OH, but much less effectively than the *n*-alkane of similar vapor pressure (*n*-pentadecane data comes from Presto et al., 2010 [72]). In Figure 2.4 we compare SOA formation from *n*-tridecanal with SOA formation from *n*-pentadecane and *n*-dodecane. The yield curves for *n*-pentadecane and *n*-dodecane in Figure 2.4 are parameterizations based on published measurements from our laboratory [72]. All experiments were performed under high-NO_x conditions, as NO_x can influence SOA mass yields [73].

We could compare precursors based on vapor pressure or carbon number, and here we do both. *n*-Tridecanal and *n*-pentadecane have very similar vapor pressures because two methylene groups or one carbonyl group have roughly equivalent effects on the vapor pressure of a molecule [43]. If the *n*-pentadecane and *n*-tridecanal oxidation mechanisms were identical, their SOA mass yields should be similar because every oxidation step would reduce or increase the vapor pressure of the next generation of molecules by a similar factor. However, that is not the case. The SOA mass yields for *n*-tridecanal are about a factor of 3 lower than those for *n*-pentadecane at any given SOA mass concentration, as shown in Figure 2.4. In fact, the SOA formation from *n*-tridecanal is virtually identical to the SOA formation from *n*-dodecane, which has one *fewer* carbon atom.

An obvious reason why *n*-tridecanal SOA mass yields are lower than *n*-pentadecane yields is the high selectivity for OH attack on the aldehydic hydrogen. Approximately 54% of the initial OH attack is on this hydrogen (Figure 2.3), which ultimately results in fragmentation and the elimination of a CO₂ molecule. The PAN intermediate is also far too volatile to partition significantly to the SOA [43]. We thus expect abstraction of the aldehydic hydrogen to be a

relatively inefficient pathway for SOA formation, and *n*-aldehydes in general to be less efficient SOA sources than *n*-alkanes, as observed.

There are two potential explanations for the observed SOA formation efficiency for *n*-tridecanal and the relationship to the *n*-alkane mass-yield curves shown in Figure 2.4. The first is that the bulk of the first-generation reaction products follow the reaction pathway shown in Figure 2.1, as discussed above. This pathway involves the elimination of a single carbon, and so it seems reasonable that the mass yields for *n*-tridecanal would be similar to those for *n*-dodecane, which has one fewer carbon. The second is that approximately one-third to one-half of the OH attack occurs along the carbon backbone, which will preserve the carbon number in the first-generation products. Thus it is plausible that the SOA yields are at least one-third as large as those observed for *n*-pentadecane, which has a similar vapor pressure (see Figure D in the Appendices). Overall, we favor the first explanation because we believe that most of the SOA formation from these relatively volatile precursors involves multiple generations of oxidation [72]. Consequently, first-generation products from OH attack on the carbon backbone will retain the aldehydic functionality, and subsequent OH reactions will still strongly favor attack on that moiety, resulting in fragmentation. Whether during the first generation or subsequent generations of oxidation, the aldehyde will thus eventually fragment, dropping the system onto a mechanistic trajectory similar to an *n*-alkane with one fewer carbon (*n*-dodecane in this case). It is also important to mention that oligomer formation due to heterogeneous reactions in the aldehyde-OH-High NO_x system is probably not a strong SOA source; otherwise SOA formation would be much higher than presented in here.

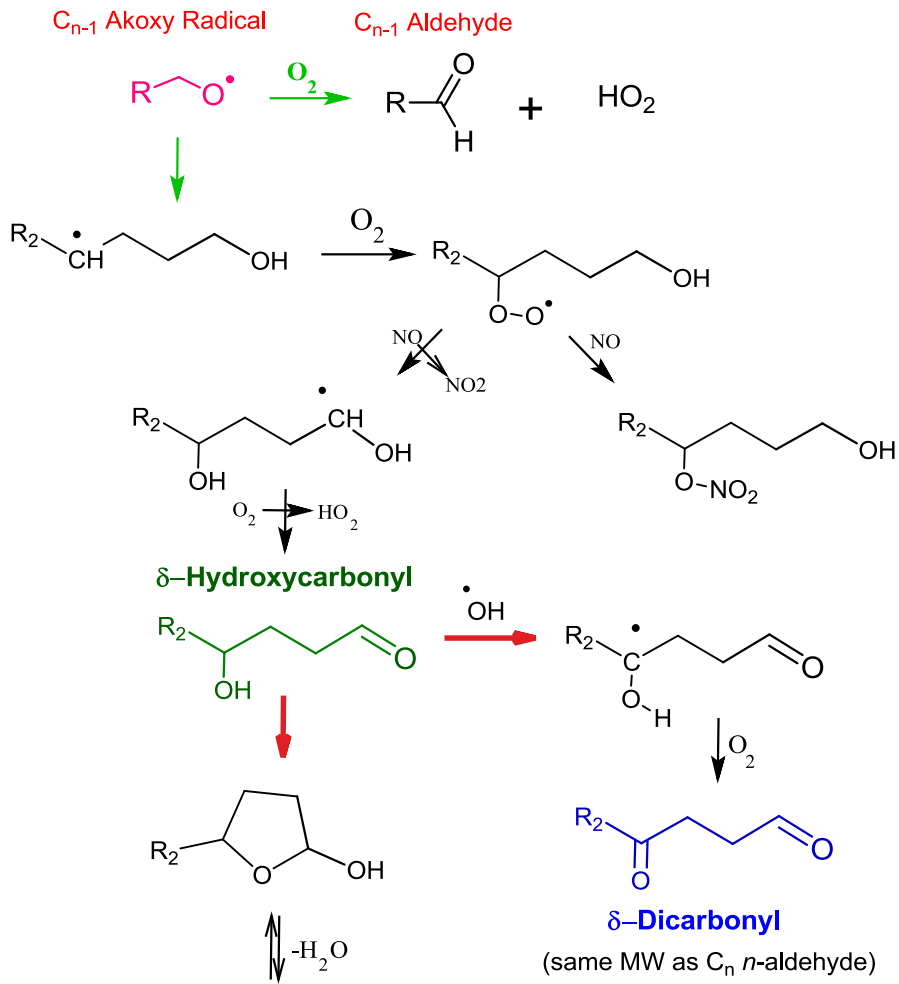
To further explore these hypotheses, we have compared the mass spectra of *n*-tridecanal and *n*-dodecane SOA using a Quadrupole Aerodyne Aerosol Mass Spectrometer (Q-

AMS). Specifically, we compared f_{44} (the ratio of $m/z=44$, CO_2^+ , to total organic-aerosol mass), and f_{44} is very similar for *n*-dodecane and *n*-tridecanal OH oxidation experiments. The spectra are shown in the Appendices, Figure G. This implies a similar level of oxidation of the aerosol material for both species. We have examined f_{30} (NO^+) also, and plotted it in Figure H in the Appendices. f_{30} indicates the presence of organic nitrates in the aerosol phase, and it is lower for *n*-tridecanal than for *n*-dodecane. Aerosol organic nitrates result from OH attack on the carbon backbone; this attack occurs only ~40% of the time for *n*-tridecanal but almost always for *n*-dodecane. The SOA formed through the attack of the aldehydic hydrogen does not form alkyl nitrates as can be seen in Figure 2.1. Thus, while the aldehydes efficiently form PANs, alkyl nitrates in SOA appear to be more common for *n*-alkanes.

In order to determine the SOA contribution from PAN, we examined the SOA mass yield of *n*-tridecanal under high NO_2 levels. By having significantly more NO_2 than NO, PAN is formed predominantly. When PAN is the dominant species, SOA mass yields drop by an order of magnitude (the Appendices, Figure E). This is consistent with SAR calculations of the PAN vapor pressure – it is simply too volatile to favor the condensed phase with these precursors. However, PAN formation does not explain the low SOA yields observed in general for the *n*-aldehydes; for the data shown in Figure 2.4, the PAN yield is only 5%. The SOA difference is caused primarily by the *n*-aldehyde fragmentation path in Figure 2.1. None the less, when PAN is formed, it has the potential to further reduce SOA formation. PAN is significantly more volatile than the homologue carboxylic acid with same carbon number. Even though the process of carboxylic acid formation in the atmosphere is not well understood, alkanes form them after various generations of oxidation [9]. Aldehydes have the potential to make acids as well [74] if the alkoxyacyl radical isomerizes [59], but this potential is diminished when the terminal carbon is protected as a peroxyacyl nitrate.

Gas-phase reaction mechanism details. Our gas-phase results (Figure 2.3) show that alkoxy isomerization overwhelms reaction with O_2 for large alkoxy radicals (which forms the C_{n-1} aldehyde), consistent with the well-established trends for alkanes [59, 61]. However, there is a difference. The isomerization pathway only becomes truly dominant at a carbon number of 10 (for an *n*-undecanal precursor), which is at least 3 more carbons than is required for the *n*-alkanes. Consequently, either the primary alkoxy radicals formed from *n*-aldehydes are somewhat more effective at reacting with oxygen to form the corresponding carbonyl than the secondary alkoxy radicals formed by *n*-alkanes, or the primary alkoxy radicals are less effective at internal H-atom abstraction.

We can also constrain the mechanism following isomerization. Following the Lim et al., 2005 [59] mechanism of long, straight-chain alkoxy radicals, the isomerization product (green arrow, Figure 2.1) of the *n*-aldehyde may be a δ -hydroxycarbonyl (green molecule, Figure 2.5) with an aldehyde group in position 1, and hydroxyl in 4 [59, 75, 76]. These compounds are able to cyclize to form a hemiacetal and subsequently a substituted dihydrofuran (brown molecule, Figure 2.5). However, relative humidity levels affect the ability to cyclize because dehydration is involved. Lower water vapor concentrations promote the cyclization, forming the dihydrofuran molecule [77]. For example, Holt et al., 2005 noticed that the C_5 and C_6 δ -hydroxycarbonyls did not cyclize when the relative humidity was increased from 5% to 50% [77, 78]. While the experiments discussed here were conducted at low relative humidity (< 20%), some of the δ -hydroxycarbonyl may still lead to a dicarbonyl [79] following reaction with OH (the hydroxyl group becomes a carbonyl) similar to the one proposed by Aschmann et al., 2003 [79]. This pathway is shown in Figure 2.5.



Substituted Dihydrofuran

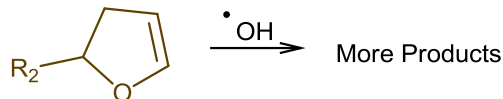


Figure 2.5. A continuation of the reaction mechanism shown in Figure 2.1, following the ‘isomerization’ pathway. This becomes important for larger n -aldehydes. The red arrows represent the branching point between cyclization and δ -dicarbonyl formation, and it is dependent on relative humidity. Holt et al., 2005 [77] shows that low relative humidity and long straight chain molecules favor cyclization. Figure 2.2 shows a decoupling from the inferred n -undecanal and the m/z 171. This decoupling might be related to the creation of δ -dicarbonyl, since it has the same molecular weight as the C_n n -aldehyde. This decoupling happens to all the aldehydes studied (Refer to the Appendices, Figures A, B, C).

Formation of this C_{n-1} δ -dicarbonyl could explain why the signal at the nominal m/z of the parent C_n n -aldehyde (see Figure 2.2 and the Appendices data, Figures A, B and C) diverges

from the inferred concentration of the aldehyde. Both the C_{n-1} δ -dicarbonyl and the parent C_n n -aldehyde have the same molecular weight, but they do not necessarily have the same sensitivity to the PTR-MS. Hence, it is not possible to determine the relative concentration of the C_{n-1} δ -dicarbonyl without a proper calibration. We are not implying that this is the only path to form a C_{n-1} δ -dicarbonyl; however, the hydrogens attached to the H_2C-OH on the δ -hydroxycarbonyl are highly reactive, approximately 3 times more reactive than hydrogens on a methylene group according to Kwok et al., 1995 [42].

2.5 Environmental Significance

There are higher anthropogenic emissions from n -aldehydes than the corresponding n -alkanes, making them potentially important as precursors of SOA. The importance of these larger emissions is reduced by the fact that n -aldehydes fragment easily (Figure 2.1) in the first steps of oxidation, limiting the amount of SOA formed when compared to an n -alkane. It is the very large n -aldehydes (higher or equal to C_{13}) that have a significant contribution to SOA formation. The data presented here show that a large C_n n -aldehyde SOA yield is similar to the SOA yield of a C_{n-1} n -alkane under similar conditions of $VOC:NO_x$ and a relatively low $NO_2:NO$, since high NO_2 favors PAN formation.

However, the most abundant aldehydes in the atmosphere might be the ones formed from the ozonolysis of monoterpenes and other biogenic unsaturated species. Since biogenic emissions are much higher than anthropogenic ones, and most biogenic species contain a double bond, the amount of aldehydes in the atmosphere is potentially large. When these aldehydes are oxidized by OH-radical attack under high NO_x conditions, they will quickly shorten their backbone size by giving up a CO_2 (similar to Figure 2.1) making their SOA contribution lower than that of similar vapor pressure anthropogenic emissions. However, sufficiently large

aldehydes derived from ozonolysis will still form SOA quite rapidly, and so their contribution to additional SOA formation during aging processes cannot be ignored.

Acknowledgments

This research was supported by the Electric Power Research Institute grant EPP25369C12290 and the EPA STAR program through the National Center for Environmental Research (NCER). This paper has not been subject to EPA's required peer and policy review, and therefore does not necessarily reflect the views of the Agency. No official endorsement should be inferred.

Chapter 3 – Fragmentation vs. Functionalization: Chemical Aging and Organic Aerosol Formation

Abstract

The transformation process that a carbon backbone undergoes in the atmosphere is complex and dynamic. Understanding all these changes for all the species in detail is impractical; however, choosing different molecules that resemble progressively higher stages of oxidation or aging and studying them can give us an insight into general characteristics and mechanisms. Here we determine secondary organic aerosol (SOA) mass yields of two sequences of molecules reacting with the OH radical at high NO_x. Each sequence consists of species with similar vapor pressures, but a succession of oxidation states. The first sequence consists of *n*-pentadecane, *n*-tridecanal, 2-, 7-tridecanone, and pinonaldehyde. The second sequence consists of *n*-nonadecane, *n*-heptadecanal and *cis*-pinonic acid. Oxidized molecules presented lower relative SOA mass yields compared to similar vapor pressure *n*-alkanes; however, oxidation state alone was not enough to predict how efficiently a molecule forms SOA. Certain functionalities are able to fragment more easily than others, and even the position of these functionalities on a molecule can have an effect. *n*-Alkanes tend to have the highest yields, and *n*-aldehydes the lowest. *n*-Ketones have slightly higher yields when the ketone moiety is located on the side of the molecule and not in the center. In general, oxidation products remain efficient SOA sources, though fragmentation makes them less effective than comparable alkanes.

3.1 Introduction

Organic oxidation mechanisms in the atmosphere are very complex and dynamic. After a molecule is emitted, it is transformed via reaction with the OH radical, ozone, NO_3 radical, and photolysis, etc., forming a rich array of products. The number of product molecules increases with increasing carbon number in the precursor-molecule as well as with the extent of oxidation [7, 9]. Consequently, mechanisms associated with organic aerosol, which generally involve higher than average carbon numbers and significant oxidation [80], are especially complex. Smog-chamber experiments have constrained parts of many reaction mechanisms; for example the first-generation products of *n*-alkanes with the OH radical have been identified in detail [23, 59, 81], but in most cases only the first hours of reaction are well understood. A typical aerosol particle resides in the atmosphere between one to two weeks [5, 82] before removal. This time scale is significantly longer than most smog-chamber experiments. There is thus a critical need to understand later-generation chemistry of the oxygenated compounds likely to be involved in the full life cycle of organics, and especially organic aerosol, in the atmosphere.

Studying the transformation of chemical species for weeks in smog-chamber experiments under ambient conditions is not possible; hence some studies have increased the oxidant concentration (e.g. OH radical) to simulate multiple days of oxidation [25, 83, 84]. These studies, done in flow tubes, have started to yield insight into chemical aging. However, there is limited research on this topic, and the very high oxidant exposures may skew the oxidation mechanisms. Understanding the details of how molecules age in the atmosphere is crucial for models that predict secondary organic aerosol (SOA) formation [5] as well as subsequent transformation [85]. One way to elucidate this multiple-generation chemistry is to follow it one generation at a time. The idea is to carefully select compounds that are either themselves

important intermediates, or that represent important classes of compounds with similar properties. Here we take this approach.

Efforts are underway to try to classify atmospherically relevant organic material in terms of properties important to the condensed phase. The most important property is volatility – it determines whether a compound is in the condensed phase at all [10]. Oxygenation has been proposed as a second important property because it progressively increases during oxidation chemistry and also appears to correlate well with hygroscopicity, another key property [3]. We can describe volatility in terms of the saturation concentration, C^0 [10, 37, 86], which is operationally defined as the organic aerosol concentration (C_{OA}) at which half of a given compound will be found in the condensed phase [10]. For oxygenation we employ the oxygen-to-carbon ratio O:C [3, 37].

It is useful to break reaction mechanisms into a succession of steps connecting one stable molecule to another. We can classify these steps as functionalization, fragmentation and accretion [9, 85] according to the effect on the product carbon number. These three processes are illustrated in Figure 3.1. Functionalization involves the addition of oxygenated functional groups (thus an increase in O:C) to a molecule with no change in carbon number, decreasing its vapor pressure in most cases and making it more likely to partition into the aerosol phase. Fragmentation refers to carbon-carbon bond cleavage resulting in at least two separate organic products (i.e. a reduction in carbon number). In some cases, this path creates higher vapor pressure species, and in others, the vapor pressure decreases because the products are typically also functionalized. A good example is the ozonolysis reaction of monoterpenes. While the double bond is broken, at least two oxygens are added, often significantly decreasing the vapor pressure of the products compared to the parent-molecule. Finally, accretion, also named

oligomerization, refers to association reactions (typically in the condensed phase) resulting in an increase in carbon number (with no change in O:C) and a dramatic reduction in vapor pressure [26, 27]. While not all accretion reactions lead to lower vapor pressure species (for example esterification), often the increase in carbon number outweighs any reduction in polarity.

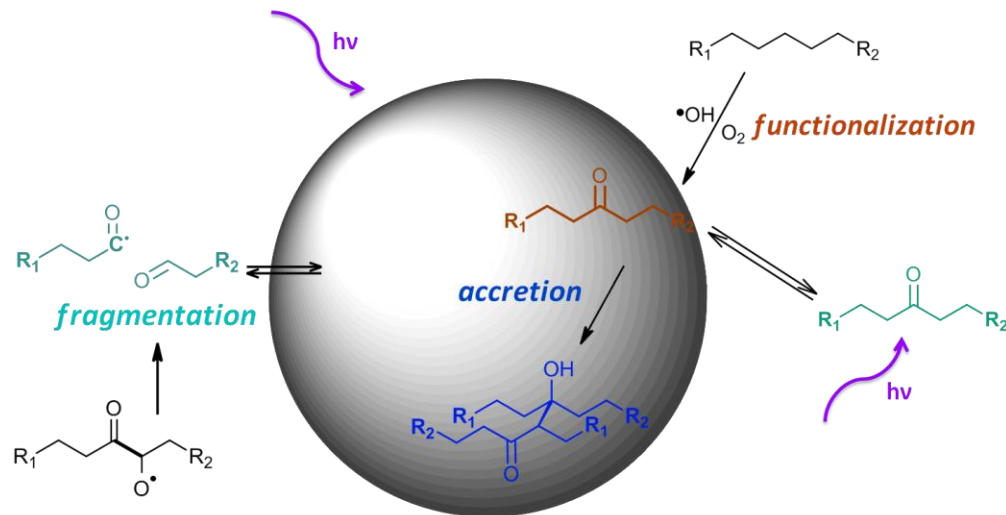


Figure 3.1. Major mechanisms in gas and aerosol-phase oxidation. The three major chemical mechanisms that a carbon backbone undergoes in the atmosphere are represented along with their interaction with aerosols. They are described and revised in Kroll and Seinfeld, 2008 [9] and Rudich et al., 2007 [85]. Both, functionalization and accretion tend to decrease the vapor pressure of species by either adding polarity to the molecule or by accreting with other molecules. Fragmentation cleaves carbon-carbon bonds of molecules, generally increasing the vapor pressure of products; however, a good exception is the ozonolysis of monoterpenes, where both fragmentation and functionalization happen simultaneously, adding polarity and decreasing the overall vapor pressure of the products. The competition of these three mechanisms define the fate of molecules in the atmosphere, but it is not clear how this competition plays out while molecules and particles age.

The relative effects of these three pathways on organic-aerosol levels and properties remain uncertain. Thermodynamics demands that complete fragmentation (formation of CO₂) would be the outcome if oxidation continued far enough [4], but most carbon emissions return to the surface before complete oxidation [7]. Ambient organic aerosol is highly oxidized [29] (with average oxygen to carbon ratios for aerosols varying from 0.5 to 0.9 [29, 87]), with

significant carboxylic acid functionality [85], but this does not directly indicate how much of a role fragmentation or accretion plays.

Another issue is the phase in which the chemistry occurs. The primary focus here is on gas-phase chemistry, where both functionalization and fragmentation reactions can occur readily. Heterogeneous uptake of oxidants (i.e. OH) can have similar effects [25]. Accretion reactions occur in the condensed phase, either in a primarily organic phase or in the aqueous phase. For the experiments reported here the relative humidity was kept low (RH < 10%), and so any condensed phase chemistry occurred in the organic phase. It is also possible that reactive uptake of organic peroxy radicals (RO_2) could influence the organic oxidation mechanism and also SOA formation. However, all experiments described here were performed under high- NO_x conditions. The timescale for collisions with aerosols (the condensational sink) was significantly longer than the fast $\text{RO}_2 + \text{NO}$ reaction [88, 89], so peroxy uptake was not significant for the experiments presented here.

While organic aerosol ages in the atmosphere, its oxygenation (indicated by the oxygen to carbon ratio, O:C) tends to increase, changing its properties with time [29]. We would therefore like to examine the fragmentation susceptibility and SOA formation of individual molecules versus oxygenation. In order to do this, we selected two different sequences of molecules, each sequence consisting of atmospherically relevant vapor pressures (Figure 3.2). Specifically, we work with molecules that have saturation concentrations (vapor pressures in mass concentration units) of $\sim 10^5$ and $\sim 10^3 \text{ } \mu\text{g m}^{-3}$. For each sequence, we concentrate on molecules that have a different O:C, and that are atmospherically relevant. The highest O:C we have worked with so far is ~ 0.3 : atmospherically relevant molecules with higher O:C are more difficult to synthesize, separate or obtain commercially. In this manner we are systematically

constructing a sequence of oxidation steps, using model compounds to represent both locations in the 2D space as well as successive generations of oxidation. Since vapor pressure data are not available for all of the species we worked with, we used the SIMPOL model from Pankow and Asher, 2008 [43] and fits from Donahue et al., 2011 [37] to estimate them. The major characteristic encountered is that a molecule with n carbons has a similar vapor pressure to a molecule with $n-2$ carbons and 1 oxygen (with carbonyl functionality). This characteristic is used only as a guide.

Each sequence contains species with similar vapor pressures because comparison of their SOA mass yields reflects the competition between fragmentation, functionalization and possibly accretion if important. If two different chemical species with identical vapor pressures had very similar chemical oxidation paths (e.g. competition of functionalization, fragmentation and accretion) their SOA mass yields are expected to be similar as well. That is because with every generation of products formed, their overall vapor pressures increase or decrease by a similar amount. If the SOA mass yields are very different, then the different classes of reaction pathways (fragmentation, functionalization and accretion) contribute differently to the oxidation mechanism. This approach is similar to that employed by Ziemann and co-workers to explore the effects of branching, unsaturation and cyclization on hydrocarbon SOA formation [60, 76], but our focus is on the effects of oxygenated functionality as a model for later-generation chemistry.

The $10^5 \mu\text{g m}^{-3}$ sequence is *n*-pentadecane, *n*-tridecanal, pinonaldehyde, 2-tridecanone, and 7-tridecanone. *n*-Pentadecane is the “anchor” species in the sequence, defining the nominal SOA mass yields we expect from a $\sim 10^5 \mu\text{g m}^{-3}$ species. Both *n*-pentadecane and *n*-tridecanal [45, 46] are good models of important anthropogenic emissions with respect to

chemical and structural characteristics (e.g. vapor pressure, oxidation state, etc.). Pinonaldehyde is a major product of the oxidation of α -pinene [90, 91]; multiple studies indicate that the molar yield formation of pinonaldehyde from both α -pinene ozonolysis and OH radical reaction can approach 50% [31, 32], making it a good model-molecule of the first-generation products from the oxidation of monoterpenes. Finally, 2-tridecanone and 7-tridecanone allow us to explore the relationship between the position of carbonyl functionality in the molecule and its ability to fragment. The $10^3 \mu\text{g m}^{-3}$ sequence is *n*-nonadecane, *n*-heptadecanal and *cis*-pinonic acid. Both *n*-nonadecane and *n*-heptadecanal are chosen as homologous to *n*-pentadecane and *n*-tridecanal. *cis*-Pinonic acid is similar to pinonaldehyde and it is also a first-generation product of α -pinene oxidation [32].

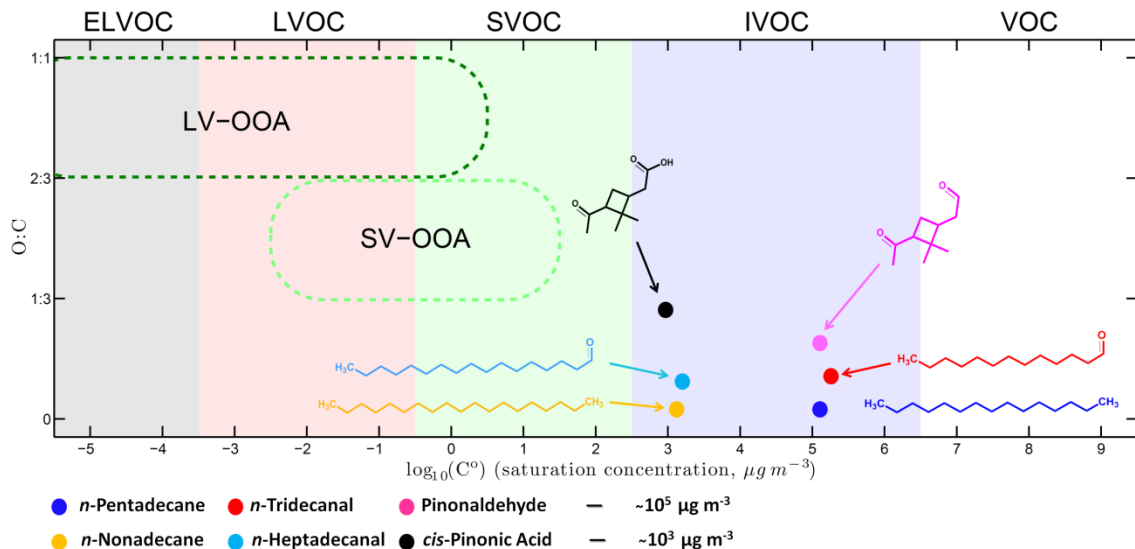


Figure 3.2. Two sequences of molecules with progressively increasing oxidation state but similar vapor pressures ($\sim 10^5$ and $\sim 10^3 \mu\text{g m}^{-3}$), shown in a two-dimensional volatility-oxidation state space. The $10^5 \mu\text{g m}^{-3}$ sequence is: *n*-pentadecane, *n*-tridecanal, pinonaldehyde, and 2- and 7-tridecanone (co-located with *n*-tridecanal). The $10^3 \mu\text{g m}^{-3}$ sequence is: *n*-nonadecane, *n*-heptadecanal and *cis*-pinonic acid. The species lie in the intermediate volatile organic carbon (IVOC) range occupied by many first-generation oxidation products associated with secondary organic aerosol (SOA) formation. Pinonaldehyde and *cis*-pinonic acid are first-generation products of α -pinene oxidation. Ambient oxidized organic aerosol (OOA) lies in the ranges indicated, with SV-OOA being fresher, less oxidized and more volatile and LV-OOA being more aged and less volatile.

Our hypothesis claims that there is a relationship between the oxidation state of a molecule and its ability to form SOA. More oxidized molecules can fragment more easily, as shown by Kroll et al., 2009 [25], reducing their ability to form organic aerosol when reacting with the OH radical. Chapter 2 of this thesis and Chacon-Madrid et al., 2010 [92] showed that *n*-aldehydes fragment significantly more than *n*-alkanes with similar vapor pressures, thus forming less SOA. When examining the gas-phase chemistry of different volatile organic compounds (VOCs) with the OH radical in the presence of NO_x [23, 28, 62], it is clear the alkoxy radical is the leading intermediate that fragments molecules, especially when other functionalities are already present [61, 62].

Our objectives are to *a*) understand the relationship between the oxidation state of a molecule and its ability to form organic aerosol, *b*) realize how important fragmentation *versus* functionalization paths are while a molecule ages in the atmosphere and *c*) report SOA mass yields of atmospherically relevant species for which there is limited or no information in the literature. Our model-system does not present highly oxidized precursors as seen in Figure 3.2, limiting our conclusions to precursors similar to those found in the early steps of OH radical oxidation sequences. This limitation has to do with the difficulty of synthesizing, separating or obtaining commercially material that resembles low volatility-oxidized organic aerosol (LV-OOA) [29].

3.2 Experimental

We conducted experiments in the Carnegie Mellon University smog chamber. Many details of our experimental procedures are described elsewhere [65]. The FEP Teflon (Welch Fluorocarbon) chamber has a maximum volume capacity of 12 m³. The bag is suspended inside a temperature-controlled room, which was held at 295 K for these experiments. All the

experiments were conducted under high- NO_x conditions (maximum of 4 ppbC/ppb- NO_x). Table B in the Appendices lists the specific concentrations and important concentration ratios for all the experiments. Particle number-size distributions were monitored using a scanning mobility particle sizer operating in recirculating mode (SMPS, TSI classifier model 3080, CPC model 3772 or 3010, 15 - 700 nm D_p). The concentrations of the different organic species were monitored with a unit mass-resolution proton transfer reaction-mass spectrometer (PTR-MS, Ionicon GmbH). For each experiment, HONO photolysis was used to create OH radicals. Additional nitric oxide (NO) was added to achieve the desired VOC: NO_x ratio. Ammonium sulfate particles (Sigma Aldrich, 99.99%) were used as inert seeds for condensation. These were formed from an aqueous solution with a nebulizer (TSI 3075), then dried and neutralized. We used seed concentrations of $\sim 10^4$ particles cm^{-3} or ~ 10 to 15 $\mu\text{g m}^{-3}$. The organic species used were *n*-tridecanal (Alfa Aesar, 94%), pinonaldehyde (synthesized in Carnegie Mellon Laboratory, $\sim 85\%$), 2-tridecanone (MP Biomedicals), 7-tridecanone (MP Biomedicals), *n*-nonadecane (Ultra, 99%), *n*-heptadecanal (synthesized in Carnegie Mellon Laboratory, $\sim 85\%$) and *cis*-pinonic acid (98%, Aldrich). These molecules were all used without further purification. UV lights (General Electric 10526 black lights) with a $J_{\text{NO}_2} = 0.06 \text{ min}^{-1}$ were used to initiate photo-oxidation after all the components were mixed in the chamber.

3.2.1 Injection of molecules into the chamber

Molecules in the $10^5 \mu\text{g m}^{-3}$ sequence were injected directly into the chamber via a septum. Molecules in the $10^3 \mu\text{g m}^{-3}$ sequence (Figure 3.2) were injected into the chamber using a resistively heated vaporizer. This vaporizer has a resistive graphite tip where the material of interest is placed, which is suspended directly in the chamber. This vaporizer heats up to about 200° C in about two minutes. A steel tube is used to allow a flow of air to dissipate the material

from the tip into the chamber. Some graphite is ejected from the tip while heated, but the concentrations are significantly lower than the organic precursors. Based on PTR-MS mass spectra of the injection products, there was no evidence of precursor decomposition during vaporization.

3.2.2 SOA Mass Yield and Wall Loss Calculations

This topic is approached for the first time in Chapter 2, section 2.2.2 and reviewed in here. The SOA mass yield from a reaction is defined as the mass of organic aerosol formed divided by the mass of precursor consumed [12],

$$Y = \frac{C_{OA}}{\Delta C_{precursor}} \quad (2.4)$$

where C_{OA} is the mass of organic aerosol created, and $\Delta C_{precursor}$ is the mass of the precursor organic species consumed to form the organic aerosol (C_{OA}) and other products. We determined SOA mass yields for the different organic species based on volume growth on the inorganic seeds, measured with the SMPS.

Total SOA production (C_{OA}) is determined by using the ratio of suspended organic aerosol (C_{OA}^{sus}) to suspended ammonium sulfate (C_{seed}^{sus}) and the initial concentration of ammonium sulfate $C_{seed}^{sus}(t = 0)$, as described by Hildebrandt et al., 2009 [65]:

$$C_{OA}(t) = \frac{C_{OA}^{sus}(t)}{C_{seed}^{sus}(t)} C_{seed}^{sus}(t = 0) \quad (2.5)$$

$C_{seed}^{sus}(t)$ is obtained by fitting an exponential decay to the ammonium sulfate volume concentration (measured with the SMPS and verified with an Aerosol Mass Spectrometer) over the interval between seed injection (and mixing) in the chamber and the onset of photo-

oxidation. Extrapolation of this signal after the photo-oxidation process starts defines the seed mass concentration as a function of time.

At time 0 (onset of photo-oxidation) and later, the difference between the total aerosol mass concentration in the chamber (measured with an SMPS) and the extrapolated ammonium-sulfate mass concentration is considered the $C_{OA}^{sus}(t)$. To obtain the total $C_{OA}(t)$ from the suspended mass concentration we correct for wall losses, assuming that organic particles lost to the wall are in equilibrium with the suspended particles and vapor-phase species, and also that the organic to seed mass ratio remains the same for suspended and deposited particles. . This is the upper-limit estimate for SOA production explained in Weitkamp et al., 2007 [67]. There is approximately a 20% difference in SOA mass yields for each species studied when assuming particles lost to the walls are in equilibrium with the suspended particles (upper limit) versus assuming that no further condensation occurs once particles have deposited (lower limit). This percentage has been observed in current and past experiments [92].

3.2.3 Measurement of reactants

The concentrations of reactants were monitored with a unit mass-resolution proton transfer reaction-mass spectrometer (PTR-MS). The fragments used to track concentrations are those of the MW + 1 for *n*-tridecanal, pinonaldehyde, 2- and 7-tridecanone. The PTR-MS sensitivity at these fragment masses was previously calibrated with those species. A key assumption is that interferences from other species were minimal. An exception to this was *n*-tridecanal, discussed in Chacon-Madrid et al., 2010 [92], where a C_{n-1} dicarbonyl is formed due to isomerization.

We used *m/z* 43 and 57 to follow the concentrations and respective consumption of *n*-heptadecanal and *n*-nonadecane. The signal corresponding to their MW + 1 was too low, thus a

higher-intensity but less selective fragment was used. The specifics of using m/z 43 and 57 with a PTR-MS are described in Jobson et al., 2005 [93] and are also applied in Presto et al., 2010 [72]. The difficulty with using either m/z 43 and 57 as a proxy of reactant concentration is that with time, the signal does not decay as quickly as the precursor is consumed. This is because first- and second-generation products contribute to m/z 43 and 57 as well. In some cases this interference is reduced because the products partition into the aerosol phase and do not produce a PTR-MS signal. We also use methanol as a radical tracer in all experiments. We measured it with a PTR-MS (specifically m/z 33) to determine the concentration of OH radicals during the experiments. OH concentrations and kinetic rate constants allow us to predict concentrations of the different precursors and compare with the initial decay of m/z 43 and 57. Methanol concentrations in all the experiments conducted were lower than the precursor-molecules themselves. This is done to minimize the effect of methanol on the radical balance. Also, the relatively low rate constant of methanol + OH radical minimizes its effect on the overall chemistry.

3.2.4 Synthesis of Organic Species

We synthesized *n*-heptadecanal and pinonaldehyde following McMurry et al., 1987 [94], as they are not commercially available. Products were formed via ozonolysis in solution, as shown in Figure I in the Appendices. 1-Octadecene (Acros Organics, 90%) and α -pinene (Aldrich, 99%) were used as reactants for *n*-heptadecanal and pinonaldehyde, respectively. The synthesis started with formation of the secondary ozonide, which was kept stable by maintaining a temperature of -78°C with a dry-ice ethanol slurry. After the ozonide was formed, dimethyl sulfide (DMS) was added to reduce the ozonide to the respective carbonyls. After adding DMS, the products were held at room temperature for about three hours, after which they were

extracted with water to remove water-soluble contaminants. Finally, a simple distillation procedure vaporized solvents and other volatile impurities. We used Nuclear Magnetic Resonance (H^1 NMR, HSQC and Tocsy) to determine products and yields from the synthesis. The spectra are shown in the Appendices in Figures J through M.

3.3 Results

SOA mass yields for the $10^5 \mu\text{g m}^{-3}$ sequence (*n*-tridecanal, pinonaldehyde, 2- and 7-tridecanone, and *n*-pentadecane) are presented in Figure 3.3 and 3.4. All of these species were exposed to similar OH and NO_x concentrations, and none of the reagents showed significant losses to the walls before the OH-radical source was turned on, indicating that wall losses such as those reported by Matsunaga and Ziemann [95], were not a problem. The OH radical was always in excess than any of the parent molecule studied. *n*-Pentadecane SOA mass yields are shown as a function reproducing data from Presto et al., 2010 [72] and *n*-tridecanal yields are from Chacon-Madrid et al., 2010 [92]. We shall use the *n*-pentadecane mass yield curve for reference throughout this discussion. *n*-Pentadecane oxidation produces significantly more SOA than either pinonaldehyde or *n*-tridecanal, but within uncertainty, yields for those two aldehydes are identical, as shown in Figure 3.3. The 2- and 7-tridecanone SOA mass yields are presented in Figure 3.4. Both *n*-ketones have significantly lower SOA mass yields than the reference *n*-alkane, and the 7-tridecanone yields are identical to *n*-tridecanal yields, within error. The 2-tridecanone mass yields are larger than the *n*-tridecanal yields in the 30 to 50 $\mu\text{g m}^{-3}$ range of SOA formed.

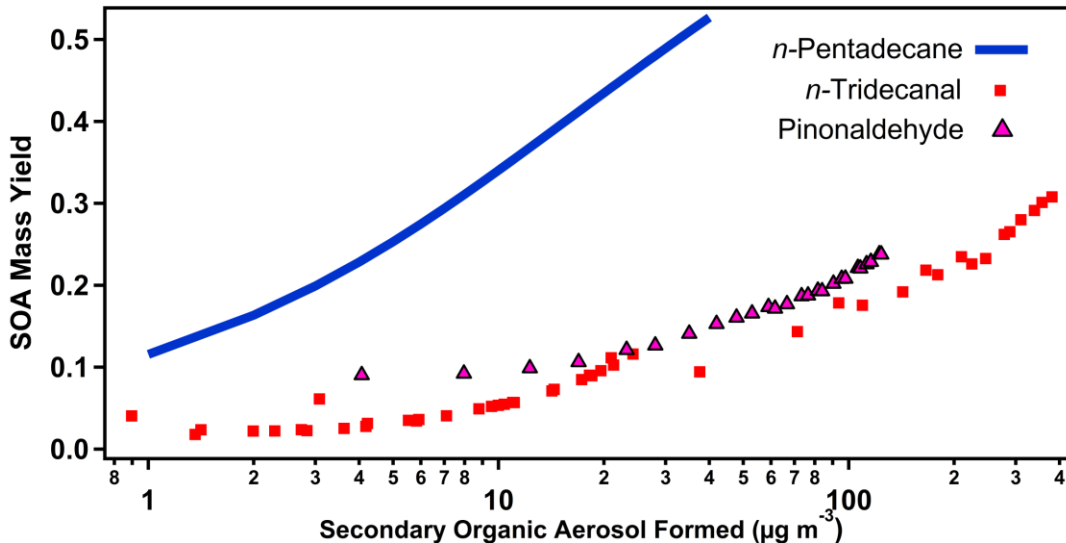


Figure 3.3. SOA mass yields of organic species with vapor pressures of $10^5 \mu\text{g m}^{-3}$. *n*-Tridecanal, pinonaldehyde and *n*-pentadecane SOA mass yields after the OH radical reaction at high NO_x are presented here. *n*-Pentadecane yields are a fit that comes from Presto et al., 2010 [72]. The suppression of SOA yields for *n*-tridecanal and pinonaldehyde vs. *n*-pentadecane are related to the tendency of the aldehydic moiety to fragment relatively quickly as detailed in Chacon-Madrid et al., 2010 [92]. At this point, it is not clear how the ketone and cyclobutane moieties influence the SOA formation from pinonaldehyde, if at all.

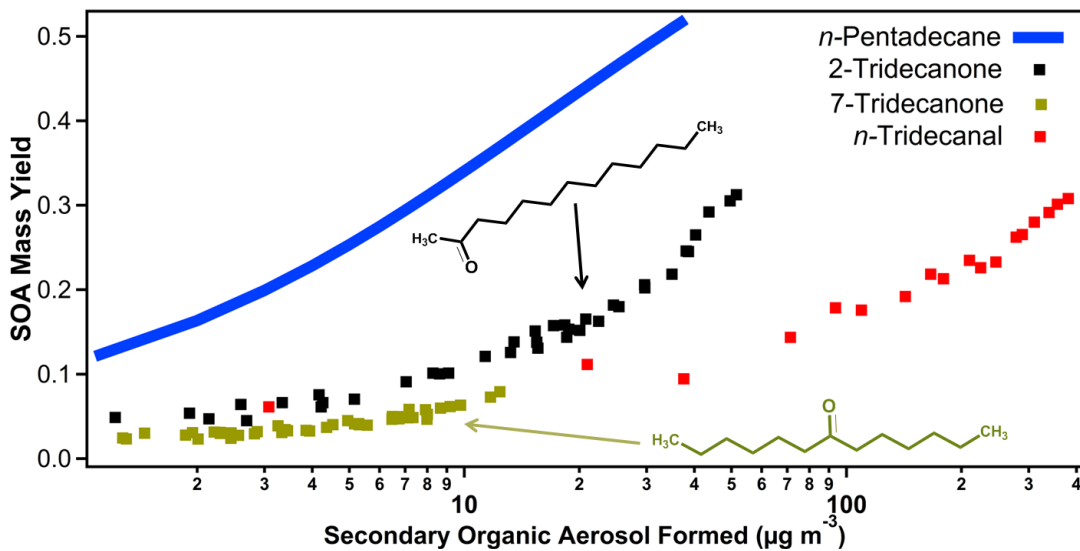


Figure 3.4. SOA mass yields of ketones with vapor pressures of $10^5 \mu\text{g m}^{-3}$. 2- and 7-tridecanone SOA mass yields are slightly different. The lower efficiency of 7-tridecanone to form SOA might be related to higher fragmentation paths when it reacts with the OH radical as compared to 2-tridecanone. Additionally, splitting the molecule in the middle might have bigger consequences on SOA production versus splitting it on the side (e.g. 2-tridecanone). However, the differences in SOA yields are not as pronounced as the mechanisms would suggest. Photolysis might play a more important role on the oxidation products of 2-tridecanone.

SOA mass yields for the $10^3 \mu\text{g m}^{-3}$ sequence (*n*-heptadecanal and *n*-nonadecane) are shown in Figure 3.5. Because the vapor pressures of the precursors themselves are quite low, we kept the injections and subsequent SOA formation to a relatively low (and atmospherically relevant) range of $< 10 \mu\text{g m}^{-3}$. We do not report yields for *cis*-pinonic acid in Figure 3.5 because we were not confident we could accurately measure its vapor concentrations with the PTR-MS. Nonetheless, *cis*-pinonic acid oxidation produced a significant amount of SOA, with mass yields appearing to be larger than *n*-heptadecanal but lower than *n*-nonadecane.

The precision of the experiments can be seen in Figure 3.3. The SOA mass yields of *n*-tridecanal are composed of two different experiments, one in the region of 0 to $\sim 25 \mu\text{g m}^{-3}$, and the other in the region of ~ 25 to $\sim 400 \mu\text{g m}^{-3}$. The two experiments form an overlapping yield curve. Pinonaldehyde has a similar mechanism to *n*-tridecanal when reacting with the OH radical and a similar vapor pressure. Figure 3.3 shows that yields of pinonaldehyde match those of *n*-tridecanal, again demonstrating the good precision of the measurements. All the experiments performed resulted in SOA mass yields above blank experiments, including the aldehydes.

All the different experiments performed reached equilibrium between the organic aerosol-phase and the gas-phase within the experimental time frame. Particles grew rapidly during the first hour of each experiment due to the high OH radical concentration, but after the first to second hour of photo-oxidation, the particles stopped growing. There was no evidence for any substantial delay in condensational growth that would be associated with a significant delay in equilibration. This is consistent with other experiments performed in our laboratories [96, 97]. Consequently, we believe that there were no substantial mass-transfer limitations

during these experiments that would affect our conclusions regarding the competition between fragmentation, functionalization and accretion effects on SOA formation.

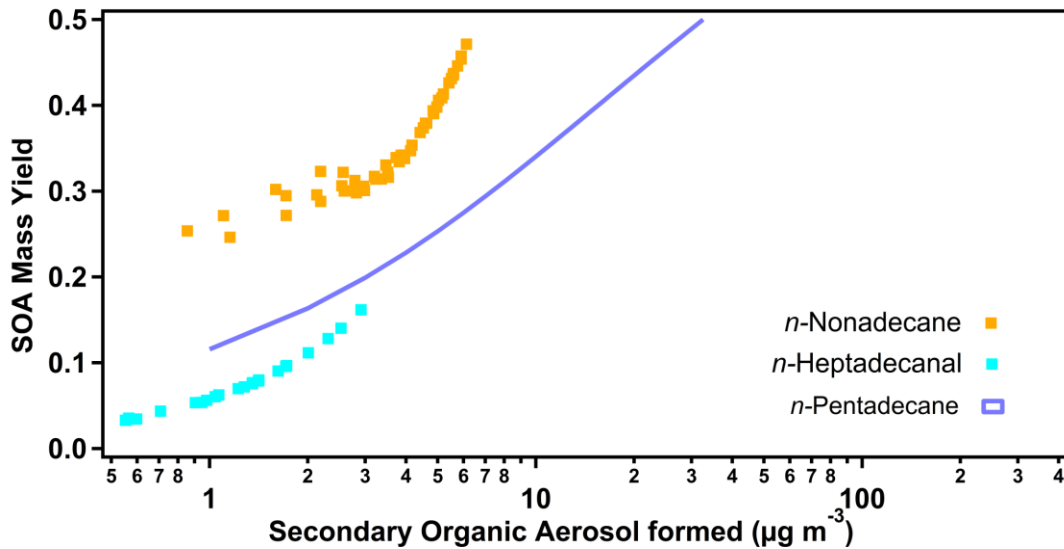


Figure 3.5. SOA mass yields of organic species with vapor pressure of $\sim 10^3 \mu\text{g m}^{-3}$. *n*-Pentadecane (from the $10^5 \mu\text{g m}^{-3}$ sequence) is shown as a reference. The differences in SOA mass yields between *n*-nonadecane and *n*-heptadecanal are not surprising. The aldehydic moiety is very reactive and causes fragmentation at high NO_x , while the *n*-nonadecane does not have relevant first-generation fragmentation paths.

3.4 Discussion

3.4.1 *n*-Tridecanal and Pinonaldehyde vs. *n*-Pentadecane

The aldehydic moiety appears to dominate *n*-tridecanal and pinonaldehyde chemistry as compared with *n*-pentadecane. This is responsible for the differences in SOA mass yields seen in Figure 3.3. Fragmentation overwhelms the first-generation chemical mechanism of pinonaldehyde and *n*-tridecanal as discussed in Chacon-Madrid et al., 2010 [92]. The fragmentation path is important in the presence of NO_x [23]. The chemical mechanism of a generic aldehyde reacting with OH radical in the presence of NO_x is presented in Chapter 2, Figure 2.1.

Fragmentation in the first generation of aldehyde oxidation evidently only occurs when the OH radical attacks the aldehydic moiety, which tends to be very reactive. For example, according to structure activity relationships (SAR) from Kwok and Atkinson, 1995 [42], the aldehydic moiety is attacked ~54% and ~79% of the time (relative to other sites in the molecule) for *n*-tridecanal and pinonaldehyde, respectively, when attacked by OH. Not every attack on the aldehydic moiety ends in fragmentation, but the molecules that do not fragment after aldehydic attack form peroxyacyl nitrates (PANs) [98], which in this case are too volatile to form SOA.

The fragmentation path is thought to be negligible for *n*-pentadecane, at least in the first oxidation steps [59, 81]. As shown in Figure 3.3, a higher SOA mass yield is the result of functionalizing a molecule without significant fragmentation. Linear *n*-alkanes are especially strong SOA precursors because branched alkanes can fragment more easily, as shown by Lim and Ziemann, 2009a,b [60, 76] and others [99]. While the first-generation oxidation products from pentadecane include carbonyls, they are larger and less volatile than *n*-tridecanal or pinonaldehyde. Since the first oxidation steps for *n*-pentadecane do not include fragmentation, its oxidized products will have significantly lower vapor pressures, making them more likely to partition into the aerosol phase [10, 11].

3.4.2 *n*-Tridecanal *versus* Pinonaldehyde

The two important structural differences between *n*-tridecanal and pinonaldehyde are the four-member cycle and the ketone functionality present in pinonaldehyde but not in *n*-tridecanal. Regardless, the aldehydic moiety is the most reactive in both molecules. Since the aldehydic moiety leads to a significant amount of fragmentation in the presence of NO_x, it is not a surprise

to see similar SOA mass yields in these aldehydes that are significantly lower than those of *n*-pentadecane.

The high fragmentation of *n*-tridecanal products was discussed in Chacon-Madrid et al., 2010 [92]. Figure 3.6 presents strong evidence of pinonaldehyde fragmentation to form *nor*-pinonaldehyde. In the figure, $t = 0$ is the start of photo-oxidation. The initial OH radical concentration (determined by consumption of methanol) was $\sim 10^7$ molecule cm^{-3} ; the OH concentration dropped by an order of magnitude after the first hour. After about 1.5 h of photo-oxidation, the *nor*-pinonaldehyde signal started to decline because the reaction with OH exceeded its production due to declining pinonaldehyde levels. These data show that *nor*-pinonaldehyde (with 9 carbons) forms with a $\sim 50\%$ molar yield. This is much larger than the $\sim 4\%$ molar yield of *n*-dodecanal formation from *n*-tridecanal presented in Chacon-Madrid et al., 2010 [92], showing that the C_{n-1} alkoxy radical from pinonaldehyde, with a stiff cyclic backbone, is not capable of isomerizing (Figure 2.1, Chapter 2).

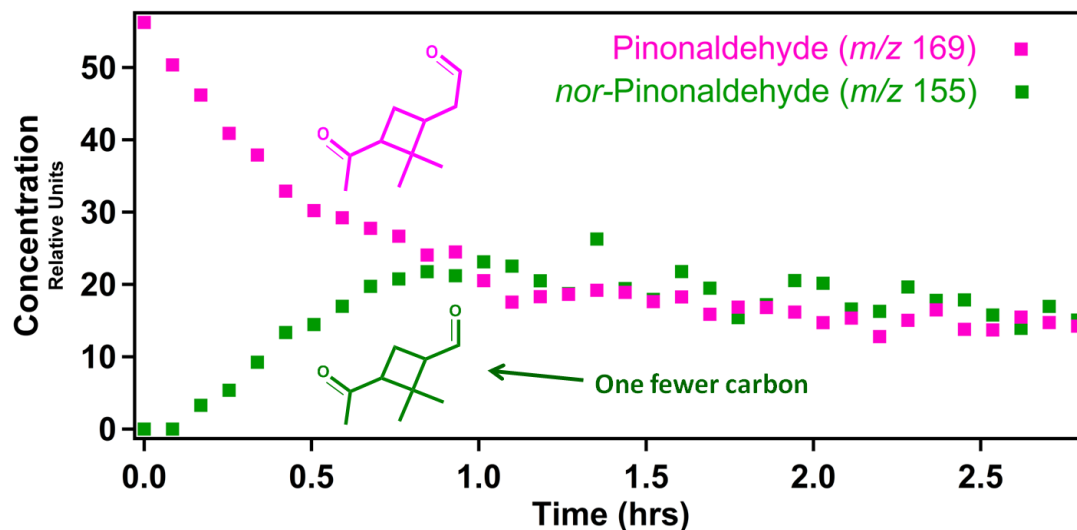


Figure 3.6. Pinonaldehyde + OH radical in the presence of NO_x . Consumption of m/z 169 (molecular weight of pinonaldehyde + 1 in a PTR-MS), and the formation of m/z 155 (molecular weight of *nor*-pinonaldehyde +1). *nor*-Pinonaldehyde molar yield from the OH radical oxidation of pinonaldehyde in the presence of NO_x is about $\sim 50\%$.

n-Tridecanal and pinonaldehyde SOA mass yields are identical within uncertainty (Figure 3.3). Two factors may explain this similarity. First, the initial attack by OH on *n*-tridecanal and pinonaldehyde happens overwhelmingly on the aldehydic moiety, resulting in product-species with one fewer carbon as their major products. Second, even though the aldehydic moiety on pinonaldehyde may be slightly more reactive than *n*-tridecanal (giving more fragmentation), the attack on the rest of the molecule (mainly the four-member-cycle) can be very efficient at adding polarity without causing the molecule to split in two different products.

3.4.3 2- versus 7-Tridecanone SOA mass yields

These two molecules are an ideal model system to explore the importance of the position of the ketone functionality in a molecule and its effect on SOA production. Broadly, if the ketone functionality promotes fragmentation, 7-tridecanone SOA yields could be very small (the molecule would split in half), while 2-tridecanone SOA yields might be intermediate. A hotspot of first-generation reactivity of ketones with the OH radical is the β -hydrogens [100] (Figure 3.7). For 7-tridecanone, the β -hydrogens are thought to account for ~47% of the first-generation reaction with the OH radical (following Kwok and Atkinson, 1995 [42]). For 2-tridecanone, attack on β -hydrogens is only ~27% because there is only one β -carbon. A partial mechanism for 7-tridecanone is presented in Figure 3.7, showing the attack on the β -hydrogens that can lead to fragmentation. This fragmentation path results in the formation of *n*-hexanal, which we observed by PTR-MS (Figure N, Appendices). This particular fragmentation path might not be important for 2-tridecanone because of the low reactivity of the terminal CH_3- with the β -alkoxy radical at the isomerization stage. Attack on the α -hydrogens could also lead to fragmentation: this path could lead to an α -alkoxy radical that would preferably fragment [9]. However, the

reactivity of the α -hydrogens by OH radical is thought to be slightly reduced because of the presence of the carbonyl [100], making this a minor pathway.

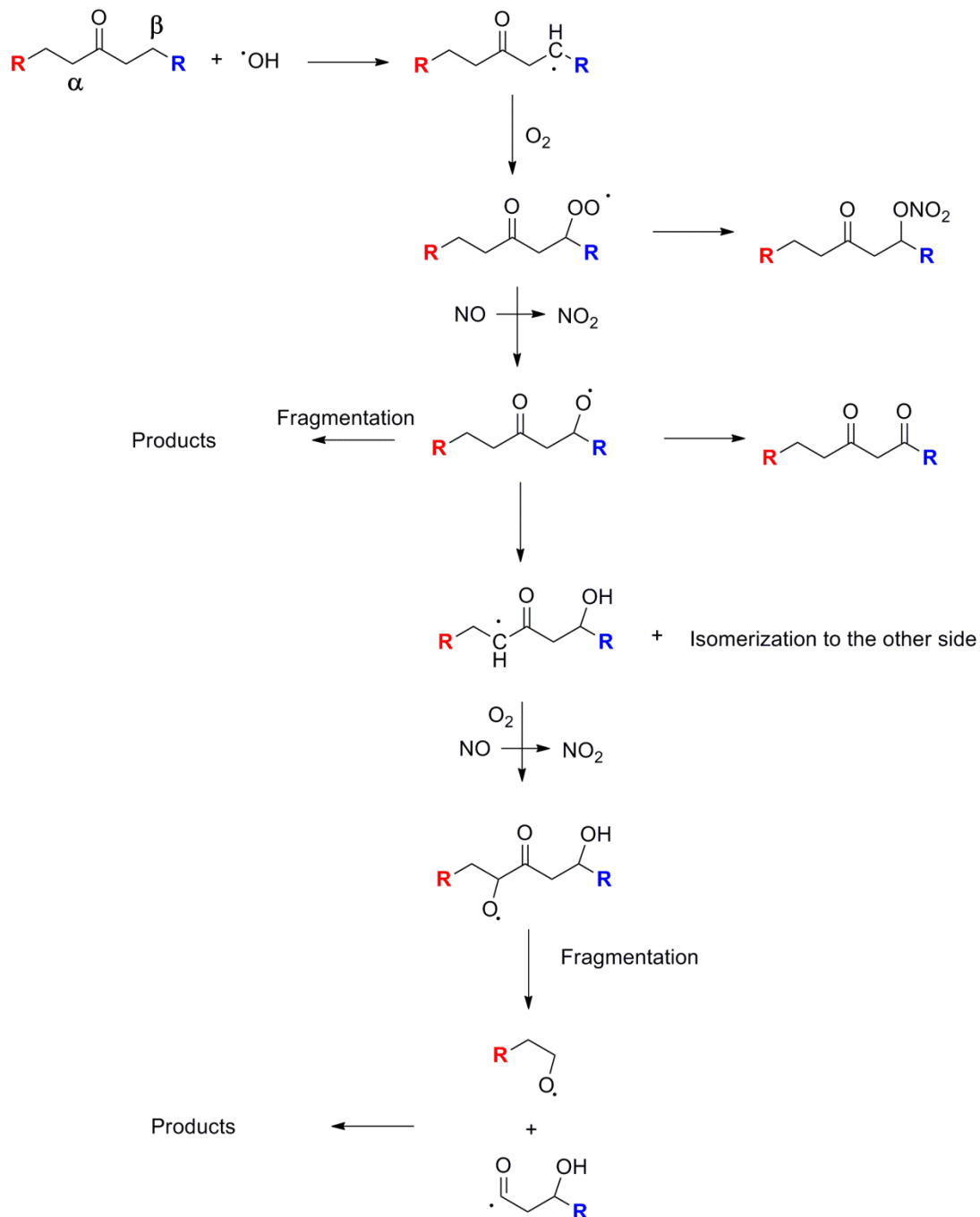


Figure 3.7. A partial high- NO_x OH-radical oxidation mechanism of 7-tridecanone, emphasizing the OH radical attack of the β -hydrogens. Figure N in the Appendices shows evidence of *n*-hexanal formation from the OH radical oxidation of 7-tridecanone at high NO_x .

The consequence of having a ketone functional group in the center versus the side can be seen in Figure 3.4. Fragmenting a molecule in the center divides it into two higher vapor-pressure product molecules, which suppresses SOA formation. It is clear in Figure 3.4 that 2-tridecanone is more efficient at forming SOA, as expected. However, it is somewhat surprising that the 2-tridecanone SOA yields are as low as they are. This could be due to photolysis of the oxidation products, given that Presto et al., 2005 [97] has shown that UV lights can have an important suppression effect on SOA formation, but this requires further investigation.

3.4.4 *n*-Nonadecane, *n*-Heptadecanal and *cis*-Pinonic Acid

The less volatile sequence follows a similar pattern as the more volatile sequence, as shown in Figure 3.5. *n*-Nonadecane has significantly higher SOA mass yields than *n*-heptadecanal. The aldehyde again presents lower SOA mass yields due to higher fragmentation. It is not obvious that this should be so. As an *n*-aldehyde becomes as large as *n*-heptadecane, its reactivity and SOA yields might resemble that of an *n*-alkane of comparable volatility rather than smaller aldehydes, simply because the long carbon backbone and not the aldehydic moiety would become the principal site of OH attack [92]. Furthermore, a molecule as large as *n*-heptadecane might have a slightly different oxidation mechanism than smaller *n*-aldehydes (<C₁₁), even if the aldehydic moiety plays a role. For example, alkoxy radicals formed on the carbon backbone of *n*-heptadecanal are more likely to isomerize towards the aldehydic functionality, promoting fragmentation. This path was proposed by Jenkin et al., 2000 [63], where an acyl-oxy radical formed from the ozonolysis of α -pinene attacks an internal aldehydic moiety. However, we do not have direct evidence to support this proposed pathway. Another reason for the relatively low SOA yields from *n*-heptadecanal could be higher photolysis rates for the reaction products, compared to *n*-nonadecane.

As mentioned before, we did not present SOA mass yields for *cis*-pinonic acid in Figure 3.5 because of difficulty measuring the *cis*-pinonic acid concentration. Nonetheless, based on injected quantities, yields appeared to be higher than the similar vapor pressure aldehyde but lower than the respective *n*-alkane. The probable strength of the SOA yields from *cis*-pinonic acid is related to its cyclic structure. The first-generation OH radical attack favors two of the tertiary-carbons and the secondary-carbon placed in the cycle. Even if an intermediate alkoxy radical is able to create a carbon-carbon scission, only one product is formed instead of two of higher-volatility.

3.5 Environmental Significance

Understanding how SOA formation capability evolves through the full oxidation sequence of organics in the atmosphere is critical in order to improve predictions of ambient SOA formation and evolution. Most chemical transport models (CTMs) under-predict the concentrations of organic aerosol [101, 102]. This may be due to the lack of multi-generation oxidation mechanisms in CTMs. In this paper, we have systematically explored the oxidation of different molecules that are proxies for first-generation oxidation products. From *n*-pentadecane, *n*-tridecanal, 2-, 7-tridecanone and pinonaldehyde to *n*-nonadecane, *n*-heptadecanal and *cis*-pinonic acid, we noticed a higher susceptibility for more oxidized molecules to fragment more easily than less oxidized species of similar vapor pressures, based on SOA mass yields. However, neither oxidation state nor O:C is enough to predict the ability of a species to produce SOA. All oxidized organics produce less SOA than *n*-alkanes of similar vapor pressures, but there are specific moieties – such as aldehydes under high-NO_x conditions – that can fragment efficiently in the first generation of the OH radical attack. The presence of these moieties, rather than O:C in general, appears to be important to SOA formation.

Our major conclusion is that even though carbon backbones become more susceptible to fragmentation as they age, that aging can still add substantially to organic aerosol formation. While more oxidized molecules are more likely to fragment, they will also contribute significantly to organic aerosol formation. For example, pinonaldehyde, a major product of α -pinene, has SOA yields very similar to those of α -pinene itself [103]. *cis*-Pinonic acid also has substantial yields. It is critical to understand the contribution of SOA from aging mechanisms and implement them in CTMs in order to better predict organic aerosol levels and properties. This work represents the beginning of that process – it does not include highly oxidized species and makes no conclusions with regards to the heterogeneous oxidation of such species. Ultimately, we hope to be able to select key model species throughout the 2D space shown in Figure 3.2 in order to constrain the full kinetics and mechanisms of organic-aerosol evolution caused by gas-phase photo-oxidation.

Acknowledgments

This research was supported by the Electric Power Research Institute grant EPP25369C12290 and the EPA STAR program through the National Center for Environmental Research (NCER). This paper has not been subject to EPA's required peer and policy review, and therefore does not necessarily reflect the views of the Agency. No official endorsement should be inferred.

Chapter 4 – Photo-oxidation of pinonaldehyde at low NO_x: from chemistry to organic aerosol formation

Abstract

Pinonaldehyde oxidation by OH radicals under low-NO_x conditions produces significant secondary organic aerosol (SOA) mass yields. Under concurrent UV illumination, mass yields are lower than high-NO_x yields published earlier by our group. However, when OH radicals are produced via dark ozonolysis the SOA mass yields are comparable at high and low NO_x. Because pinonaldehyde is a major first-generation gas-phase product of α -pinene oxidation by either ozone or OH radicals, its potential to form SOA serves as a molecular counterpoint to bulk SOA aging experiments involving SOA formed from α -pinene. Both the general tendency for aging reactions to produce more SOA and the sensitivity of the low-NO_x products to UV photolysis observed in the bulk clearly occur for this single species as well. Photochemical oxidation of pinonaldehyde and analogous first-generation terpene oxidation products are potentially a significant source of additional SOA in biogenically influenced air masses.

4.1 Introduction

Organic aerosols are dynamic in part because the organic compounds that comprise it can undergo multiple generations of oxidation in the atmosphere. At each step, the reaction products will depend on ambient conditions, and yet most attention to date has focused on first-generation oxidation products. α -Pinene is the monoterpene with the highest estimated emissions [104], and pinonaldehyde is one of the highest yield yet most volatile products of α -pinene oxidation by ozone and OH radicals, with molar yields ranging from 20-25% [31, 32]. Pinonaldehyde is an excellent first-generation product to study because it can give insight into the chemistry and additional SOA formation potential of other products from monoterpene photo-oxidation. C_{10} -keto-aldehydes are one such example, since most have very similar chemical structures [33, 36, 105, 106]. There are also limited data on the chemistry of pinonaldehyde and chemically similar compounds in the literature [91], though we recently described SOA chemistry under high- NO_x conditions [107]. It is also important to explore its chemistry in low- NO_x conditions, given that products of biogenic species are concentrated in areas where NO_x concentrations are low [105, 108]. That is the focus here.

4.1.1 Pinonaldehyde as a key molecule

Due to the significant amount of non-methane hydrocarbon emissions in the form of monoterpenes [109], it is important to study their later-generation photo-oxidation products and their ongoing contributions to organic-aerosol formation. By doing so, we can develop a better understanding of photo-chemical aerosol aging, which we define as the continuous photochemistry of progressively oxidized material either as vapors or part of aerosols [3, 25, 85, 107]. Chemical Transport Models (CTMs) can benefit greatly by properly including SOA

formation from biogenic later-generation products, especially since there has been an underestimation of organic aerosol formation from computer simulations [110].

We concentrate on pinonaldehyde because of its high-yield formation as a product of α -pinene and its fast reactivity with the OH radical [91]. Its structure, presented in Figure 4.1, consists of a C_{10} -keto-aldehyde constructed around a substituted cyclobutane. Similar structures can be found in other products of oxidation from different monoterpenes, such as caronaldehyde and limononaldehyde, among others [35, 36, 111]. Pinonaldehyde can therefore give us an understanding of SOA formation potential from other similar first-generation products of biogenic nature. Because it is relatively volatile and prone to fragmentation, it is in some sense a worst-case example of aging chemistry; if pinonaldehyde produces substantial SOA under both high- and low- NO_x conditions, it is extremely likely that many other less volatile first-generation α -pinene oxidation products will be as or more effective as sources of additional SOA.

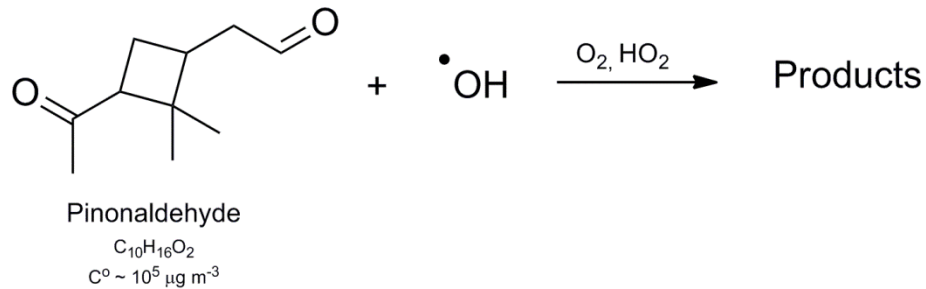


Figure 4.1. Pinonaldehyde ($C_{10}H_{16}O_2$) is a C_{10} -keto-aldehyde structure with a characteristic cyclobutane. Similar structures can be found in other products of photo-oxidation from different monoterpenes. It is a highly reactive molecule, with an OH-radical lifetime in the order of hours.

4.1.2 Chemistry of aldehydes under low- NO_x conditions

$\text{OH} + \text{hydrocarbon}$ chemistry at low NO_x is very different than at high NO_x . Notable differences are the absence of organic nitrate (R-ONO_2) formation at low NO_x and the strong production of hydroperoxides (ROOH) [9, 34, 112]. Evidence of ROOH formation has been presented by Docherty et al., [113] as well by Maksymiuk et al., [114] in 2D-NMR samples of terpene ozonolysis products, absent of NO_x

The aldehydic hydrogen is the most reactive site in the pinonaldehyde molecule when attacked by the OH radical [23, 92]. According to structure-reactivity relationships from Kwok and Atkinson, [42], OH attacks the aldehydic hydrogen $\sim 79\%$ of the time versus $\sim 21\%$ in the rest of the molecule. Figure 4.2 presents a simplified reaction path of a generic aldehyde + OH . When aldehydes are attacked by the OH radical, an acyl-hydroperoxide (RC(O)OOH ; blue structure, Figure 4.2), also called peroxyacid, can be formed [115-117]. Photolysis can then play an important role, however, breaking the acyl-hydroperoxide into an acyl-oxy radical (green structure, Figure 4.2), which can also be formed from $\text{R(O)OO} + \text{RO}_2$.

The important characteristic of aldehyde + OH photo-oxidation, in the presence or absence of NO_x , is that it systematically forms first-generation products with one fewer carbon atoms. Under high- NO_x conditions *n*-aldehyde SOA mass yields are significantly smaller than yields from a similar vapor pressure *n*-alkane [92]; yields are close to those for a much more volatile *n*-alkane with 1 carbon less than the aldehyde. It is one of our objectives to understand the importance of this fragmentation path under low- NO_x conditions.

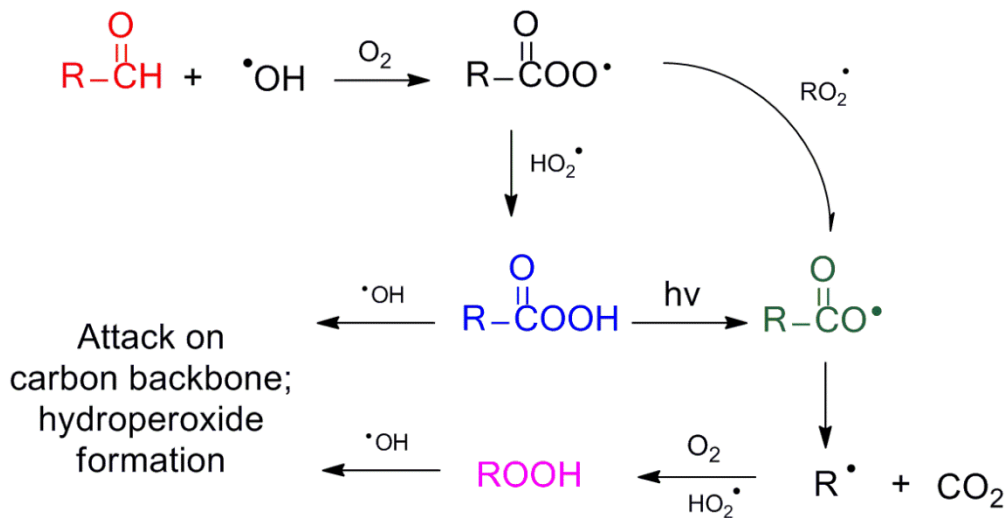


Figure 4.2. A simplified aldehyde + OH radical chemical-path in the absence of NO_x. After the aldehyde (red structure) is attacked, an acyl-peroxy radical is formed. In the absence of NO_x, the acyl-peroxy radical forms a peroxyacid (blue structure) or an acyl-oxy radical (green structure) when reacting with HO₂ or RO₂, respectively. The acyl-oxy radical decomposes quickly, losing one carbon.

4.1.3 Objectives

Our goals are to (a) present SOA mass yields under low-NO_x conditions for pinonaldehyde over an atmospherically relevant range of organic aerosol concentrations (C_{OA}) and compare results to those of *n*-tridecanal and α -pinene for similar conditions, (b) understand the difference in SOA mass yields for pinonaldehyde between low- and high-NO_x conditions, and (c) determine whether first-generation products of biogenic photo-oxidation (such as pinonaldehyde) are significant additional contributors of SOA.

Comparison of *n*-tridecanal and pinonaldehyde gives us insight into the aldehydic moiety and its ability to form SOA under different concentrations of NO_x. α -Pinene and pinonaldehyde yields are compared to infer how much SOA is formed by first-generation products. We also determine SOA mass yields of pinonaldehyde in the dark, using tetramethylethylene (TME) + O₃

as a source of OH radical. A dark experiment allows us to determine the effect of UV lights on pinonaldehyde photo-oxidation.

4.2 Experimental

The experiments are conducted in the Carnegie Mellon University smog-chamber. The details of experimental procedures are described elsewhere [65]. The FEP Teflon (Welch Fluorocarbon) chamber has a volume capacity between 10 and 12 m³. The bag is suspended inside a temperature-controlled room, which is held at 295 K for all experiments described here. The experiments are conducted under low-NO_x conditions (< 10 ppb). Particle number and size distributions are monitored with a scanning mobility particle sizer (SMPS) operating in recirculation mode (TSI classifier model 3080, CPC model 3772 or 3010, 15 - 700 nm D_p). The concentrations of the gas-phase organic species are monitored with a unit mass-resolution proton transfer reaction-mass spectrometer (PTR-MS, Ionicon GmbH). For each experiment, hydrogen peroxide (H₂O₂, Sigma Aldrich, 50/50 in water) photolysis is used to create OH radicals, and the relative humidity is kept under ~20%. Ammonium sulfate particles (Sigma Aldrich, 99.99%) are used as inert seeds for condensation of low-volatility organic oxidation products. These are formed from an aqueous solution with a nebulizer (TSI 3075), then dried and neutralized. We use seed concentrations of ~10⁴ particles cm⁻³ with mass in the range of ~10 to 20 µg m⁻³. The organic species used are *n*-tridecanal (Alfa Aesar, 94%), pinonaldehyde (synthesized in Carnegie Mellon Laboratory, ~85%), and α-pinene (Sigma Aldrich, >99%). These molecules are all used without further purification. UV lights (General Electric 10526 black lights) with a $J_{NO_2} < 0.06 \text{ min}^{-1}$ are used for initiation and during photo-oxidation after all the components are mixed in the chamber. For dark experiments, tetratmethylethylene (TME, Aldrich, 99%) ozonolysis was performed as a source of OH radicals [118].

4.2.1 SOA Mass Yields and Wall Loss Calculations

This topic is approached for the first time in Chapter 2 and 3, sections 2.2.2 and 3.2.2 and reviewed in here. The SOA mass yield from a chemical precursor is calculated as the ratio of organic aerosol mass formed divided by the mass of precursor consumed [12],

$$Y = \frac{C_{OA}}{\Delta C_{precursor}} \quad (2.4)$$

C_{OA} is the organic aerosol mass formed, and $\Delta C_{precursor}$ is the mass of the precursor organic species consumed while forming C_{OA} and other, gas-phase products. We determined SOA mass yields for the different organic precursors based on volume growth of organic aerosol, measured with the SMPS, during each oxidation experiment.

Because Eq. 2.4 is a mass balance, one must account for organic aerosol mass losses during an experiment – especially wall losses. Suspended particles can deposit to the chamber walls, and condensable organic vapors can either condense onto those deposited particles, or they can be lost to the chamber walls. Here we assume that condensable vapors interact with particles deposited on the chamber walls, and that the mass growth of those deposited particles follows that of the suspended particles. In this case the total SOA production (C_{OA}) is determined by using the ratio of suspended organic aerosol (C_{OA}^{sus}) to suspended ammonium sulfate (C_{seed}^{sus}) and the initial concentration of ammonium sulfate C_{seed}^{sus} ($t = 0$), as described by Hildebrandt et al. [65]:

$$C_{OA}(t) = \frac{C_{OA}^{sus}(t)}{C_{seed}^{sus}(t)} C_{seed}^{sus}(t = 0) \quad (2.5)$$

$C_{seed}^{sus}(t)$ is obtained by fitting an exponential decay to the ammonium sulfate volume concentration (measured with the SMPS and verified with a High Resolution-Aerosol Mass

Spectrometer) over the interval between seed injection (and mixing) in the chamber and the onset of photo-oxidation. Extrapolation of this signal after the photo-oxidation process starts defines the seed mass concentration as a function of time.

At time 0 (onset of photo-oxidation) and later, the difference between the total aerosol mass concentration in the chamber (measured with an SMPS) and the extrapolated ammonium sulfate mass concentration is considered $C_{OA}^{sus}(t)$. To obtain the total $C_{OA}(t)$ from the suspended mass concentration, we correct for wall losses, assuming that organic particles lost to the wall are in equilibrium with the suspended particles and vapor-phase species, and also that the organic to seed mass ratio remains the same for suspended and deposited particles. This is the upper-limit estimate for SOA production explained in Weitkamp et al., 2007 [67]. There is approximately a 20% difference in SOA mass yields for each species studied when assuming particles lost to the walls are in equilibrium with the suspended particles (upper limit) versus assuming that no further condensation occurs once particles have deposited (lower limit). This percentage has been observed in current and past experiments [92, 107]. The SOA mass yields in this work are presented using an aerosol density of unity ($1 \mu\text{g m}^{-3}$).

4.2.2 Measurement of reactants

The concentrations of reactants are monitored with a unit mass-resolution PTR-MS. The fragments used to track concentrations are those of the MW + 1 or MW + 1 – 18 (dehydrated form) for *n*-tridecanal, pinonaldehyde and α -pinene. The PTR-MS sensitivity at these fragment masses was previously calibrated with those species. A key assumption is that interferences from other species were minimal.

We also use methanol as an OH radical tracer in all experiments. We measure it with the PTR-MS (at m/z 33) to determine the concentration of OH radicals during the experiments. OH concentrations and kinetic rate constants allow us to predict concentrations of the different precursors and compare with the initial decay of their respective MW + 1 or MW + 1 – 18 (dehydrated form). Methanol concentrations in all experiments are lower or equal to those of the precursor molecules, and methanol is also substantially less reactive with OH. Consequently the methanol has a minimal effect on the radical balance.

4.2.3 Synthesis of Pinonaldehyde

We synthesize pinonaldehyde following McMurry et al. [94], as it is not commercially available. Products are formed via ozonolysis in solution, as shown in Figure I in the Appendices. α -Pinene (Sigma Aldrich, >99%) is used as the parent reactant for pinonaldehyde. The synthesis starts with formation of the secondary ozonide, which is kept stable by maintaining a temperature of -78°C with a dry-ice ethanol slurry. After the ozonide is formed, dimethyl sulfide (DMS) is added to reduce the ozonide to pinonaldehyde. After adding DMS, the products are held at room temperature for about three hours, after which they are extracted with water to remove water-soluble contaminants. Finally, a simple distillation procedure vaporizes solvents and other volatile impurities. We use Nuclear Magnetic Resonance (^1H NMR, HSQC and Tocsy) to determine products and yields from the synthesis. The spectra are shown in the Appendices, Figures J to M.

4.3 Results

Following Odum et al. [12], we plot SOA mass yields vs. the organic aerosol concentration (C_{OA}). In all experiments presented here there was no evidence for precursor decay before the onset

of photochemistry and there was no evidence for delayed condensation of organic aerosol after the cessation of photochemistry. Both issues are important for the interpretation of accurate equilibrium mass yields. We observed no evidence of precursor wall losses, in contrast to the results presented in Matsunaga and Ziemann [95]. After injection into the smog chamber, precursor concentrations were monitored for about a half an hour before start of photo-oxidation with no evident decay. This is important because losses to the walls would suppress calculated SOA mass yields. The reproducibility and precision of the experiments can be observed in Figure 4.3.

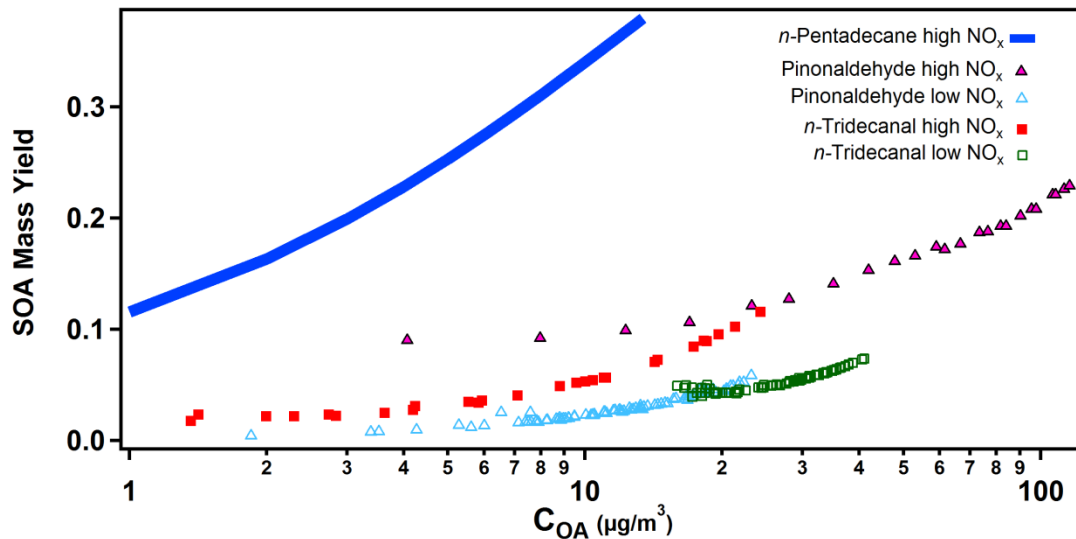


Figure 4.3. Pinonaldehyde and *n*-tridecanal SOA mass yields at high and low NO_x. The potential to form organic aerosol from pinonaldehyde + OH – and *n*-tridecanal – is less than that from *n*-pentadecane + OH under high and low NO_x. *n*-Pentadecane yields come from Presto et al. [72]. Pinonaldehyde (triangles) and *n*-tridecanal (squares), independent from NO_x concentration, suffer fragmentation paths in its first-generation chemistry that limits its SOA formation potential. *n*-Alkanes such as *n*-pentadecane do not experience significant fragmentation in their first-generation chemistry [59].

All experiments presented in this manuscript reached equilibrium between the organic aerosol-phase and the gas-phase within the experimental time frame. Specifically, particles grew rapidly during the first hour of each experiment due to the high OH radical concentration,

but after the first hour or two of photo-oxidation, the particles stopped growing. There was no evidence for any substantial delay in condensational growth that would be associated with a significant delay in equilibration. The median particle diameters were thus stable following completion of the oxidation chemistry, and so we conclude that the gas and condensed-phases were in equilibrium, as any disequilibrium would constitute a driving force for condensation (or evaporation). This is consistent with other experiments performed in our laboratories [96, 97]. Consequently, we believe that there were no substantial mass-transfer limitations during these experiments that would affect our conclusions regarding the competition between fragmentation, functionalization and accretion effects on SOA formation.

SOA mass yields for pinonaldehyde and *n*-tridecanal under high- and low-NO_x conditions are presented in Figure 4.3. In the same figure, a function from Presto et al., [72] for *n*-pentadecane (blue) SOA mass yield under high-NO_x is presented for comparison. Mass yields are plotted as a function of the organic-aerosol concentration because the products are semi-volatile. The equilibrium partitioning between the gas and condensed phases drives yields up with increasing loading, as described by Odum et al. [12]. *n*-Pentadecane, pinonaldehyde, and *n*-tridecanal have similar vapor pressures, making their SOA mass yield comparison instructive. Contrasting species of similar vapor pressure can provide information regarding chemical paths, more specifically the competition between fragmentation, functionalization and accretion [25, 107].

Because of the unusually high reactivity of the aldehydic moiety [23, 92] in the pinonaldehyde + OH reaction, it was important to compare with another aldehyde with similar vapor pressure – *n*-tridecanal. Low-NO_x yields for *n*-tridecanal for C_{OA} of < 15 $\mu\text{g m}^{-3}$ are not presented due to a high degree of uncertainty and noise. An important feature of Figure 4.3 is

the similarity between the yields of pinonaldehyde and *n*-tridecanal under low- and high-NO_x conditions, supporting our conclusion that the two aldehydes have comparable chemistry. For both of the aldehydes discussed here, high-NO_x conditions enhance SOA yields with respect to low NO_x. This is in marked contrast to first-generation SOA yields from monoterpene ozonolysis, where yields are significantly higher under low-NO_x conditions [73, 119, 120].

4.4 Discussion

We shall start with a comparison of various precursors in Figure 4.3, as this highlights the important similarities and differences of the chemistry.

4.4.1 Pinonaldehyde vs. *n*-tridecanal

The similarity at low NO_x between pinonaldehyde and *n*-tridecanal SOA yields can be explained by their similar first-generation chemistry and by the fact that both species possess similar vapor pressures ($\sim 10^5 \mu\text{g m}^{-3}$). This similarity has also been observed under high-NO_x levels [107], as shown in the Figure 4.3 as well. The aldehydic hydrogen drives most of the first-generation chemistry for both species by OH abstraction, and the functional groups formed in subsequent chemistry are likely to be similar as well. Because the aldehydic moiety dominates the initial chemistry, structural differences between *n*-tridecanal (straight chain) and pinonaldehyde (characteristic cyclo-butane and a carbonyl) are not sufficient to result in different SOA mass yields.

4.4.2 Pinonaldehyde vs. *n*-pentadecane

These two molecules have similar vapor pressures of about $\sim 10^5 \mu\text{g m}^{-3}$, but their chemistry is very different. *n*-Pentadecane, like many other large ($>\text{C}_7$) *n*-alkanes, goes through a similar

mechanistic path when reacting with the OH radical; this path has been studied extensively [23, 28, 59, 81]. The main feature of *n*-alkane first-generation chemistry is the efficient addition of oxygen to the carbon backbone by way of functionalization, mainly with carbonyls and alcohols, without suffering any major carbon-carbon fragmentation. This *n*-alkane mechanism results in products of much lower vapor pressure, enhancing SOA mass yields.

Aldehyde + OH chemistry is very different from that of *n*-alkanes. The first key difference is the high reactivity of the aldehydic hydrogen compared to $-\text{CH}_2-$ (methylene) groups in *n*-alkane carbon backbones. Consequently, most of the first-generation chemistry occurs by abstraction of the aldehydic hydrogen. According to Kwok and Atkinson [42], the first-generation attack from the OH radical on pinonaldehyde occurs $\sim 79\%$ of the time on the aldehydic hydrogen.

The OH attack on the aldehydic hydrogen leads to the eventual formation of an acyl-oxy radical (green structure, Figure 4.2) either in the presence or absence of NO_x . This acyl-oxy radical can fragment easily, yielding CO_2 and C_{n-1} products (species with one less carbon). Our main conclusion is that even though there are differences in the pinonaldehyde + OH chemistry in the presence or absence of NO_x , both mechanisms systematically fragment the aldehyde precursor. This systematic fragmentation happens rapidly, suppressing SOA mass yields when compared to those of *n*-pentadecane, as seen in Figure 4.3.

4.4.3 Pinonaldehyde: low and high NO_x

Even though both high- and low- NO_x pinonaldehyde experiments (Figure 4.3) show lower SOA yields compared to *n*-pentadecane, there is a difference between them. Pinonaldehyde photo-

oxidation at high NO_x results in higher SOA yields than at low NO_x . In order to understand this difference, it is important to distinguish between the products likely to be obtained in each case.

Major differences are the creation of hydroperoxides in the absence of NO_x and the formation of organic nitrates (mainly peroxyacetyl nitrates or PANs) when NO_x is abundant. These two moieties, when added to a carbon backbone, can reduce its vapor pressure by roughly a factor of 300 [43]. They are both exceptions to the rule that aldehyde oxidation results in loss of a carbon atom, as both moieties protect the terminal carbon. However, for pinonaldehyde the PAN or peroxide products are predicted to have saturation concentrations in the order of $300 \text{ }\mu\text{g m}^{-3}$; too large to directly produce SOA in these experiments.

A major difference is that hydroperoxides (especially peroxyacids) are sensitive to UV-light photolysis [97, 121, 122] when compared to organic nitrates. When photolysis of a hydroperoxide bond occurs, an alkoxy radical is formed, which has the ability to fragment a C-C bond. Such fragmentation can increase the vapor pressure of products when compared to the products of high- NO_x chemistry. In order to test the effect of photolysis on SOA formation potential for pinonaldehyde photo-oxidation, an experiment was performed under low- NO_x conditions in the dark. A tetramethylethylene (TME) + O_3 reaction was used as a dark source of OH radical without introducing NO_x . The experimental details of TME + O_3 as a dark source of OH radical are explained in Lambe et al. [118]; TME + O_3 products do not contribute to SOA [123].

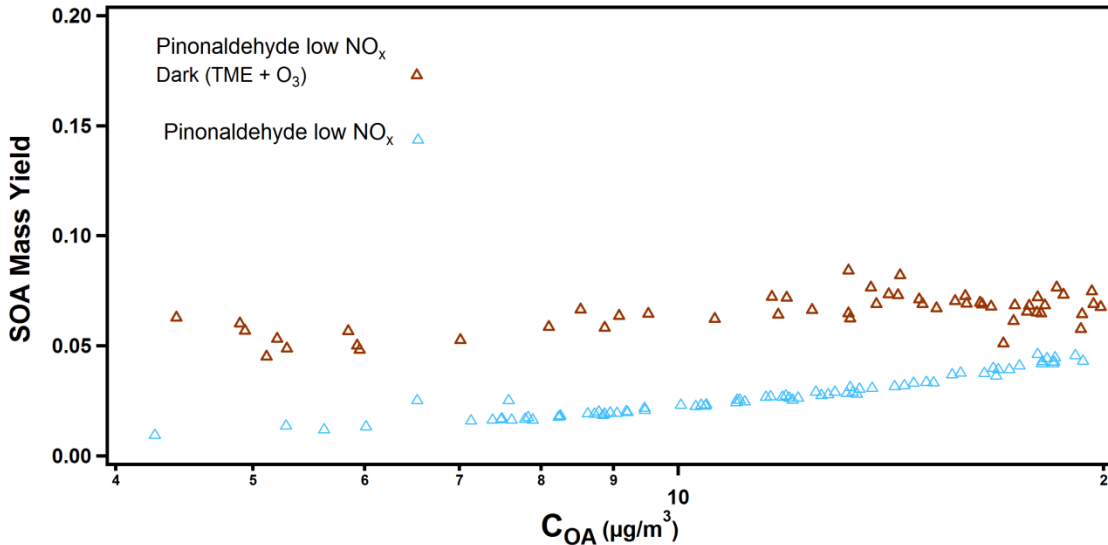


Figure 4.4. Comparison between SOA mass yields of pinonaldehyde in the absence (brown) and presence (blue) of UV light, under low NO_x. In order to understand if the difference in pinonaldehyde SOA yields between low and high NO_x is due to photolysis of hydroperoxides and subsequent fragmentation, an experiment in the dark is performed. The dark experiment (no UV light) produces more SOA than the one where the oxidation reaction is exposed to UV lights. We can infer that UV light is responsible for fragmentation paths, and it is likely that the fragmentation happens on hydroperoxide moieties since the experiments are performed under low NO_x.

Figure 4.4 shows that low-NO_x pinonaldehyde SOA mass yields are higher in the dark than in the presence of ~350 nm UV light from our black lights [97, 122]. The difference in SOA mass yields between light and dark experiments is approximately 0.04 absolute yield units, and the dark, low-NO_x yields are similar to the (illuminated) high-NO_x yields. A similar yield suppression by UV light was reported in Presto et al. [97] for α -pinene ozonolysis, and recently Henry and Donahue [122] reported significant loss of later-generation low-NO_x SOA from α -pinene in the presence of the same UV lights [122]. The yield disparity shown here supports the hypothesis that hydroperoxide photolysis forms alkoxy radicals that can fragment carbon-carbon bonds, creating products of higher volatility.

4.4.4 α -Pinene and Pinonaldehyde

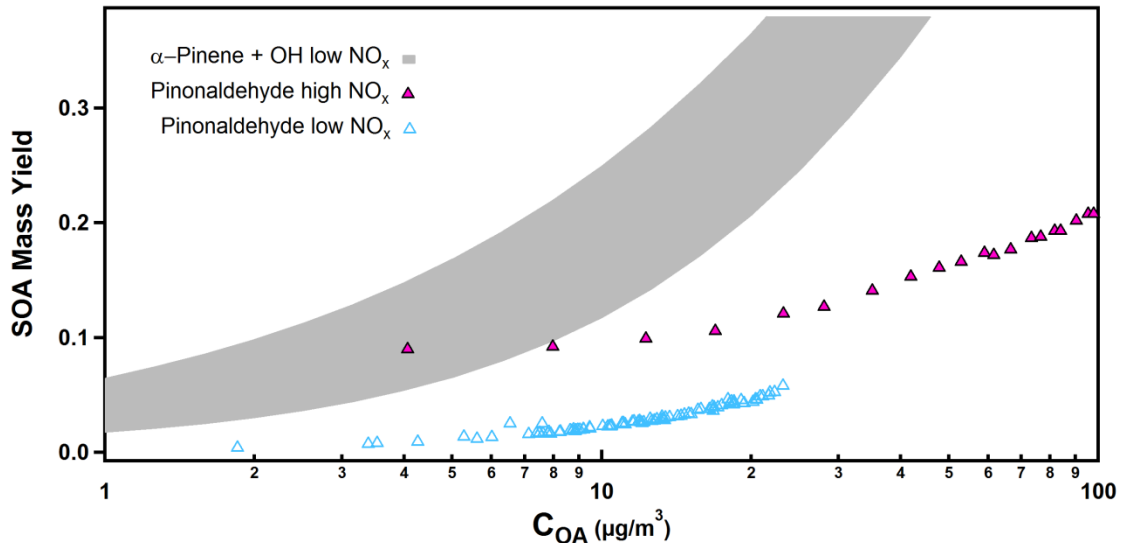


Figure 4.5. Pinonaldehyde SOA yields in the context of α -pinene SOA yields. As a first-generation product from α -pinene + OH, pinonaldehyde can form SOA at lower yields than α -pinene itself. Nonetheless, the yields of pinonaldehyde, including low NO_x , are significant and higher than zero. This figure shows how later-generation species from α -pinene photo-oxidation are capable of forming SOA, making atmospheric chemical aging an important source of SOA.

Figure 4.5 compares pinonaldehyde SOA yields to those from its parent molecule, α -pinene. This figure shows the importance of atmospheric chemical aging. It is clear that first-generation products such as pinonaldehyde are able to contribute to organic aerosol [122, 124]. Pinonaldehyde yields, both under high and low- NO_x conditions, are significant when compared to those of α -pinene + OH [125]. High- NO_x yields [107] are comparable to α -pinene, but even low- NO_x illuminated conditions result in yields that are discernibly higher than zero (almost 1/4 of α -pinene yields). This shows the importance of atmospheric chemical aging to organic aerosol formation. If a first-generation product from α -pinene + OH is able to produce significant SOA, it is likely that later-generation ones have also the potential to contribute to organic aerosol formation. This is especially important because organic aerosol material can last

for about a week in the atmosphere [82, 126], giving it sufficient time to add oxygens to carbon backbones, increasing total organic aerosol mass.

4.5 Environmental Significance and Conclusions

Atmospheric chemical aging mechanisms are challenging to understand due to their dynamic nature, but studying first-generation products can give us insight. Pinonaldehyde is able to form SOA under low- NO_x conditions, though less effectively than under high- NO_x conditions. This is especially important given that the pinonaldehyde + OH mechanism goes through a strong fragmentation path in its first-generation chemistry. The ability of pinonaldehyde to form organic aerosol shows that volatile products from α -pinene photo-oxidation can contribute to SOA, making a case for the importance of biogenic chemical aging. This is especially true since many monoterpene + OH products share similar chemical structures. Oxidation products from many terpenes are similar, and the current results hold for both pinonaldehyde and *n*-tridecanal, which are structurally quite different. Consequently, we are confident extrapolating our conclusions to terpenes as a whole.

SOA yields from pinonaldehyde + OH under UV light are lower at low NO_x than at high NO_x . This suppression can be explained by the susceptibility of hydroperoxides and peroxyacids – formed under low- NO_x conditions – to fragment, creating products of higher volatility. Strong evidence of this susceptibility to fragment in the presence of UV light was shown by performing an experiment in the dark, which produced more organic aerosol and higher yields.

In order to improve our understanding of atmospheric chemical aging from biogenic material, many more chemical species should be studied, especially later-generation products of monoterpene photo-oxidation. Studying the effect of NO_x and UV light on SOA formation is also

important in order to understand the susceptibility of hydroperoxides and peroxyacids to fragment and suppress SOA yields in systems other than pinonaldehyde. Species from monoterpene oxidation with carboxylic acid functionality, such as *cis*-pinonic acid, should be studied in detail due to the ubiquity of such a moiety [85].

Acknowledgments

This research is supported by NSF grant AGS1136479. NMR instrumentation at Carnegie Mellon is partially supported by NSF grants CHE-0130903 and CHE-1039870.

Chapter 5 – Simulations of smog-chamber experiments using the two-dimensional volatility basis set and GECKO-A: linear oxygenated precursors

Abstract

We use a two-dimensional volatility basis set (2D-VBS) box model and an explicit chemical model (the Generator for Explicit Chemistry and Kinetics of Organics in the atmosphere or GECKO-A) to simulate SOA mass yields of linear molecules. They are: *n*-pentadecane, *n*-tridecanal, 2-, 7-tridecanone, 2- and 7-tridecanol, *n*-heptdecanal and *n*-nonadecane. A 2D-VBS hybrid model with explicit treatment of first-generation products followed by a generic 2D-VBS mechanism and GECKO-A resulted in acceptable model-measurement agreement for all species. This was despite the different approaches from both simulations, where the 2D-VBS considers average chemistry and GECKO-A explicit mechanisms.

5.1 Introduction

Chemical transport models (CTMs) predict organic aerosol mass and its time evolution in an atmospheric context [5, 127]. Current three-dimensional CTMs, such as the community multiscale air quality [101, 102, 128] (CMAQ) and the comprehensive air quality model [129, 130] (CAMx), have continuously improved in the last decade regarding their predictions of

particulate matter concentration (PM_{2.5}). Nonetheless, there are still important aspects that need to be incorporated into models to achieve more accurate predictions.

An important process not widely implemented in CTMs is continuous chemical aging of organic aerosol [3]. The typical residence time for a particle in the atmosphere is about a week [82, 126], which is sufficient time for molecules to experience multiple generations of oxidation that can affect concentrations and composition of organic aerosol [85]. Aging mechanisms have been implemented in some models such as the one presented in Carlton et al. [110]. Also, Lane et al. [131], Murphy and Pandis, [127] and Murphy et al. [132] included multiple generations of chemical aging mechanisms. Additionally, they showed that it is important to understand how the organic material contributes to particulate matter (PM) as it ages; specifically how fragmentation and functionalization paths compete in chemical aging mechanisms [9, 54, 107]. Accurate aging mechanisms may lead to better descriptions of total organic-aerosol levels, but they may also permit better prediction of other properties such as the organic mass to organic carbon (OM to OC) ratio and water solubility. This can be critical for accurate comparison with existing measurement networks that provide data on, for example, OC levels but not OM, or water-soluble organic carbon (WSOC).

A general challenge for models of organic-aerosol chemistry is the enormous number of chemical species comprising the aerosol [4, 7]. Models require some form of lumping, either representing the organics with a few surrogate molecules whose chemistry and phase partitioning can be described explicitly [133], or representing condensable organics with pseudo species characterized solely by their relevant physical properties (e.g. volatility) [10, 12]. The lumping mechanisms based on pseudo species are generally constrained by smog-chamber SOA formation experiments, and so the resulting parameterizations will represent the phase

partitioning of the experimental conditions. Subsequent chemical evolution, or aging, is not straightforward to model without additional information [10].

The two-dimensional volatility basis set (2D-VBS) framework [37, 38] is a powerful prognostic tool for secondary organic aerosol (SOA) evolution [132]. The two dimensions are volatility and oxygenation, and so the framework directly describes both OM and OC. A key hypothesis is that the ensemble of molecules found in the atmosphere with a given volatility and degree of oxidation (i.e. one lumped species in the 2D-VBS) will have a common average chemical behavior. It considers continuous chemical aging and includes fragmentation and functionalization paths as the aging occurs [3, 124]. It is our intention to use the 2D-VBS as a prognostic tool of SOA production in this chapter.

Another approach to consider in this chapter for chemical-aging mechanisms is keeping track of every single molecule involved in a system with its thermodynamic properties. Because of improvements in computational power nowadays as compared to a couple of decades ago, a very detailed approach with every single reaction scheme can be generated. Tens of thousands of molecules can be tracked. This approach requires a very detailed algorithm of instructions and a very large database that contains information about chemical reactions and physico-chemical properties for all species. Aumont and co-workers have developed a Generator (computer simulation) with the previous general properties mentioned named the Generator for Explicit Chemistry and Kinetics of Organics in the Atmosphere (GECKO-A)[39]. This Generator complements the two-dimensional volatility basis set (2D-VBS) [3, 37, 38] mentioned in the previous paragraph. It is also our intention in this chapter to use GECKO-A as a prognostic tool of SOA mass yields and compare with the 2D-VBS.

Objectives of this work. The goal of this work is to use two different simulations as prognostic tools of SOA mass yields of linear oxygenated species. The two simulations are the 2D-VBS box model and GECKO-A with average and explicit chemistry treatment, respectively. The experimental data to use for comparison will be SOA production and mass yields from smog-chamber experiments presented in Chapters 2, 3 and in Chacon-Madrid et al. [92], Presto et al. [72] and Chacon-Madrid and Donahue [107]. The species for the 2D-VBS include: *n*-pentadecane, *n*-tridecanal, 2- and 7-tridecanone, 2- and 7-tridecanol. For GECKO-A we also include *n*-heptadecanal and *n*-nonadecane. The oxygenated species are models for first-generation products of hydrocarbons such as *n*-pentadecane, so we are “walking through” an oxidation mechanism by studying later-generation products one by one.

The 2D-VBS box model will be prescribed the first-generation product distribution from known chemical mechanisms as it lacks explicit chemistry. This will help in making a difference between species that have functional groups in different parts of the carbon backbone (e.g. 2- and 7-tridecanone, refer to Chapter 3).

5.1.1 The Two-Dimensional-Volatility Basis Set (2D-VBS) framework as a prognostic tool.

The details of the 2D-VBS are explained elsewhere [3, 37, 38, 124]; however, we will review a few key points.

The 2D-VBS is a discretized version of a two-dimensional space in which organic compounds are characterized by their saturation concentration (C^* in $\mu\text{g m}^{-3}$) and degree of oxidation – here O:C (molar ratio of oxygen to carbon atoms). The 2D-VBS box model predicts chemical aging of bulk organic aerosol, capturing average chemical behavior. Similar frameworks have been developed [4, 134], but the unique attribute of the 2D-VBS is that

volatility (C^*) is an attribute of the lumped species rather than being calculated from other properties [124]. The chemical mechanism in the 2D-VBS describes how material from one bin (a specific C^* , O:C pair) is transformed after reaction – with OH radicals here – into products in a number of other bins. The 2D-VBS tracks and conserves carbon, so with known C:H:O it separately accounts for OC and OM. The nominal formula ($C_xH_yO_z$) of a given bin is reasonably constrained [37], but the specific structure, branching, location of functional groups, etc., is not just unknown, it is assumed to be a diverse mixture of different structural and functional isomers and analogues. Thus, the transformations in a 2D-VBS mechanism represent the average behavior of these isomers. This complements fully explicit models like the Generator for Explicit Chemistry and Kinetics of Organics in the Atmosphere (GECKO-A) that includes schemes with every compound and chemical reaction, potentially numbering 10,000 or more [39-41]. We will expand on GECKO-A in the next section.

The 2D-VBS splits an oxidation process into two pathways: functionalization and fragmentation [3, 132]. Functionalization refers to reactions that add oxygenated functionality to the carbon backbone without breaking it. Fragmentation refers to reactions that do break the carbon backbone. Typically at least one fragment is also a radical that adds new oxygenated functional groups. The functionalization scheme assumes that one generation of oxidation results in products with C^* lowered by between 1 and 6 decades (mostly 2 to 4), and 1 to 3 added oxygens. The fragmentation scheme assumes that C-C bonds cleave at a random position (on average). Fragmentation thus disperses products over a wide C^* and O:C range. We use O:C to determine the branching ratio (β) between fragmentation and functionalization, with $\beta = (O:C)^{1/6}$ [3]. At an O:C = 0.5, $\beta = 0.89$; which means that ~89 % of carbon mass will fragment, moving most products into higher volatility bins. The total organic aerosol mass (C_{OA}) is determined iteratively based on equilibrium partitioning [10].

Heterogeneous oxidation of OA by the OH radical is also considered; however, it is done with an effective rate constant that is an order of magnitude slower than gas-phase kinetics. Diffusion limitations make heterogeneous oxidation a factor of 5-10 slower than analogous homogenous oxidation [135]. Heterogeneous uptake has a minimal influence on the results shown here.

The 2D-VBS mechanism is designed to describe the *average* behavior of organics, based on the assumption that oxidation of even one large precursor will rapidly lead to a very diverse set of product molecules, not to mention mixtures of precursors in the atmosphere. However, when considering OA formation from individual reactant molecules, it does not distinguish between functional-group and structural isomers. For example, functional-group isomers such as *n*-tridecanal and 2-tridecanone are both photo-oxidized exactly in the same way independently of which one is fragmented more in its first-generation chemistry [107]. Also, structural isomers like 2- and 7-tridecanone (or 2- and 7-tridecanol) would be treated equally.

We hypothesize that by describing the first-generation chemistry of such isomers, either functional-group or structural, and subsequently use the 2D-VBS box model, we can predict OA adequately.

5.1.2 Generator for Explicit Chemistry and Kinetics of Organics in the Atmosphere (GECKO-A).

The details of GECKO-A are explained in detail in Aumont et al., [39] and Camredon et al., [40]; however, we will comment on general features of the Generator. Even though Aumont et al., [39] and Camredon et al., [40] concentrated on smaller species (< C₈), recently Valorso et al., [41] used GECKO-A to simulate α -pinene (C₁₀) photo-oxidation experiments presented by Ng et al. [120]. The Generator bases its schemes for chemical-mechanisms on well-established reaction paths – e.g. Atkinson, [28]; Atkinson and Arey, [23]; Lim and Ziemann, [59]. Published

kinetic rate constants are used when available – for example, those available in Atkinson and Arey [23] – and in the cases they are not available, structure reactivity relationships like the ones from Kwok and Atkinson [42] are used to estimate these missing parameters. Gas/particle partitioning of the different species is utilized assuming a basic thermodynamic process of absorption [11]. Vapor pressures of species are determined using different structure activity relationships [43, 136, 137]. In this work we will use structure activity relationships from Nannoolal et al., [137] as it is believed to provide the best vapor pressure estimates according to the Barley and McFiggans [138] study.

Because we will present simulations of large species ($\geq C_{13}$), it is important to mention other specific aspects of GECKO-A. Since explicit chemical schemes for such species are very large and far beyond computational limits, systematic reduction methods are used in GECKO-A: (i) gas-phase chemistry for non-volatile species – vapor pressures below 10^{-13} atm or approximately $10^{-3} \mu\text{g m}^{-3}$ – is not considered from the scheme, and (ii) generated chemical schemes are reduced using a lumping method. This method consists on substitution of one species by another if they are position isomers; this lowers the amount of species in the chemical schemes, hence the computational power needed.

5.2 Methods and Simulations

5.2.1 The 2D-VBS.

The photoxidative degradation of each reactant is simulated with the 2D-VBS box model twice. In the first case, there is no explicit first-generation chemistry included in the simulation. In the second case, the first step of chemistry is treated explicitly. The first generation of each simulation is illustrated in a 1D-VBS format in Figure 5.1 for each precursor molecule studied here, as well as in more detail in the Appendices (Figs. O and P). The default VBS products are

shown in gray and the explicit ones in red. In each case the first-generation products are subsequently aged with the default 2D-VBS mechanism. We can thus test whether explicit treatment of the first-generation chemistry improves 2D-VBS performance but also whether the generic mechanism used for later-generation aging performs well.

We do not fit the 1st generation. Rather, the explicit 1st-generation products are based on known hydrocarbon + OH chemistry [23, 28, 59]. The stoichiometry of the products come from the expected first-generation attacks on the different sites of the reactant molecule predicted by structure reactivity relationships (Appendices, Fig. P) [42]; products of fragmentation are expected to come from OH attack on α -carbons (side-carbons to functional group) and also from attack on carbons where the alkoxy radicals can isomerize by 1,5-hydrogen-shift towards the α -carbons. We present an example of this chemistry path in Figure 3.7, Chapter 3; also *n*-tridecanal chemistry is presented in Figure 2.1, Chapter 2. The decay of the parent-reactant for the computer simulations – for both cases in Figure 5.1 – is obtained from experimental data; this decay trace is also used to determine OH radical concentrations in the system.

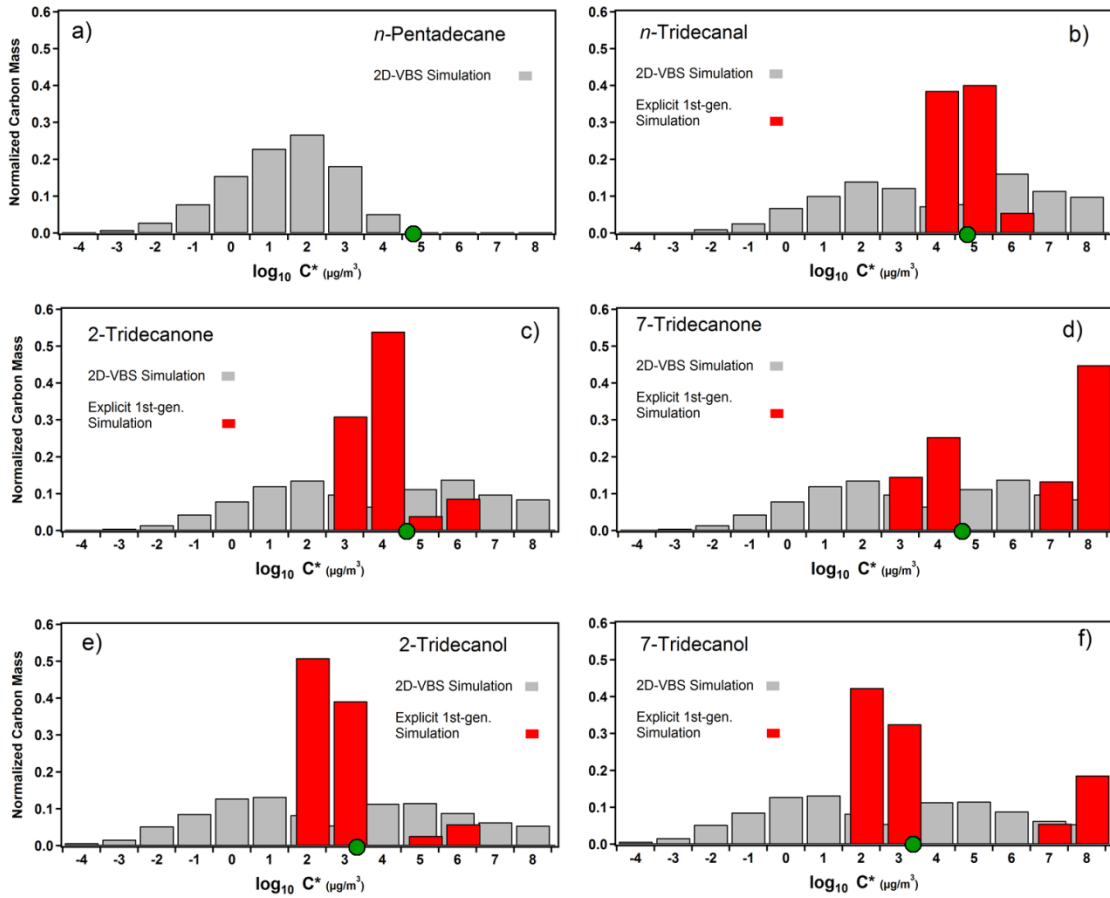


Figure 5.1. Product volatility distribution of generic 2D-VBS (gray) vs. explicit 1st-generation treatments (red) for different precursors (volatility indicated with a green circle – ●). The red bars are slightly offset to reveal gray bars behind. These panels show the product distribution volatility of the expected first-generation products of OH oxidation for two different cases. The first case is the 2D-VBS Simulation; this distribution is obtained from the average chemistry implied by the box model for bulk organic material [3, 124]. The second case – explicit 1st-gen. – presents a distribution that is obtained from the literature hydrocarbon + OH chemistry for individual molecules [23, 28, 59]. The main reason for the differences between both cases is that the 2D-VBS considers average chemistry of bulk organic material which is quite different from that of linear mono-oxygenated molecules. However, we believe that after establishing only the first-generation, the 2D-VBS box model can acceptably predict experimental SOA mass yields. *n*-Pentadecane does not suffer strong fragmentation paths in its first-generation chemistry, this is why we only present its product-distribution from the 2D-VBS [59].

The first-generation products are presented in Figure P in the Appendices and also as red bars in Figure 5.1. The red species in Figure P represent products of fragmentation paths, and the blue species those of functionalization. The stoichiometry has been rounded to the closest 0.05 due

to the uncertainty in structure reactivity relationships of Kwok and Atkinson [42]. The oxygen in the products of fragmentation (red species Figure P in the Appendices) represent a carbonyl or an ether-functionality typical of dihydrofurans [59] – both functionalities have similar effect on vapor pressure [43]. The functionality products (blue species Fig. P in the Appendices) possess two oxygens, one from its original moiety and the second corresponds to a carbonyl or ether-functionality (dihydrofuran).

Estimating saturation concentrations for the products of first-generation of oxidation is necessary to place them in the 2D-VBS (Figure 5.1). Experimental data is very limited; hence, we use structure activity relationships. There are multiple literature papers that estimate vapor pressures [43, 136, 137]. Here we use SIMPOL from Pankow and Asher [43]. However, all methods present a degree of uncertainty in vapor pressure calculation, adding to the uncertainty of our results (explicit 1st-generation scheme).

5.3 The 2D-VBS: Results and Discussion

In Figure 5.2 we present SOA mass yields as a function of total organic aerosol formed (C_{OA}) for six different species: *n*-pentadecane, *n*-tridecanal, 2-, 7-tridecanone, 2- and 7-tridecanol. Experimental data comes from Presto et al. [72] (*n*-pentadecane) and Chacon-Madrid and Donahue [107] for carbonyls (experimental conditions are presented in Table D, Appendices); however, here the SOA mass yields have been corrected for a typical OA density of 1.4 g cm⁻³ [80, 85].

In each panel of Figure 5.2 we present three different results: (i) the default 2D-VBS box model simulation (black solid line), (ii) explicit 1st-generation followed by 2D-VBS box model simulation (violet solid line) and (iii) experimental SOA mass yields (each species has a different

color for experimental data). Figure 5.2a, *n*-pentadecane, is the only panel without an explicit 1st-generation simulation since *n*-pentadecane does not suffer major fragmentation paths in its first-generation chemistry [59].

All experiments presented here were performed under high-NO_x conditions (maximum of 2 ppbC/ppb NO_x), while the 2D-VBS box model simulations are for generic conditions [37]. High-NO_x conditions lead to organic nitrate (-ONO₂) formation which can reduce vapor pressure by ~2.5 orders of magnitude [43]. Low-NO_x conditions favor hydroperoxide (-OOH) formation [34, 112-114], which can lower vapor pressures by a similar factor. Therefore, the vapor pressure of products – and SOA mass yields – of high and low-NO_x cases might not be very different, unless very UV-sensitive products are formed [122, 139].

In most cases the default 2D-VBS box model over estimates the experimental SOA mass yields. This is because it was not designed for individual molecules but bulk organic aerosol material – capturing average chemistry – that includes species that easily fragment and those that functionalize more effectively. However, the predictive ability of SOA mass yields from the box model with explicit first-generation chemistry is acceptable and within the experimental uncertainty for all of the species studied here. Experimental SOA yields have a minimum uncertainty of \pm 20% [107] [65], and the explicit model falls within that range of the data for most of the species over most of the concentration ranges presented in Figure 5.2. We must emphasize that the explicit first-generation mechanism is based on a-priori consideration of the chemistry and contains no fitting to the data. The model-measurement agreement for the explicit case is thus a strong confirmation of the underlying mechanism.

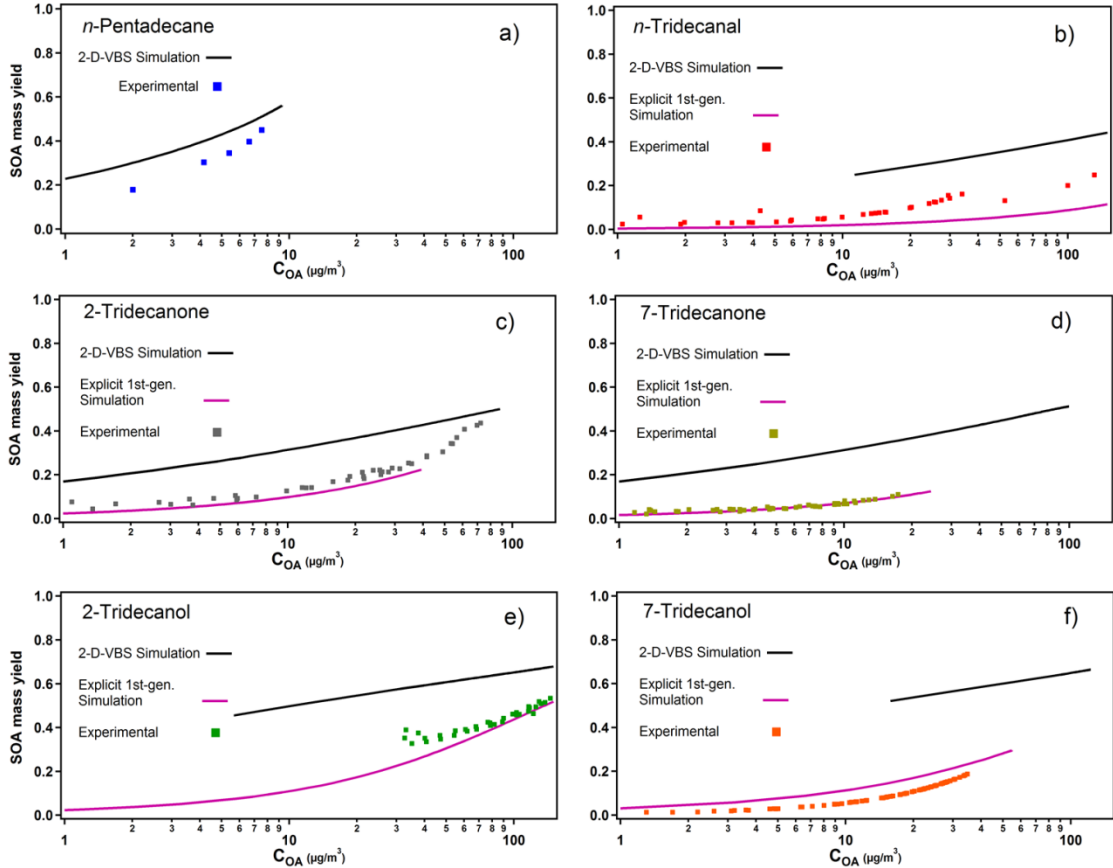


Figure 5.2. Simulations vs. Experimental Results. Each panel presents SOA mass yields for three sets of results; (i) 2D-VBS Simulation (solid black), (ii) Explicit 1st-gen. Simulation (solid violet) and (iii) experimental results [72, 92, 107]. For all oxygenated species we encounter an acceptable agreement between the experimental data and the Explicit 1st-gen. Simulation. This means that establishing only the first-generation chemistry and then use the 2D-VBS box model is sufficient to present acceptable agreements between simulations and experimental data. *n*-Pentadecane does not need first-generation products to be established; the 2D-VBS Simulation predicts SOA mass yields adequately.

5.3.1 *n*-Pentadecane.

The 2D-VBS simulation and the experimental SOA mass yields for *n*-pentadecane agree within the experimental uncertainty (Figure 5.2a). The good accord between these two sets of data can be attributed to a good representation by the 2D-VBS of the initial chemistry of alkanes (shown in Figure 5.1a) as well as reasonable fragmentation vs. functionalization paths for the ensemble of later-generation *n*-alkane products. Also, the assignment in the box model of saturation concentrations of products as a function of carbon and oxygen number was built for straight-chain species [37].

5.3.2 *n*-Tridecanal.

The explicit 1st-generation simulation in Figure 5.2b captures the fragmentation path that *n*-tridecanal undergoes in its first-generation chemistry [92] as opposed to the default 2D-VBS scheme, which severely overestimates SOA formation. The modest underestimation of the explicit simulation may be the assignment of products for the first-generation chemistry (Fig. P in the Appendices). Our assumption is that first-generation photo-oxidation of *n*-tridecanal forms three different species. They are: a C₁₂O (corresponding to *n*-dodecanal), CO₂ (which is irrelevant for SOA formation purposes) and a C₁₃O₂ (corresponding to a dicarbonyl or carbonyl with a dihydrofuran). Both, the C₁₂O and C₁₃O₂ species have one fewer oxygen than a typical isomerization reaction would predict [59, 62, 81]. We chose such structures because isomerization reactions lead to dehydration under low relative humidity (our conditions for all experiments were of low relative humidity), expelling an oxygen from the carbon backbone and forming a dihydrofuran [77]. However, the dihydrofuran can be in equilibrium with a hydroxy-carbonyl species with one more oxygen. Representing this equilibrium in the simulation was not

straightforward, so we decided to represent the first-generation products with $C_{12}O$, $C_{13}O_2$ and CO_2 . This would slightly underestimate experimental yields, as seen in Figure 5.2b.

5.3.3 Other Precursors: Position of functional groups.

The sets of 2-, 7-tridecanone and 2-, 7-tridecanol present an instructive sequence to understand the effect of functional-group positioning on SOA formation potential. A major difference between the ketones and the alcohols is the order of magnitude difference in their vapor pressures; alcohols are less volatile. Nonetheless, both the alcohol and ketone pairs probe the influence of functional-group location. Consequently, 7-tridecanone and 7-tridecanol have systematically lower SOA yields than 2-tridecanone and 2-tridecanol, respectively. This is similar to results presented by Lim and Ziemann [60, 76] where substituted alkanes have lower SOA yields than analogous straight-chain alkanes. Tridecanone yields had been reported in Chacon-Madrid and Donahue [107]. Tridecanol yields are presented here for the first time.

SOA yields are suppressed when the functional group is in the center due to creation of fragments (e. g. hexanal and heptanal for 7-tridecanone and 7-tridecanol) of higher vapor pressure when compared to the case where the functional group is on the side. For example, a $C_{10}O$ (expected product from 2-tridecanone and 2-tridecanol) can contribute to later-generation SOA more effectively than a C_6O and C_7O . The position dependence of substituents is evident in Figure 5.1 – low C^* yields for functional groups in the 2-position (Figure 5.1c and e) are much larger than yields with the functional group in the 7- position (Figure 5.1d and f).

The agreement between the explicit 1st-generation simulations (violet solid lines) and experimental data for the tridecanones and tridecanols is very good (Figure 5.2c, d, e and f). This performance shows how the 2D-VBS box model is a powerful tool for predicting SOA, not

only of bulk material, but individual molecules. And predicting SOA formation for an individual molecule can be done, at least in similar cases to the ones presented in here, after determining only the first-generation products of photo-oxidation.

The small discrepancies between experimental data and the explicit 1st-generation box model can also be attributed to uncertainty in the structure reactivity relationships from Kwok and Atkinson [42]. SRRs are used to determine the stoichiometry of products of fragmentation and functionalization in here (Fig. P in the Appendices). We believe that the SRR can be instructive in general to capture the likelihood of fragmentation, but its calculations have a relatively high degree of uncertainty.

5.4 GECKO-A: Results and Discussions

We are presenting the experimental SOA mass yields of the aforementioned species initially published in Chacon-Madrid et al. [92] and Chacon-Madrid and Donahue [107]; however, the published normalized SOA mass yields have been corrected for an OA density of 1.4 g cm⁻³ in here [80]. Because of their sensitivity to organic aerosol mass formed (C_{OA}), SOA mass yields are presented as a function of C_{OA} [12]. This dependence is due to partitioning between the gas and particle phases [10]. Experimental data is compared with GECKO-A simulations that use experimental inputs such as initial OH radical concentration ($\sim 10^7$ mol cm⁻³), UV-light intensity ($J_{NO_2} \sim 0.06$) and high-NO_x conditions (maximum of 4 ppbC/ppb NO_x). All experimental data has been corrected for wall-losses, and the details of such calculations are explained elsewhere [65, 107]. Experimental conditions are presented in Tables B and D in the Appendices.

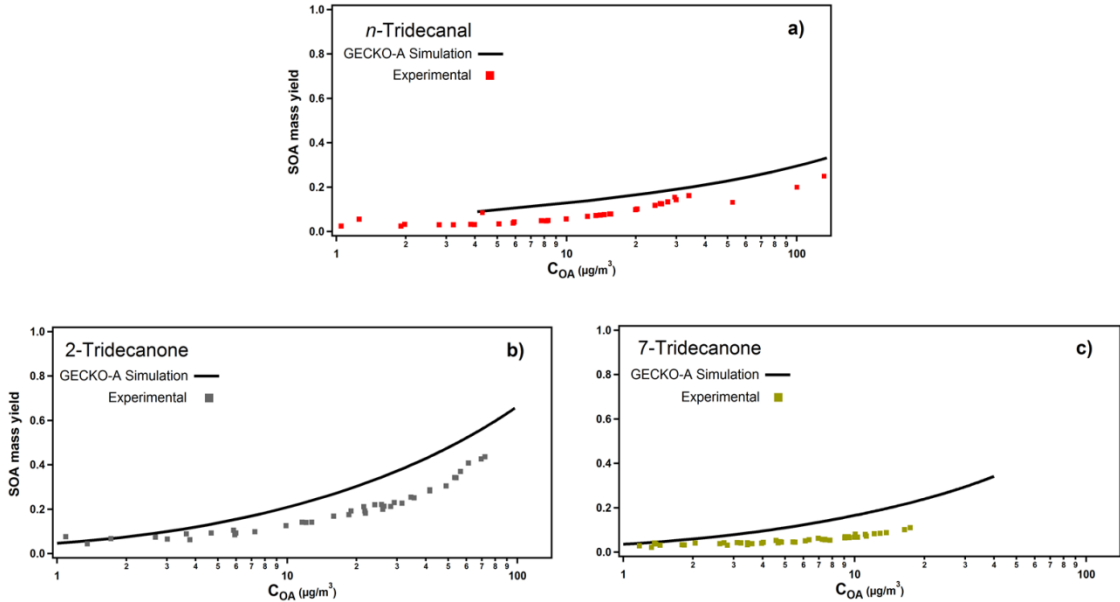


Figure 5.3. GECKO-A simulations of SOA mass yields for three different carbonyls – all with thirteen carbons – present an over-prediction when compared to experiments [92, 107]. However, when considering experimental uncertainty in the order of $\sim 20\%$, the comparisons are very encouraging. Also, the agreement between GECKO-A and experiments are similar – if not better – in here than with α -pinene oxidation experiments [41, 120].

A clear trend when comparing GECKO-A with experimental data is its systematic over-prediction of SOA mass yields for most species, as it can be seen in Figure 5.3 and 5.4. The over-prediction can also be seen in Figure Q and R in the Appendices. Nonetheless, in most cases – with exception of Figure 5.4a, *n*-heptadecanal – the over-prediction is not large regarding SOA yields. Over-prediction of SOA formation from GECKO-A had been observed in previous comparisons. For example, Valorso et al., [41] uses the Generator to predict organic aerosol formation of α -pinene under varying concentrations of NO_x ; from high to low, as presented in Ng et al., [120]. All simulations systematically over-predicted SOA, independently of the method used to estimate vapor-pressures [43, 136, 137]. In this work, we use only the Nannoolal et al., [137] method to estimate vapor pressures as stated before. This method has produced the best predictions of OA in other comparisons. However, it is important to mention that even though

GECKO-A presented over-predictions of α -pinene photo-oxidation in Valorso et al., [41], its qualitative forecast of OA time-evolution features has been very acceptable. In a similar way, this work shows a very acceptable qualitative description of SOA mass yields for most molecules – to a lesser extent *n*-heptadecanal and 7-tridecanone. The agreement is especially strong for the beginning portion of most experiments shown in Figure 5.3 and 5.4.

Experimental Uncertainty. One of the first aspects to consider when comparing GECKO-A with experimental data is reproducibility and level of uncertainty of such data. Experimental SOA mass yields in this work present an uncertainty of at least $\pm 20\%$. This can be seen in multiple chamber experiments with aldehydic species presented in Chacon-Madrid et al., [92], Chacon-Madrid and Donahue [107] and Chacon-Madrid et al., [140]. Also, experiments performed with toluene photo-oxidation confirm that level of uncertainty [65]. Consequently, Figure 5.3a, b, the beginning of simulation in Figure 5.3c (7-tridecanone), and Figure 5.4b, c and d present acceptable SOA yields simulations considering the experimental uncertainty.

Structure Activity Relationships. GECKO-A depends on structure reactivity relationships (SRRs) [42] to determine the proportion of OH-radical attack on each carbon-site of a molecule. The only exception happens when there is direct information available from the literature. For the vast majority of molecules, there is very limited information; consequently SRRs direct most of OH-chemistry placement. SRRs have shown excellent predictions for simple and small molecules (e.g. *n*-alkanes), but the agreements are less than ideal for complex species with multiple functional groups. This less-than-ideal predictions can make GECKO-A less reliable as the system becomes more chemically complex. The Generator also depends on structure activity relationships for prediction of vapor pressures. Predictions of vapor pressures become

less reliable as the number of functionalities increases in a carbon backbone. Similarly to SRRs, vapor pressure estimates can add to the uncertainty of the Generator.

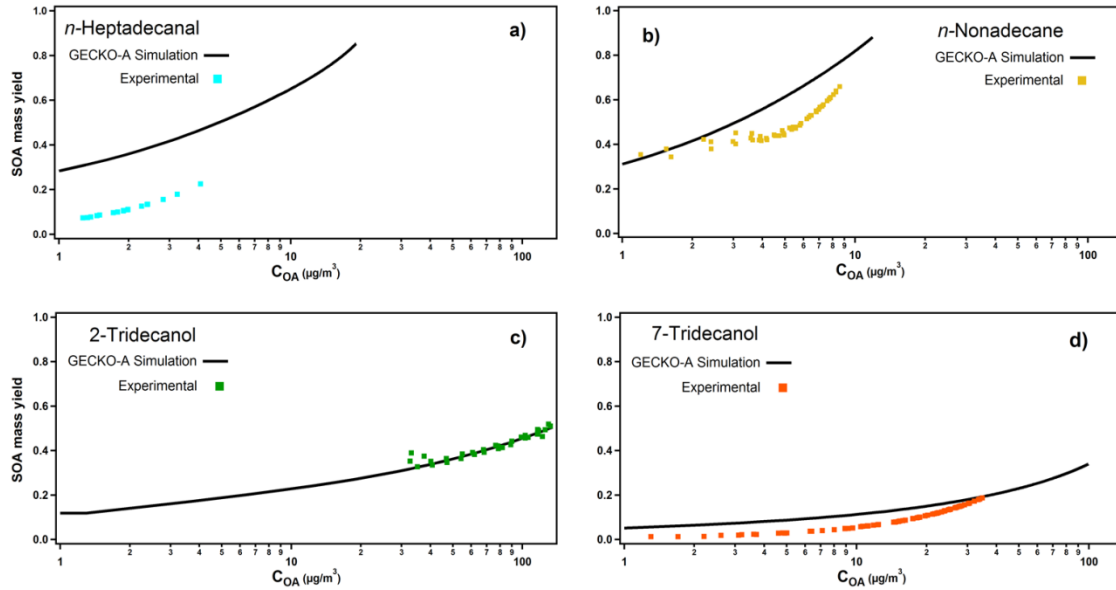


Figure 5.4. The species presented in this panel are of lower volatility than those in Fig. 5.3. The agreements between GECKO-A and most experimental yields are also very acceptable in this Figure. *n*-Heptadecanal is the only species for which the differences are much larger than the ~20% of experimental uncertainty. Considering that GECKO-A has to rely on different structure activity relationships [42, 137] that possess a high degree of uncertainty, these results are very encouraging. Other aspects, such as vapor losses to walls of later-generation products, have to be approached in future experiments.

Vapor losses. An aspect that would cause GECKO-A to over-estimate experimental SOA mass yields with respect to experimental results is not considering losses of vapors to the walls of smog-chambers – if they happen to be important and relevant. We think it is unlikely that most parent-molecules presented in here were lost to the walls. In fact, before photo-oxidation most of these precursors were observed for ~15 minutes without seeing decay. As further evidence, Figure S in the Appendices shows proton transfer reaction-mass spectrometer (PTR-MS) data of a series of *n*-aldehydes with vapor pressures of at least ~ 10^5 μg m⁻³. All of these species were

injected into the Carnegie Mellon Smog-Chamber made of Teflon (Welch Fluorocarbon) and with a volume capacity between 10 and 12 m³. They were not exposed to UV-light or oxidation, and their concentrations in the chamber were between ~200 and ~300 µg m⁻³. Figure S in the Appendices shows how all these species are not lost to the walls after being inside the chamber for about one hour.

However, losses to the walls (like the ones shown by Matsunaga and Ziemann [95]) from multi-functionalized that are likely to appear as photo-oxidation progresses are possible. Also, oxidized and less volatile species, such as *n*-heptadecanal, can potentially be lost to the walls. This could explain an acceptable agreement for SOA mass yields between all species presented in here, with exception of *n*-heptadecanal (Figure 5.4a).

5.5 Environmental Significance

Both, the 2D-VBS box model and GECKO-A demonstrate encouraging potential as a prognostic tool for simulating SOA formation and evolution. Even though the box model was created for bulk organic aerosol with average chemistry, it is capable – as shown here – of predicting OA mass formation of individual molecules. This can be done by simply establishing the first-generation chemistry of the individual molecule.

When applied to simulations of the real atmosphere, the averaging nature of the 2D-VBS mechanism is an asset, as it is highly unlikely that one or even a handful of unique organic compounds dominate the OA mass at any location or time. On the other hand, the results from this work suggest that it may be important to treat freshly emitted OA mass with aging chemistry that is more representative of the major compounds from particular sources (if

known). It is expected, though, that as oxidation reactions continue to transform this OA mass, its constituents will become more varied and treating their chemistry with the general (average) 2D-VBS mechanism will be more suitable. Transport models that simulate this aging process already take into account a parameterization of SOA formation based on yields from smog-chamber experiments carried out over a few hours. The approach used in the current work is analogous, but there are subtle differences. The first-generation yields used here attempt to isolate the products from the first attack by an oxidant on the precursor gas. Traditional chamber yields take into account however many generations of chemistry occur in the experiment. The implications of this difference, especially in three-dimensional photochemical transport models, are not clear. This paper focuses on six precursors to illustrate some of the subtleties of applying the 2D-VBS to modeling the aging of specific molecules. However, these compounds are not the most relevant species when addressing SOA formation in the atmosphere. It will be important for future work to apply this same approach to experiments with compounds like toluene and terpenes to determine if only one explicit step of chemistry is necessary before treatment with the 2D-VBS is adequate.

GECKO-A presents tremendous advantages over current models that predict OA formation. The most obvious one is the large amount of chemical information that it can provide, as it tracks most chemical species during a simulated photo-oxidation experiment. The Generator can also determine SOA mass yields of virtually any molecule; such yields can be useful to both experimental projects and also to Chemical Transport Models (CTMs) that simulate SOA formation [101, 102, 129]. It can be especially important to CTMs in cases where there is a high need for rich-chemistry knowledge of the system. As shown in this work, GECKO-A tends to slightly over-predict SOA mass yields of different linear and oxygenated species with thirteen carbons or more.

The slight over-prediction of GECKO-A with respect to experimental work can be attributed to a number of issues, which include (i) experimental uncertainty, (ii) use of SRRs [42] to determine the proportion of OH-radical attack on the different carbon-sites of a molecule, (iii) use of structure activity relationship to estimate vapor pressures [41] and (iv) potential losses of large and oxygenated vapors including later-generation products to smog-chamber walls – over-predicting experimental SOA mass yields.

Acknowledgments

This research was supported by the Electric Power Research Institute grant EPP25369C12290 and the EPA STAR program through the National Center for Environmental Research (NCER). This paper has not been subject to EPA's required peer and policy review, and therefore does not necessarily reflect the views of the Agency. No official endorsement should be inferred. All the computer simulations were performed in the University of Paris by Dr. Richard Valorso and Dr. Bernard Aumont in close discussion with the authors of this chapter.

Chapter 6 – Conclusions and Future Work

The work presented in this dissertation is centered on the topic of atmospheric chemical evolution. More specifically, it relates to how the ability of organic compounds to form SOA changes as they become progressively more oxidized. Multiple conclusions were found regarding the different systems analyzed to approach such subject. The most relevant findings and conclusions are summarized next:

- The aldehydic moiety was found to be highly reactive with the OH radical, as expected [23]. We found that this moiety promotes strong fragmentation mechanisms in its first-generation OH radical attack, even for large compounds ($\geq C_{13}$) [92] (Chapter 2). This fragmentation was typically characterized by forming species with one fewer carbon (e.g. *n*-heptanal would form *n*-hexanal). However, only species with large-enough carbon backbones ($\geq C_{13}$) were found to form SOA under 22° C, UV-light exposure of $J_{NO_2} = 0.06 \text{ min}^{-1}$ and relative humidity < 10%.

n-Tridecanal SOA mass yields were compared to those of *n*-pentadecane because of their similar vapor pressures which give an instructive comparison. The linear C_{13} aldehyde presented yields that were about a third of *n*-pentadecane. This suppression of yields is due to the strong fragmentation path of aldehydes in their first-generation that does not happen to *n*-alkanes in their first-generation chemistry [59]. The importance of this finding relates to the aldehydic moiety itself, which can be an abundant functional group in biogenic first-generation products of monoterpene ozonolysis or OH-radical reaction [106]. This is especially important due to the prevalence of biogenic emissions [33].

- Molecules with higher oxidation states have a greater susceptibility to fragment when reacting with the OH radical. This is especially true when compared to *n*-alkanes of similar vapor pressures [107] (Chapter 3). This conclusion comes from examining and comparing SOA mass yields for two sequences of molecules under high-NO_x conditions, at 22°C, UV-light exposure of $J_{NO_2} = 0.06 \text{ min}^{-1}$ and relative humidity < 10%. The first sequence consists of molecules with vapor pressures of $\sim 10^5 \text{ } \mu\text{g m}^{-3}$ and they are: *n*-pentadecane, *n*-tridecanal and pinonaldehyde. The second sequence is comprised of *n*-nonadecane, *n*-heptadecanal and *cis*-pinonic acid, all with vapor pressures of $\sim 10^3 \text{ } \mu\text{g m}^{-3}$. Both sequences showed systematically lower SOA mass yields for oxygenated species when compared to the respective *n*-alkanes.

Another aspect studied was how the position of the functional group on a carbon backbone can affect SOA mass yields. 2- and 7-tridecanone were examined in similar experimental conditions as before. Both species – with vapor pressures of $\sim 10^5 \text{ } \mu\text{g m}^{-3}$ – presented lower SOA yields than *n*-pentadecane also. However, 2-tridecanone yields were larger than those from 7-tridecanone. This was especially true in the region of organic aerosol concentration from ~ 20 to $\sim 50 \text{ } \mu\text{g m}^{-3}$.

These findings let us conclude that the position of the functional group can have an effect on SOA mass yields. Molecules with functional groups in the center of their carbon backbones present lower SOA yields than molecules with functional groups towards the end of their carbon backbones. When the functional group is in the center of a linear carbon backbone, fragmentation that occurs creates small products that are less likely to partition to the organic aerosol phase. In the case of a functional group towards the end of carbon backbone, one of the fragmentation products can be large enough to contribute to organic aerosol formation. The alkoxy radicals formed on the

immediate carbon-site of a functional group – such as a carbonyl – are responsible for carbon-carbon bond fragmentation [23].

- Pinonaldehyde + OH chemistry was explored under low- NO_x conditions, and its SOA mass yields were determined (Chapter 4). Pinonaldehyde SOA mass yields under low- NO_x were lower than *n*-pentadecane, but significant and higher than zero. The importance of these findings relates to the ability of first-generation products from monoterpene oxidation to form SOA. If first-generation biogenic products – like pinonaldehyde – can produce SOA in an environmental concentration range, OA formation potential from all subsequent-generation products combined can be very significant.
- A 2D-VBS box model [37, 38] is utilized to simulate experimental SOA mass yields of linear oxygenated molecules (Chapter 5). They are *n*-pentadecane, *n*-tridecanal, 2-, 7-tridecanone, 2- and 7-tridecanol. Because the box model cannot distinguish between functional groups (e.g. 2-tridecanone and *n*-tridecanal), we explicitly expressed the first-generation products in the framework. By doing so, we encountered a very good agreement between experimental and simulated yields – with explicit first-generation chemistry included.

We can conclude that the box model can be a very good prognostic tool for SOA formation of not only bulk organic aerosol, but also of systems that start with one specific molecule. This can be achieved by only expressing the first-generation chemistry. It is important to note that all the species simulated were linear and oxygenated; we cannot draw conclusions regarding different chemical structures.

- An explicit chemical generator – GECKO-A [39-41] – is also utilized to simulate experimental SOA mass yields of *n*-tridecanal, 2-, 7-tridecanone, 2-, 7-tridecanol, *n*-heptadecanal and *n*-nonadecane (Chapter 6). GECKO-A over-predicts SOA yields for all species; however, it captures the qualitative trends of OA formation. We also found good agreements between the generator and experimental results for the beginning of most experiments and a widening gap in the latter part. There is no one single culprit for this discrepancy; we think that a combination of multiple reasons could have contributed such as: (i) experimental uncertainty, (ii) use of SRRs [42] to determine the proportion of OH-radical attack on the different carbon-sites of a molecule, (iii) use of structure activity relationships to estimate vapor pressures [41] and (iv) potential losses of large and oxygenated vapors to smog-chamber walls. Nonetheless, GECKO-A can be very useful in generating approximate SOA yields of molecules to be investigated in the laboratory.

6.1 Future Work

6.1.1 Functional groups.

Throughout this thesis multiple functional groups were studied in relation to their ability to contribute to SOA mass yields. However, not all functional groups were studied. Some of the functional groups not studied explicitly as linear carbon backbones include ethers, carboxylic acids and peroxides. Ethers can be abundant functional groups in the form of dihydrofurans [59] and especially abundant in dry conditions [77]. Also, dihydrofurans can be ubiquitous species in organic aerosol material that is long enough to suffer isomerization reactions in the form of 1,5-hydrogen shifts; most linear carbon backbones with 7 carbons or more could experience such isomerization.

Linear carboxylic acids should also be studied in detail, including SOA yields determination. Acids are very abundant in aged-ambient organic aerosol [29], also as organic material ages, the formation of carboxylic acid becomes progressively more important [4, 141]. Other than studying gas-phase OH radical chemistry of carboxylic acids, it is important to understand their heterogeneous and aerosol-phase reactions; this is especially true because of the low volatility of acids [43] that makes them more likely to partition and exist in the aerosol phase [10] especially if an acid-base neutralization reaction occurs.

Peroxides, specifically hydroperoxides, can be very abundant in conditions of low- NO_x chemistry [112, 114]. Studying linear hydroperoxides can be useful in understanding low- NO_x chemistry. Analyzing *n*-alkanes in the absence of NO_x can be a good first step towards understanding hydroperoxides. A better step would consist of synthesizing a linear hydroperoxide and determining its SOA mass yield. Doing so can be a good contribution to our knowledge of atmospheric organic chemistry under low- NO_x .

Chemistry of species with multiple functional groups. All the linear chemical compounds studied in this thesis possessed either no functional group (*n*-alkanes) or only one. Addressing linear species with at least two functional groups (e. g. a carbonyl + alcohol) can be important and representative of aged material. For example, *n*-alkanes + OH under high- NO_x can form a δ -hydroxy-carbonyl [59]. It is important to acknowledge that synthesis, purification, and proper identification are tremendous challenges that need to be overcome when studying organic compounds with two or more functional groups. If such challenges are overcome, we could gain much more information on the atmospheric chemistry of highly oxygenated compounds.

6.1.2 GECKO-A and the 2D-VBS.

Simulations of many more species are needed for both GECKO-A and the 2D-VBS box model. Species that are structurally different than those presented here (e.g. cyclic and aromatic structures) are needed in order to complement this work. Also, simulations of linear structures with functional groups not reported in this thesis can be very instructive. Both simulation schemes – GECKO-A and the 2D-VBS – have to be utilized as prognostic tools in ambient systems also. The nature of the 2D-VBS will make this task easier if it does not need to know the specific molecules involved, only overall ranges of oxygenation and volatility – including concentrations. In the case of GECKO-A, a good starting point could include selecting surrogate molecules of the system to analyze.

Appendices

Table A. Most of the information presented in this table is for initial conditions. The NO₂:NO kept relatively constant for the first 30 minutes of the oxidation. The Structure Activity (SAR) rate constants were calculated from Kwok et al., 1995 and used for “inferred *n*-aldehyde” concentrations.

Species oxidized	Initial Concentration in the Smog Chamber	Initial NO ₂ :NO (ppb/ ppb)	Initial VOC ₀ /NO _x (ppbC/ ppb)	Initial OH concentration (molecule cm ⁻³)	Kwok and Atkinson Rate Constant (cm ³ molecule ⁻¹ s ⁻¹)
<i>n</i> -Tridecanal 021609	4 ppb	~300:1400	0.03	~1 × 10 ⁷	n/a
<i>n</i> -Tridecanal 031009	18 ppb	~300:1400	0.13	~7 × 10 ⁷	3.9 × 10 ⁻¹¹
<i>n</i> -Tridecanal 041709	250 ppb	~300:1400	2	~1 × 10 ⁷	3.9 × 10 ⁻¹¹
<i>n</i> -Tridecanal 082109	382 ppb	~4000:2000	0.8	~3 × 10 ⁶	3.9 × 10 ⁻¹¹
<i>n</i> -Tridecanal 030809	25 ppb	~4000:1000	0.07	~1 × 10 ⁷	3.9 × 10 ⁻¹¹
<i>n</i> -Dodecane Presto et al., 2010	19 to 58 ppb	-	0.05-0.4	-	n/a
<i>n</i> -Pentadecane Presto et al., 2010	2 to 9 ppb	-	0.03-0.1	-	n/a
<i>n</i> -Undecanal 060909	187 ppb	~900:500	1.3	~4 × 10 ⁷	3.6 × 10 ⁻¹¹
<i>n</i> -Octanal 042109	350 ppb	~500:180	4	~2 × 10 ⁷	3.2 × 10 ⁻¹¹
<i>n</i> -Pentanal 050709	189 ppb	~1200:300	0.8	~5 × 10 ⁷	2.8 × 10 ⁻¹¹

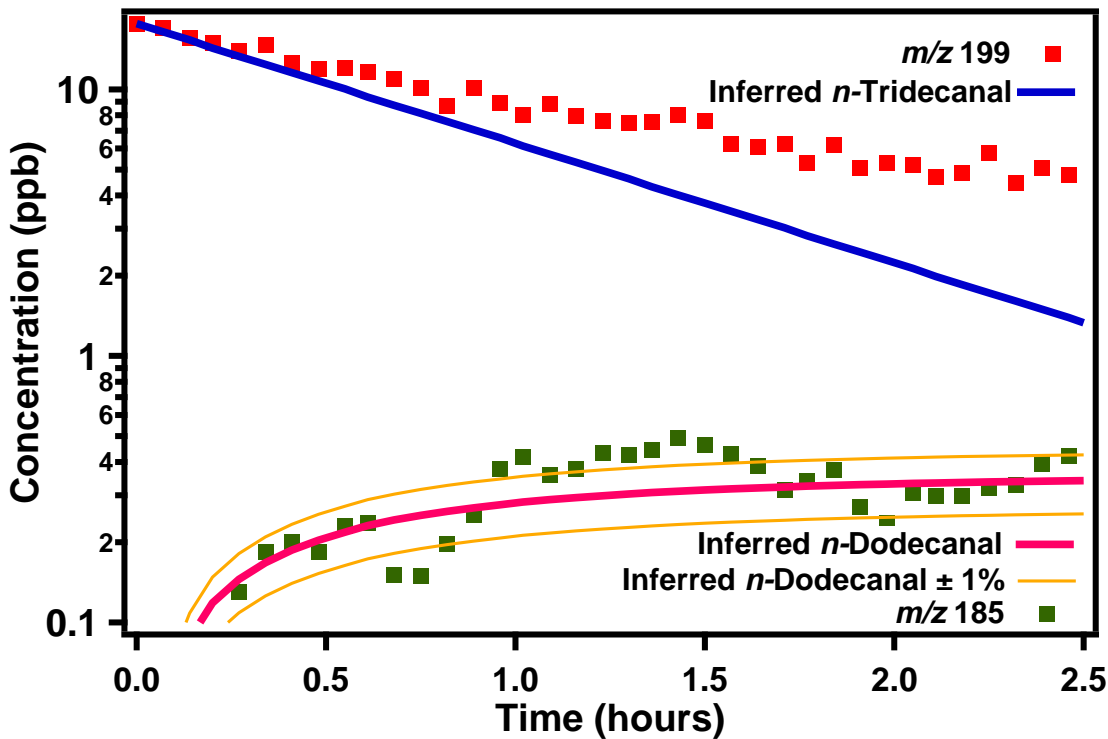


Figure A. (*n*-Tridecanal 031009). After reacting *n*-tridecanal with OH radical at high NO_x conditions, it was encountered that the *n*-dodecanal molar yield formation is $4 \pm 1\%$; however, this yield is dependent on NO₂:NO. The Inferred *n*-tridecanal is obtained by using a SAR rate constant, and an average OH concentration obtained from methanol (tracer). The discrepancies between *m/z* 199 and inferred *n*-tridecanal have to do with the formation of other species that have the same molecular weight as *n*-tridecanal (refer to Figure 2.5 in the main manuscript). The inferred *n*-dodecanal was calculated as 4% of the consumed inferred *n*-tridecanal minus any consumption due to OH radical attack.

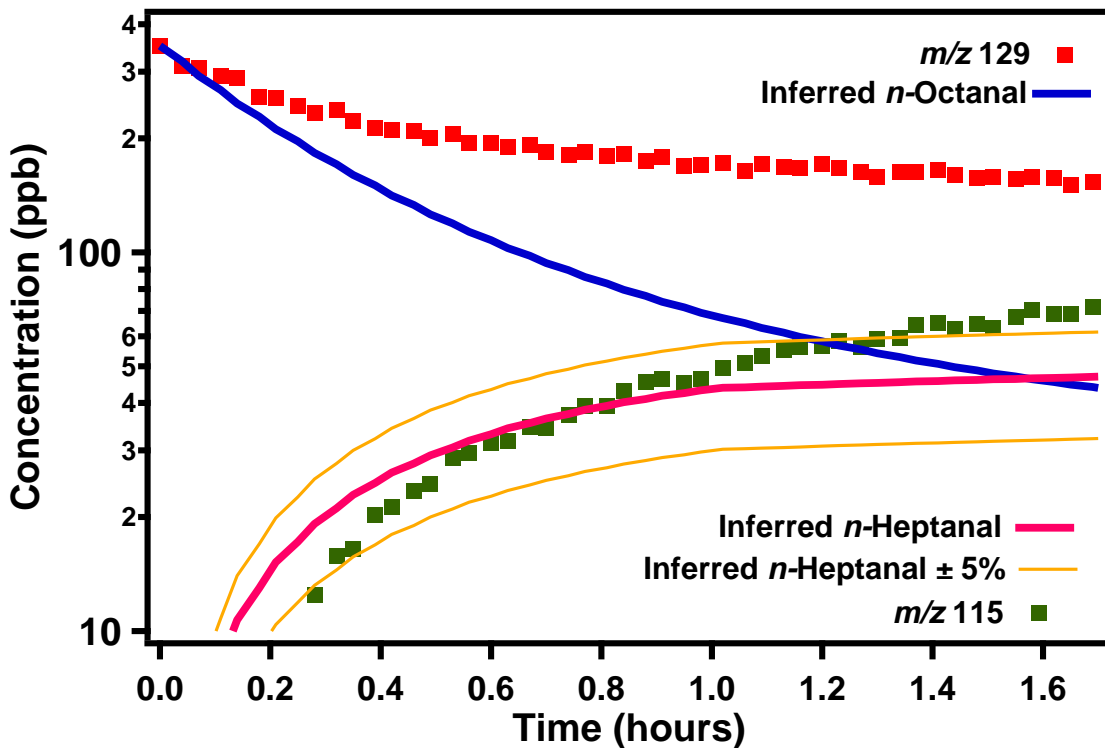


Figure B. (*n*-Octanal 042109). The molar yield formation of *n*-heptanal from the OH oxidation (at high NO_x) of *n*-octanal was determined to be 16 ± 5%. However, this yield is dependent on NO₂:NO. The inferred *n*-octanal is calculated by using a SAR rate constant (refer to Table A, Supplementary Data), and OH radical concentration obtained from the consumption of methanol. The discrepancies between *m/z* 129 and the inferred *n*-octanal are due to the formation of other species with the same molecular weight as *n*-octanal (refer to Figure 2.5 in the main manuscript). The inferred *n*-heptanal was calculated as 16% of the consumed inferred *n*-octanal minus any consumption due to OH radical attack.

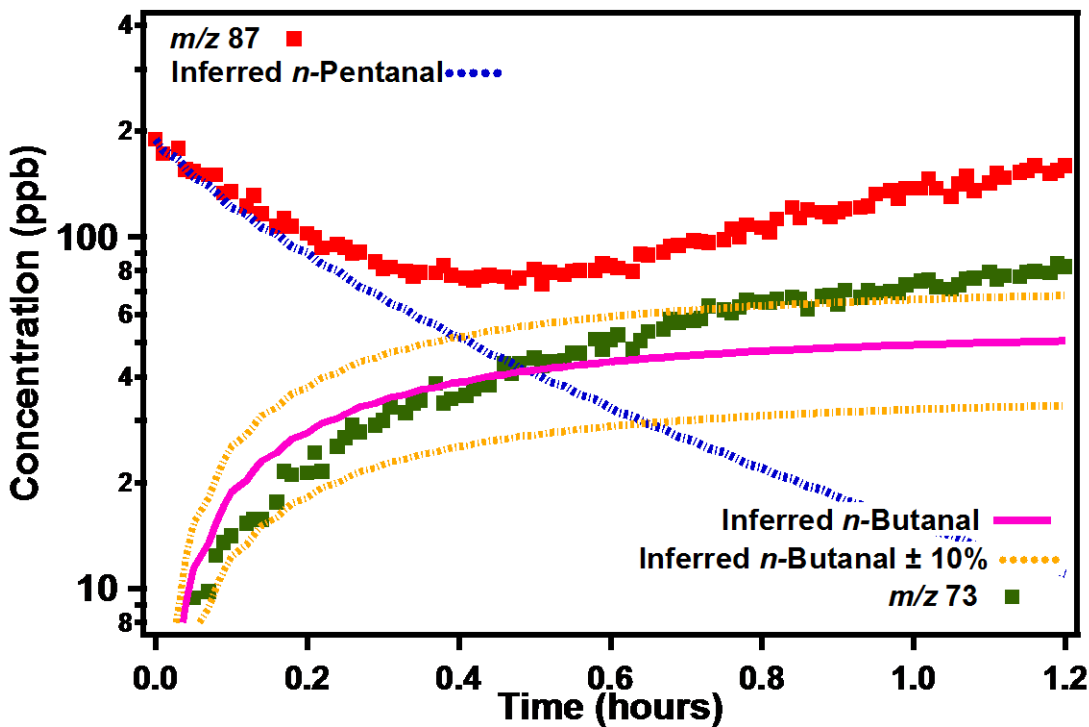


Figure C. (*n*-Pentanal 050709). It was found that the *n*-butanal molar yield formation is $29 \pm 10\%$; however, this yield is dependent on ratio of $\text{NO}_2:\text{NO}$. The Inferred *n*-pentanal is obtained by using a SAR rate constant, and an OH concentration obtained from methanol (tracer). The differences between *m/z* 87 and inferred *n*-pentanal might have to do with the formation of other species that have the same molecular weight as *n*-pentanal (refer to Figure 2.5 in the main manuscript). However, this other(s) species may have a different sensitivity to the PTR-MS. The inferred *n*-butanal was calculated as 29% of the consumed inferred *n*-pentanal minus any consumption due to OH radical attack.

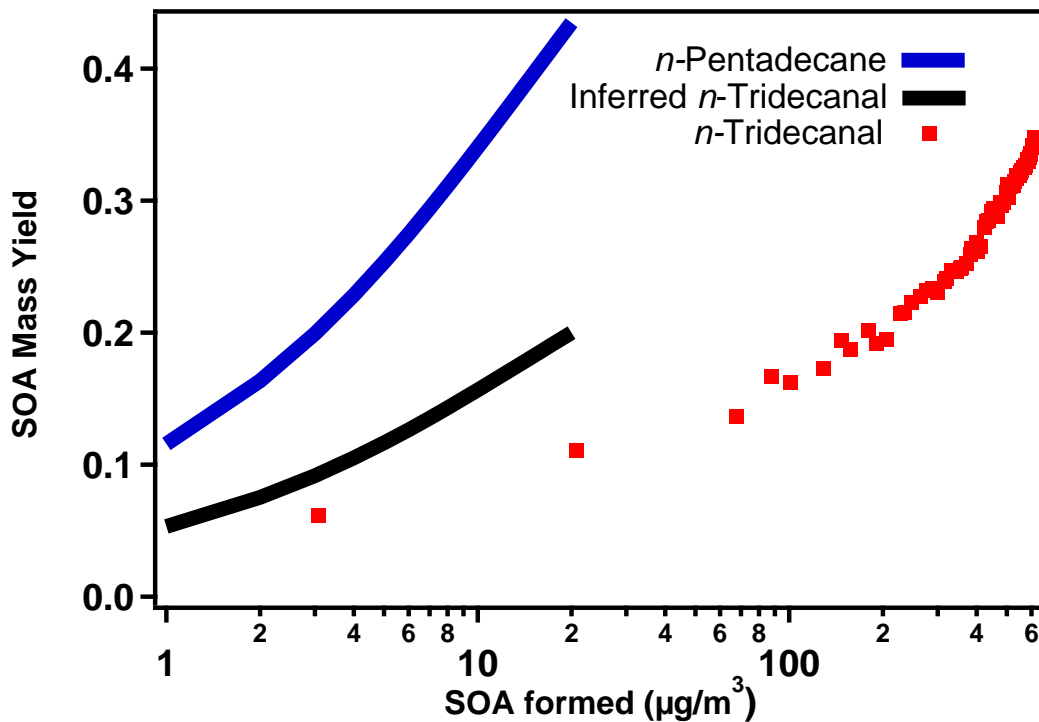


Figure D. *n*-Pentadecane yields are obtained from Presto et al., 2010, and the *n*-tridecanal yields come from this work, specifically experiment 041709 (refer to Table A). According to SAR, the OH radical attacks 54% of the time the aldehydic hydrogen of *n*-tridecanal, and 46% of the time the backbone. When the backbone is attacked, higher vapor pressure species are formed; that's not the case when the aldehydic hydrogen is attacked. *n*-Pentadecane's backbone is attacked always, as a result, *n*-tridecanal SOA yields should be about 46% of *n*-pentadecane's since both species have similar vapor pressures. The inferred *n*-tridecanal yields (black curve) is 46% of *n*-pentadecane's yields. A good match between inferred and experimental *n*-tridecanal yields is not encountered because attacking the aldehydic hydrogen (*n*-tridecanal) promotes the formation of lower vapor pressure species.

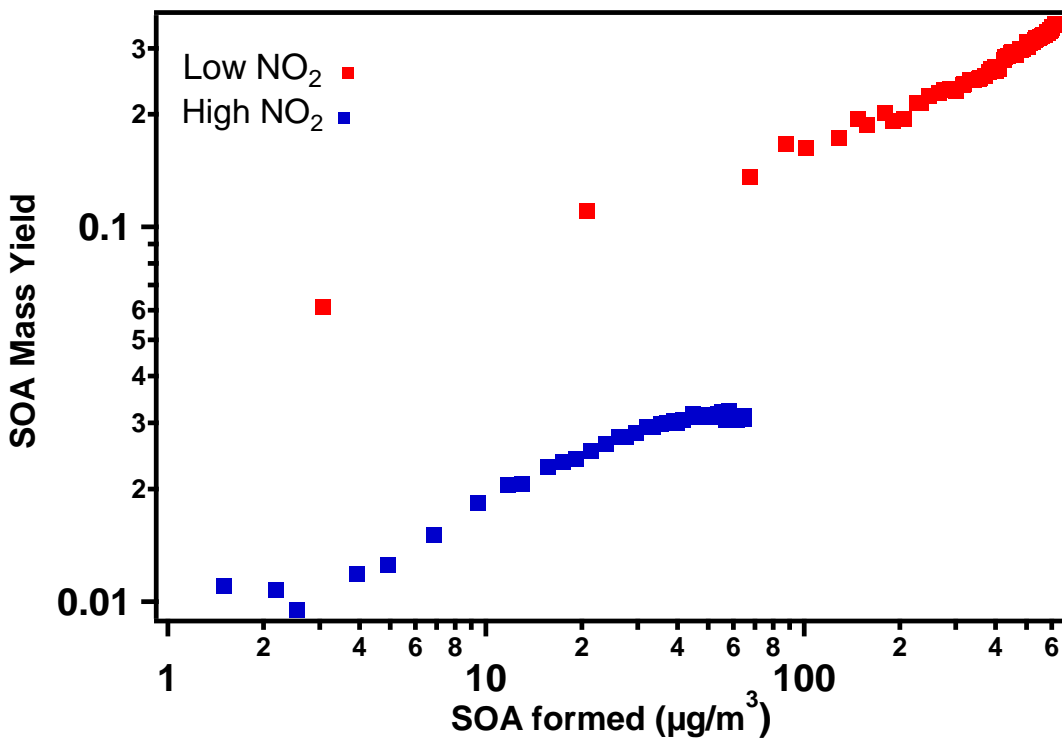


Figure E. Low (041709) versus high (082109) NO_2 *n*-tridecanal reaction with OH radical. The differences in SOA mass yields between Low and High NO_2 are considerable. The difference in VOC_0/NO_x (ppbC/ppb) between experiment 041709 and 082109 are not dramatic; however, their $\text{NO}_2:\text{NO}$ are. When there is significantly more NO_2 than NO available (experiment 082109), the formation of PAN is dominant (refer to Figure 2.1, main manuscript). Forming PAN thus has an effect on SOA formation. Presumably PAN formation limits the creation of carboxylic acids by protecting Peroxyacetyl Radical.

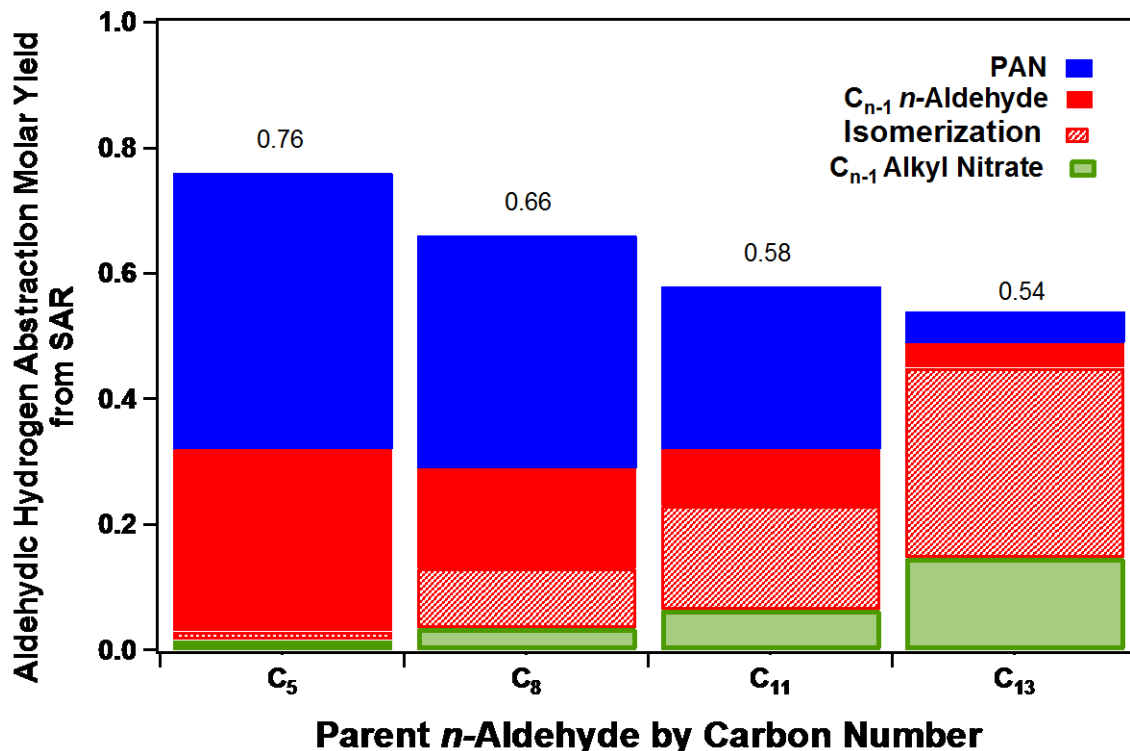


Figure F. (*n*-Pentanal 050709, *n*-Octanal 042109, *n*-Undecanal 060609, *n*-Tridecanal 031009) The height of each column is the SAR aldehydic hydrogen abstraction molar yield. After the aldehydic hydrogen abstraction, branching towards either PAN or C_{n-1} peroxy radical occurs, this last one branches into a C_{n-1} alkyl nitrate and a C_{n-1} alkoxy radical. Then the alkoxy radical branches between the C_{n-1} aldehyde and an isomerization structure. These relative yields are obtained from SAR predicted molar yields of aldehydic hydrogen abstraction induced by OH, kinetic constants for PAR branching, alkyl nitrate formation from Arey et al., 2001 and observed C_{n-1} aldehyde molar yields. This branching is only valid for the beginning of the experiment. Branching towards PAN is dependent on NO_2 concentration (blue arrows, Figure 2.1), which affects abundance of the C_{n-1} alkyl nitrate, *n*-aldehyde and the isomerization structure, but not their branching (red and green arrows, Figure 2.1).

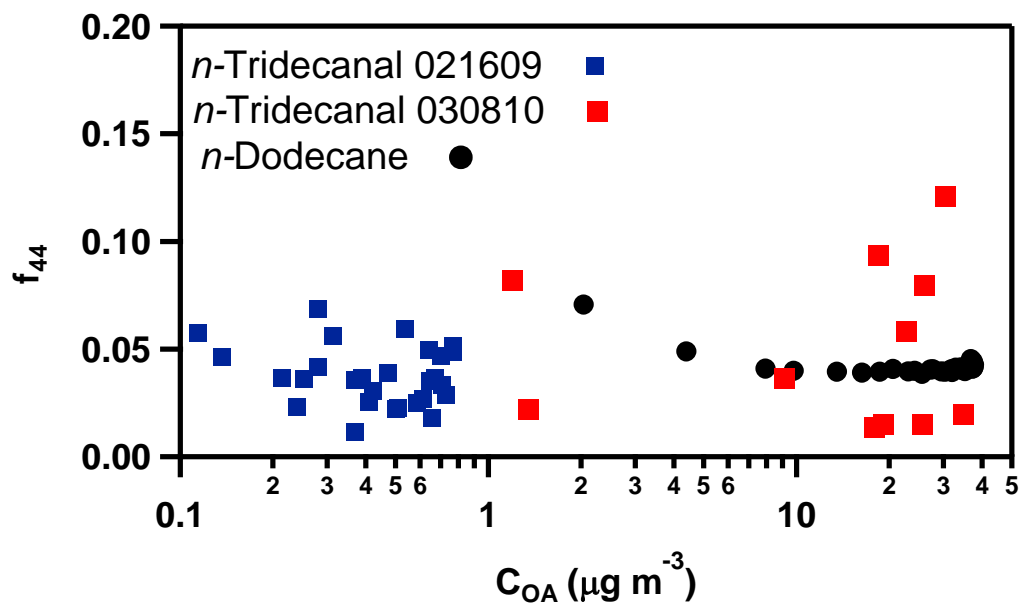


Figure G. *n*-Dodecane (Presto et al., 2010) versus *n*-tridecanal (021709 and 030810). The f_{44} is the ratio of m/z 44 to total organics detected by an AMS in the aerosol phase. This figure shows how oxidized both *n*-dodecane and *n*-tridecanal organic aerosols are. Since both molecules form a C_{12} alkoxy radical as a significant intermediate, it is expected to find similar level of oxidation in their organic aerosols.

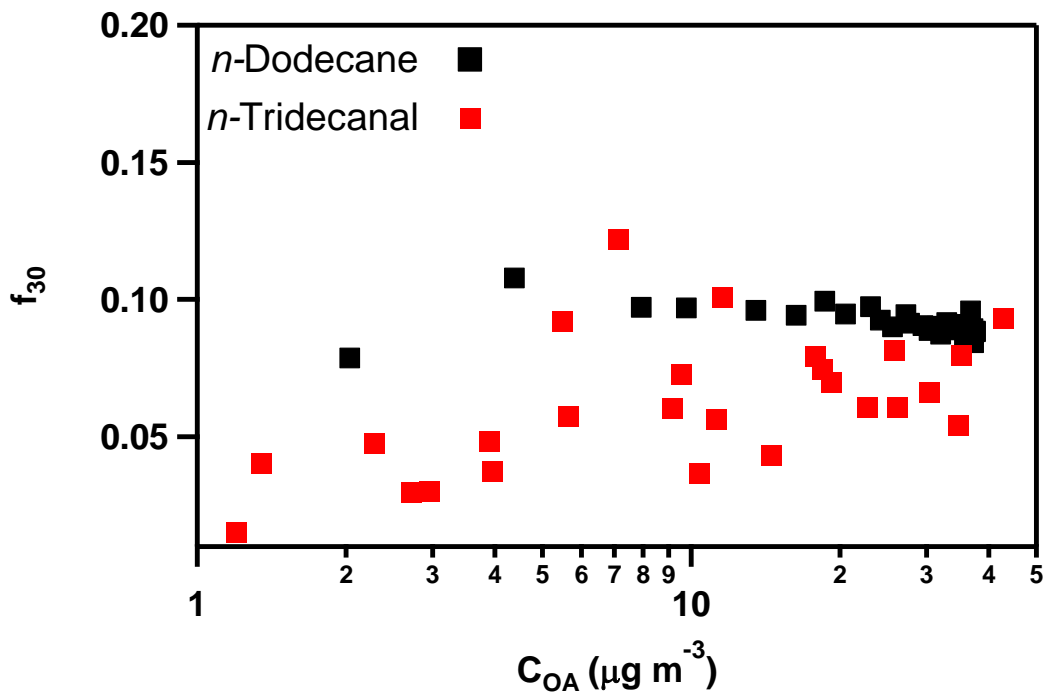


Figure H. *n*-Dodecane (Presto et al., 2010) versus *n*-tridecanal (021709). The presence of organic nitrates in the organic aerosol phase is significantly different for *n*-tridecanal versus *n*-dodecane. Most of the OH first generation reaction with *n*-tridecanal occurs at the aldehydic hydrogen, which does not form organic nitrates other than PAN. The presence of PAN is small due to a low $\text{NO}_2:\text{NO}$ for experiment 021709.

Table B. Conditions for the different experiments presented on Chapter 3 are shown on this table.

Species oxidized	Initial Concentration in the Smog Chamber	Initial NO _x (ppb)	Initial VOC ₀ /NO _x (ppbC/ppb)	Initial OH concentration (molecule cm ⁻³)
<i>n</i> -Tridecanal	~250 ppb	~1700	2	~1×10 ⁷
Pinonaldehyde	~300 ppb	~4000	0.8	~0.5×10 ⁷
<i>n</i> -Pentadecane Presto <i>et al.</i> , 2010	2 to 9 ppb	-	0.03-0.1	-
2-Tridecanone	~40 ppb	~3500	0.15	~0.5×10 ⁷
7-Tridecanone	~35 ppb	~3000	0.15	~0.5×10 ⁷
<i>n</i> -Nonadecane	~2 ppb	~1800	0.02	~0.5×10 ⁷
<i>n</i> -Heptadecanal	~3 ppb	~5000	0.01	~1×10 ⁷

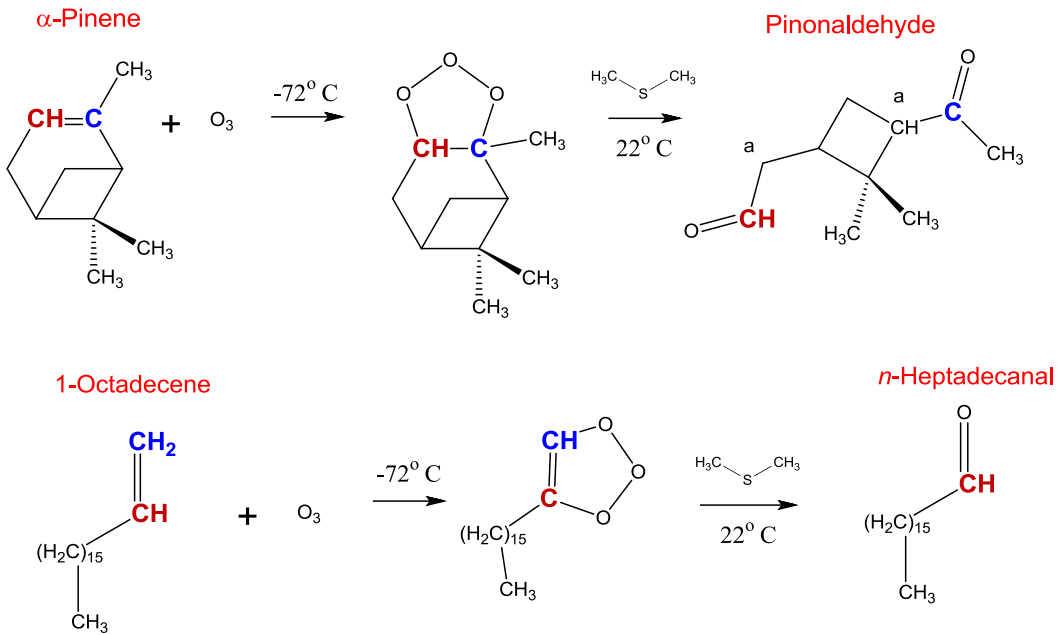


Figure I. α -Pinene and 1-octadecene were reacted (separately) with a flow of excess-ozone at $-72^\circ C$ to form the primary ozonide. Dimethylsulfide was used as a reducing agent to form the corresponding dicarbonyl. A bicarbonate solution was used to extract the carboxylic acids formed and other water soluble impurities. The procedure followed was the one by McMurry et al. (1987).

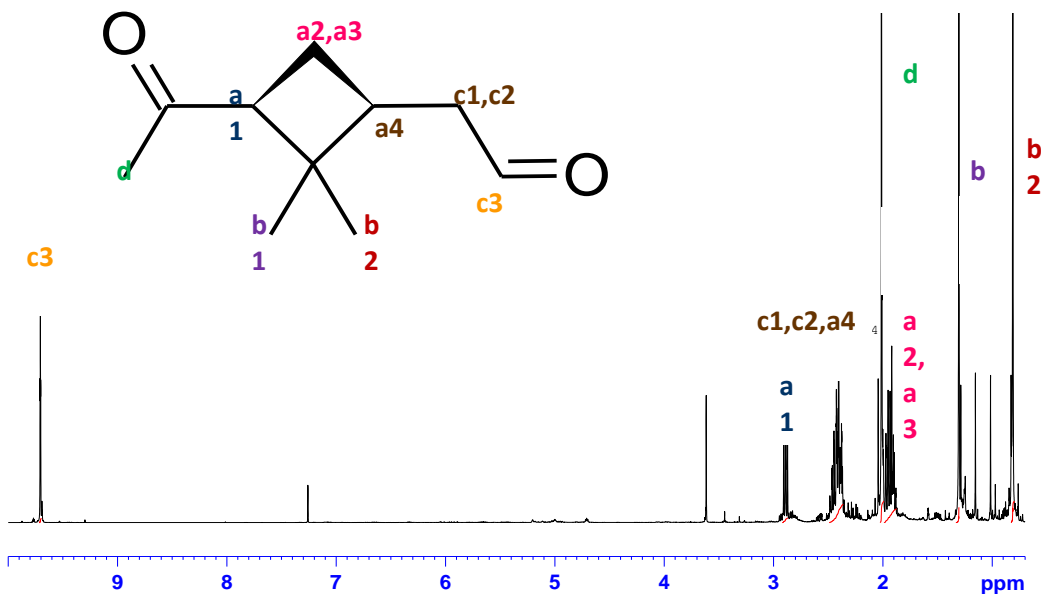


Figure J. ^1H NMR spectra were taken from the synthesized-pinonaldehyde sample in order to assess its purity level. Pinonaldehyde composed approximately ~85% of the sample, including the *cis*- and *trans*-isomers. Other minor species like peroxides were found. No acids were encountered. The biggest impurity was dimethyl sulfoxide (DMSO, at ~3.6 ppm). The signal at approximately 7.2 ppm corresponds to CDCl_3 , which was the solvent used when the NMR spectra were taken.

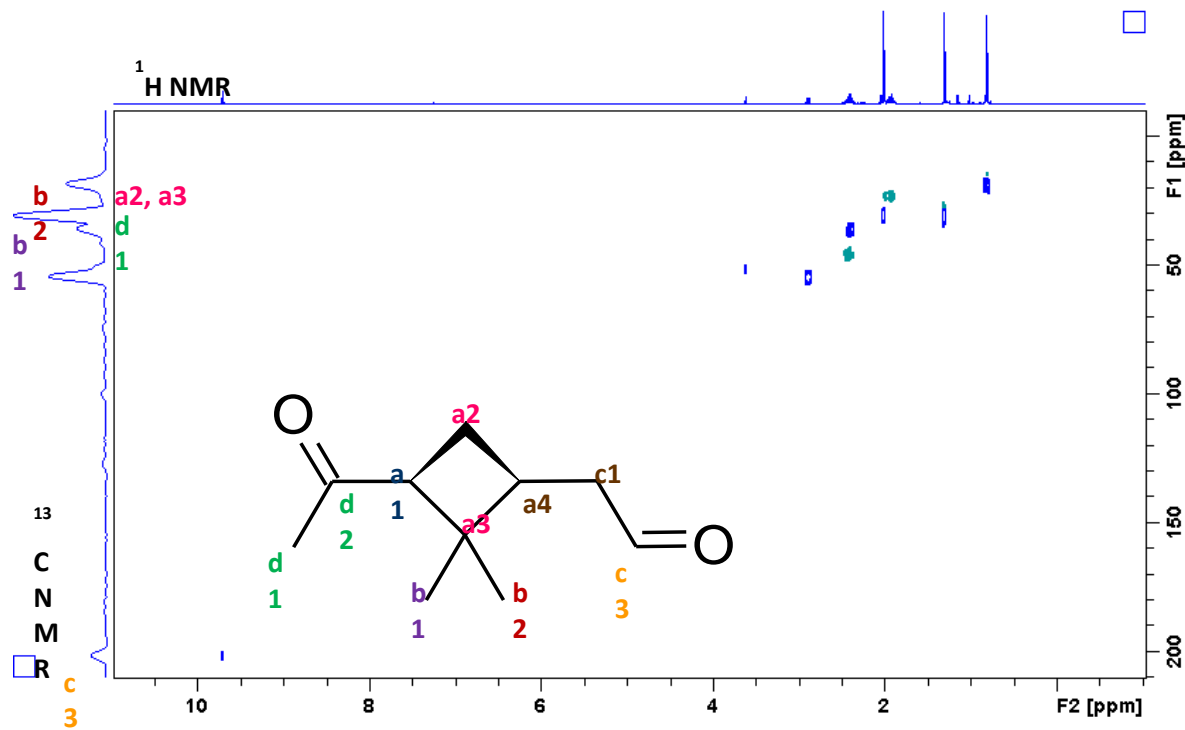


Figure K. This is a Heteronuclear Single Quantum Coherence (HSQC) spectra of the synthesized-pinonaldehyde sample that gives a strong suggestion of the abundance of the pinonaldehyde structure. There is an excellent connection between the ¹³C NMR and the ¹H NMR which shows pinonaldehyde as the most abundant species in the sample.

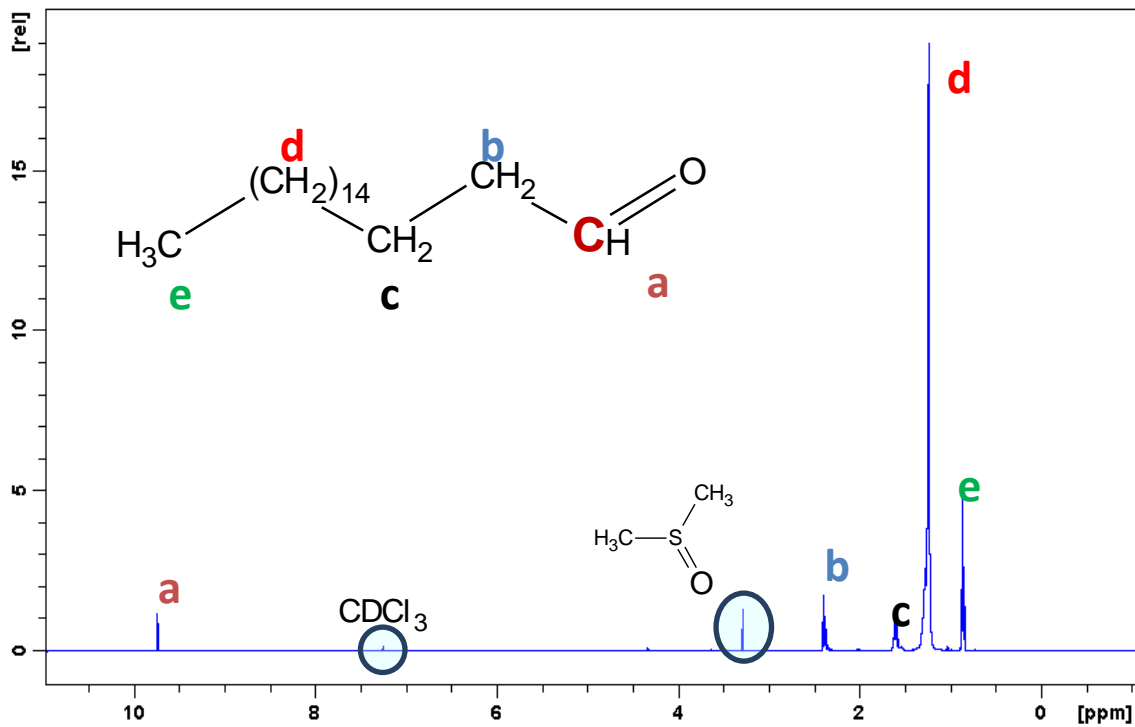


Figure L. This ^1H NMR spectra shows the presence of *n*-heptadecanal as the major product (>90%). The major contaminant is DMSO at ~ 3.3 ppm. CDCl_3 was the solvent used when the NMR spectra were taken, reason for a peak at ~ 7.2 ppm. Other than DMSO, contaminants such as peroxides are observed in minor concentrations.

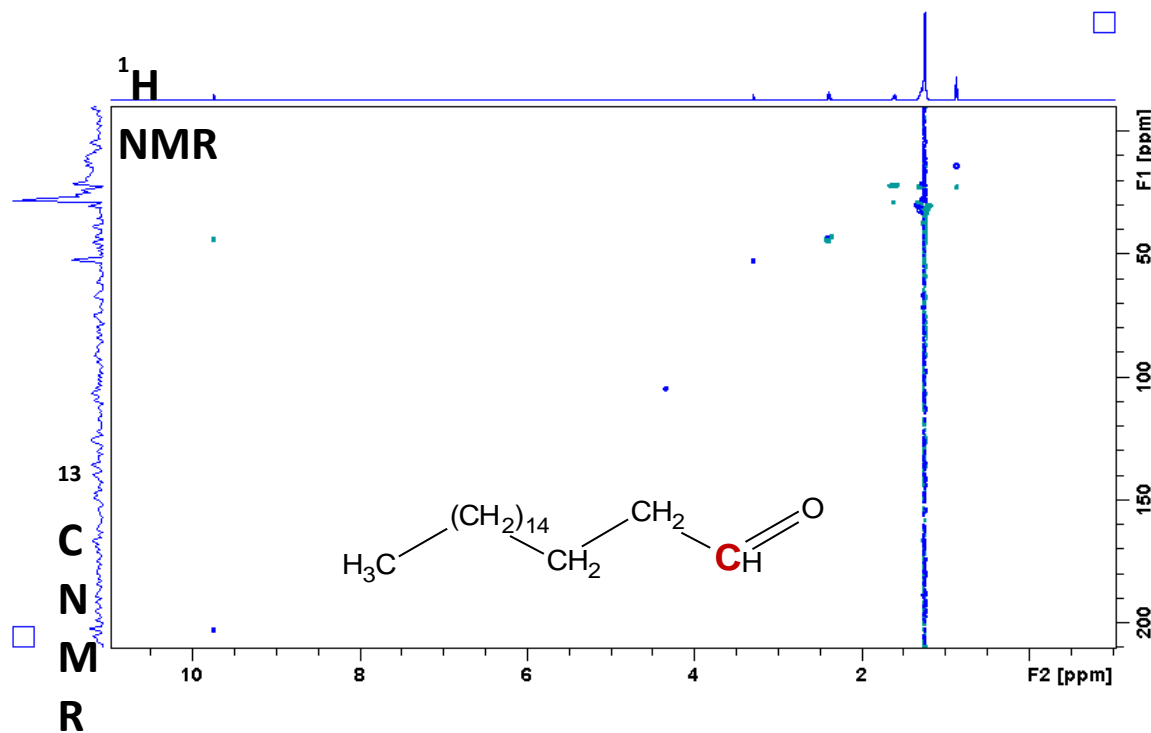


Figure M. This is an HSQC spectra of the synthesized-*n*-heptadecanal sample. This spectra strongly suggests abundance of *n*-heptadecanal in the sample. There is an excellent connection between the ^{13}C NMR and the ^1H NMR, describing *n*-heptadecanal as the most abundant species in the sample.

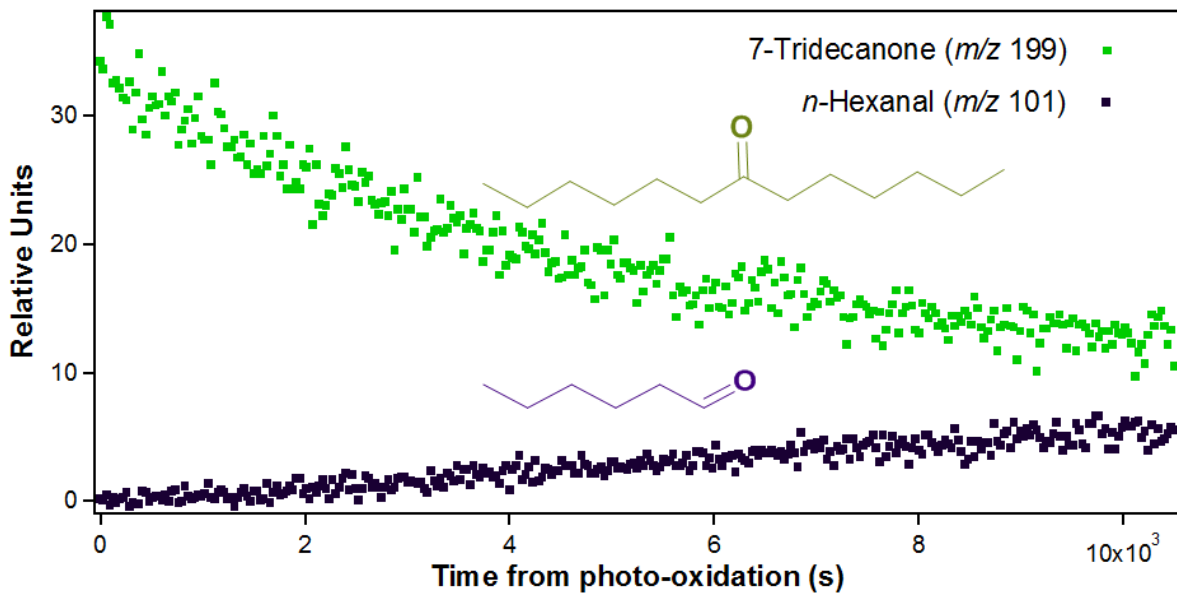


Figure N. Fragmentation of 7-tridecanone via OH radical oxidation in the presence of NO_x forms n -hexanal. The signals presented here have not been calibrated. n -Hexanal can be formed from attack on the α - and β -hydrogens of 7-tridecanone (refer to Figure 3.7, Chapter 3). The reaction of 2-tridecanone with OH in the presence of NO_x does not show the formation of its respective aldehyde. That is because chemical fragmentation is a smaller path for 2-tridecanone versus 7-tridecanone.

Table C. Conditions of all experiments performed and presented in Chapter 4.

Species oxidized	Initial Concentration in the Smog Chamber	Initial NO _x (ppb)	Initial VOC ₀ /NO _x (ppbC/ppb)	Initial OH concentration (molecule cm ⁻³)
<i>n</i> -Tridecanal High NO _x	~250 ppb	~1700	~2	~10 ⁷
Pinonaldehyde High NO _x	~300 ppb	~4000	~0.8	~0.5 X 10 ⁷
<i>n</i> -Pentadecane from Presto et al., 2010	2 to 9 ppb	-	0.03 – 0.1	-
<i>n</i> -Tridecanal Low NO _x	~69 ppb	~2000	~0.46	~0.3 X 10 ⁷
Pinonaldehyde Low NO _x	~70 ppb	~2000	~0.47	~0.3 X 10 ⁷
Pinonaldehyde Low NO _x Dark Experiment	~93 ppb	~2000	~0.35	~0.3 X 10 ⁷

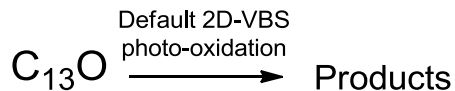
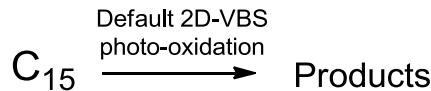


Fig. O. Default 2D-VBS photo-oxidation simulations. The box model simulation makes no distinction between structural and functional-group isomers since it was designed for bulk organic material. The relevant features for the model are oxygen-to-carbon ratio and saturation concentrations.

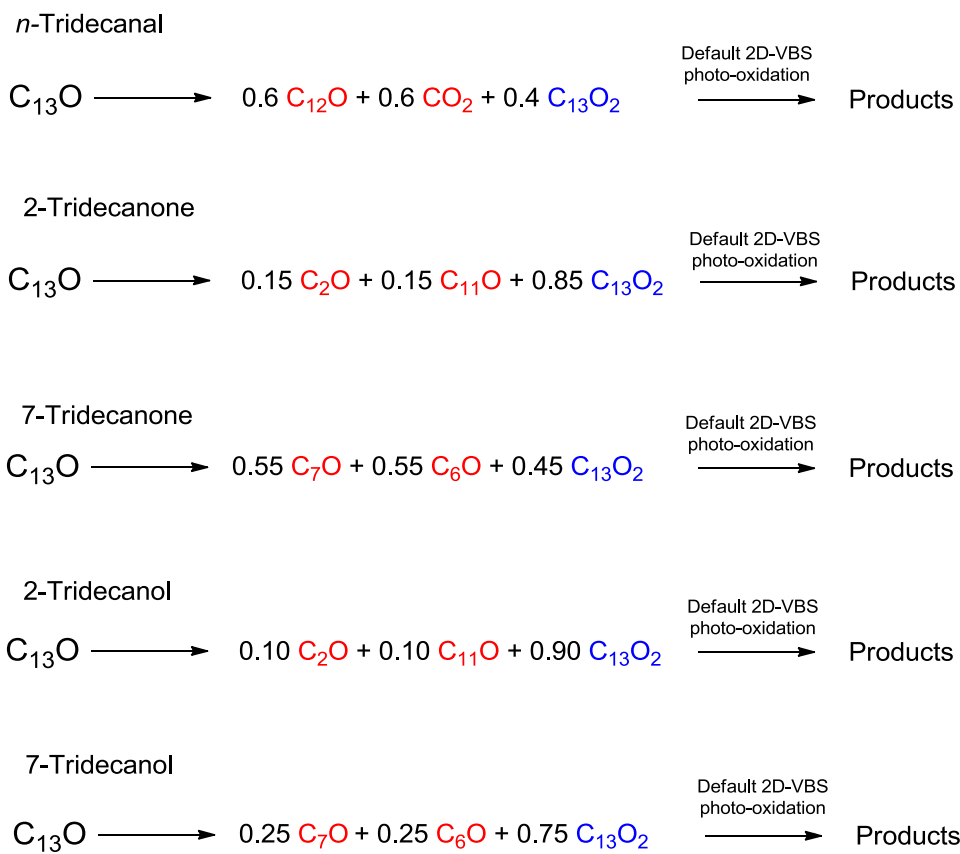


Fig. P. Explicit First Generation 2D-VBS simulations. All the species in this figure have the same oxygen-to-carbon atomic ratio and similar vapor pressures (with exception of the alcohols). We establish a first generation chemistry to assist the 2D-VBS box model.

Table D. Conditions of all experiments performed and presented in Chapter 5.

Species oxidized	Initial Concentration in the Smog Chamber	Initial NO _x (ppb)	Initial VOC ₀ /NO _x (ppbC/ppb)	Initial OH concentration (molecule cm ⁻³)
<i>n</i> -Pentadecane fit from Presto <i>et al.</i> , 2010	2 to 9 ppb	-	0.03-0.1	-
<i>n</i> -Tridecanal	~250 ppb	~1700	~2	~1×10 ⁷
2-Tridecanone	~40 ppb	~3500	0.15	~0.5×10 ⁷
7-Tridecanone	~35 ppb	~3000	0.15	~0.5×10 ⁷
2-Tridecanol	~110 ppb	~2500	0.57	~1×10 ⁷
7-Tridecanol	~43 ppb	~1400	0.40	~2×10 ⁷

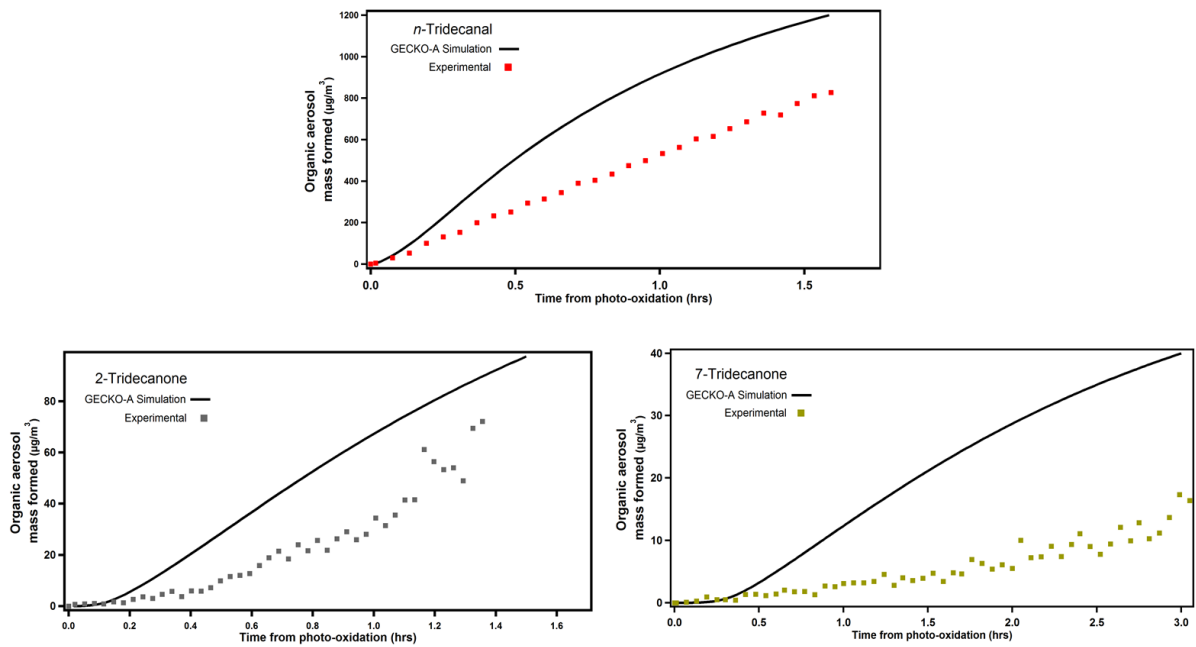


Figure Q. Time evolution of organic aerosol mass. The species presented correspond to those in Figure 5.3 from Chapter 5.

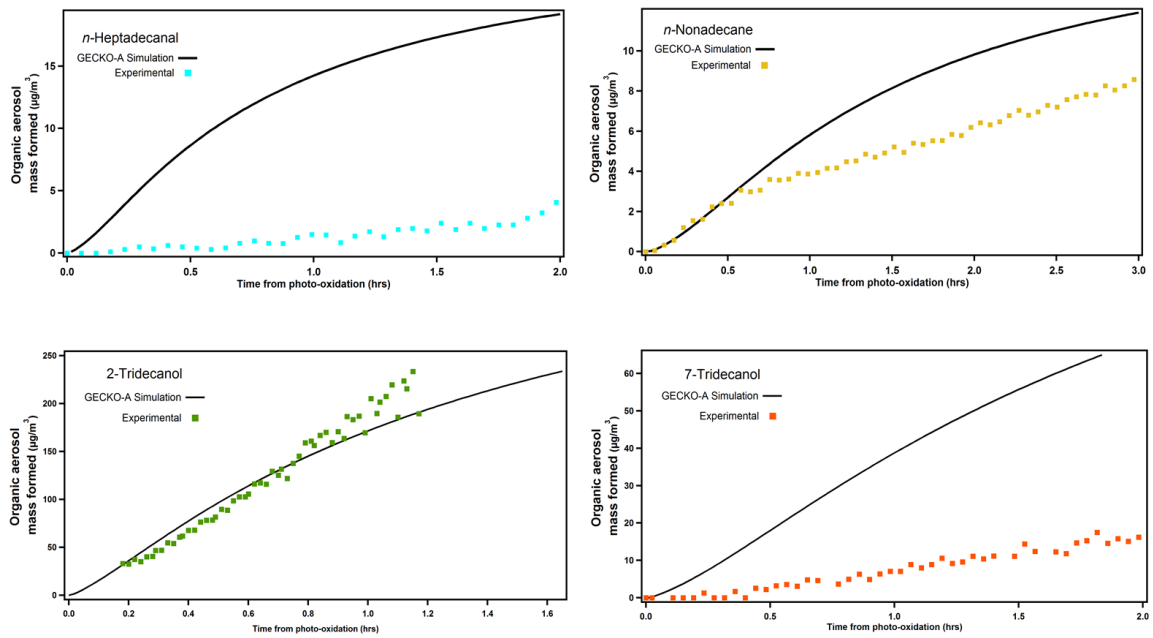


Figure R. Organic aerosol mass time evolution. The species in this figure correspond to the ones presented in Figure 5.4.

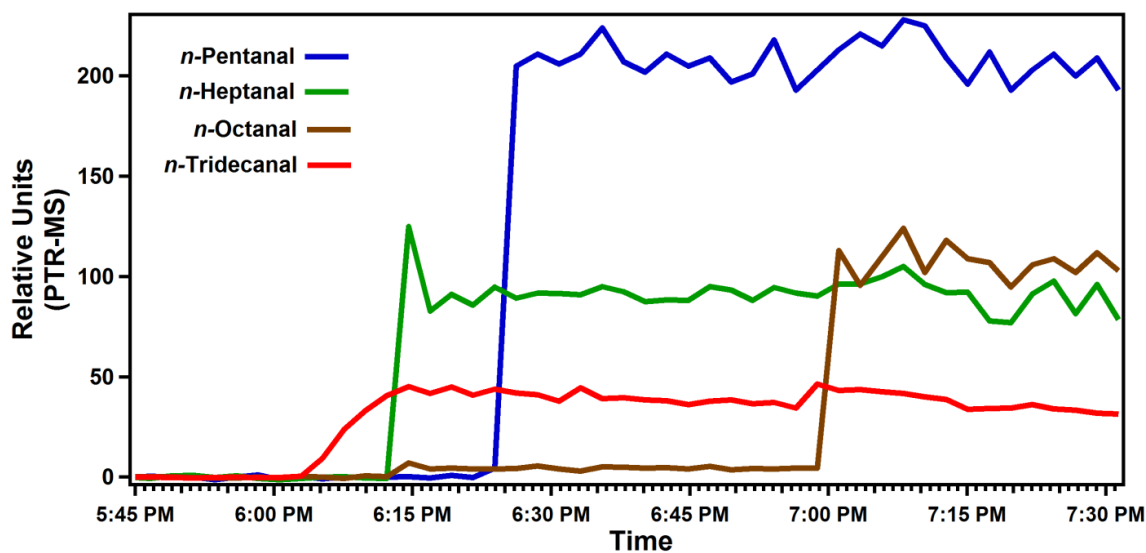


Figure S. Vapors in a Teflon Smog-Chamber. These molecules were injected into the Carnegie Mellon smog-chamber. As it can be seen, these compounds – with up to thirteen carbons and one oxygen – are not lost to chamber walls. However, we did not do the same experiment for larger – like *n*-heptadecanal – or much more oxidized molecules. Consequently, we cannot negate the possibility that larger or more oxidized material can potentially be lost to the wall, under-estimating experimental SOA yields.

References

1. Finlayson-Pitts, B.J. and J.N. Pitts. Chemistry of the upper and lower atmosphere, *Academic Press*, (2000).
2. Seinfeld, J.H. and S.N. Pandis. Atmospheric Chemistry and Physics, *John Wiley & Sons, Inc.*, (2006, 2nd. Ed.).
3. Jimenez, J.L., M.R. Canagaratna, N.M. Donahue, A.S.H. Prevot, Q. Zhang, J.H. Kroll, P.F. DeCarlo, J.D. Allan, H. Coe, N.L. Ng, A.C. Aiken, K.S. Docherty, I.M. Ulbrich, A.P. Grieshop, A.L. Robinson, J. Duplissy, J.D. Smith, K.R. Wilson, V.A. Lanz, C. Hueglin, Y.L. Sun, J. Tian, A. Laaksonen, T. Raatikainen, J. Rautiainen, P. Vaattovaara, M. Ehn, M. Kulmala, J.M. Tomlinson, D.R. Collins, M.J. Cubison, E. J. Dunlea, J.A. Huffman, T.B. Onasch, M.R. Alfarra, P.I. Williams, K. Bower, Y. Kondo, J. Schneider, F. Drewnick, S. Borrmann, S. Weimer, K. Demerjian, D. Salcedo, L. Cottrell, R. Griffin, A. Takami, T. Miyoshi, S. Hatakeyama, A. Shimono, J.Y. Sun, Y.M. Zhang, K. Dzepina, J.R. Kimmel, D. Sueper, J.T. Jayne, S.C. Herndon, A.M. Trimborn, L.R. Williams, E.C. Wood, A.M. Middlebrook, C.E. Kolb, U. Baltensperger, and D.R. Worsnop. Evolution of Organic Aerosols in the Atmosphere, *Science*, (2009). **326**(5959): p. 1525-1529.
4. Kroll, J.H., N.M. Donahue, J.L. Jimenez, S.H. Kessler, M.R. Canagaratna, K.R. Wilson, K.E. Altieri, L.R. Mazzoleni, A.S. Wozniak, H. Bluhm, E.R. Mysak, J.D. Smith, C.E. Kolb, and D.R. Worsnop. Carbon oxidation state as a metric for describing the chemistry of atmospheric organic aerosol, *Nat. Chem.*, (2011). **3**(2): p. 133-139.

5. Kanakidou, M., J.H. Seinfeld, S.N. Pandis, I. Barnes, F.J. Dentener, M.C. Facchini, R.V. Dingenen, A.N. B. Ervens, C.J. Nielsen, E. Swietlicki, J.P. Putaud, Y. Balkanski, S. Fuzzi, J. Horth, G.K. Moortgat, R. Winterhalter, C.E.L. Myhre, K. Tsigaridis, E. Vignati, E.G. Stephanou, and J. Wilson. Organic aerosol and global climate modelling: a review, *Atmos. Chem. Phys.*, (2005). **5**: p. 1053-1123.
6. Zhang, Q., J.L. Jimenez, M.R. Canagaratna, J.D. Allan, H. Coe, I. Ulbrich, M.R. Alfarra, A. Takami, A.M. Middlebrook, Y.L. Sun, K. Dzepina, E. Dunlea, K. Docherty, P.F. DeCarlo, D. Salcedo, T. Onasch, J.T. Jayne, T. Miyoshi, A. Shimono, S. Hatakeyama, N. Takegawa, Y. Kondo, J. Schneider, F. Drewnick, S. Borrmann, S. Weimer, K. Demerjian, P. Williams, K. Bower, R. Bahreini, L. Cottrell, R.J. Griffin, J. Rautiainen, J.Y. Sun, Y.M. Zhang, and D.R. Worsnop. Ubiquity and dominance of oxygenated species in organic aerosols in anthropogenically-influenced Northern Hemisphere midlatitudes, *Geophys. Res. Lett.*, (2007). **34**(13): p. L13801.
7. Goldstein, A.H. and I.E. Galbally. Known and Unexplored Organic Constituents in the Earth's Atmosphere, *Environ. Sci. Technol.*, (2007). **41**(5): p. 1514-1521.
8. Robinson, A.L., N.M. Donahue, M.K. Shrivastava, E.A. Weitkamp, A.M. Sage, A.P. Grieshop, T.E. Lane, J.R. Pierce, and S.N. Pandis. Rethinking Organic Aerosol: Semivolatile Emissions and Photochemical Aging, *Science*, (2007). **2**: p. 1259-1262.
9. Kroll, J.H. and J.H. Seinfeld. Chemistry of secondary organic aerosol: Formation and evolution of low-volatility organics in the atmosphere, *Atmos. Environ.*, (2008). **42**: p. 3593-3624.

10. Donahue, N.M., A.L. Robinson, C.O. Stanier, and S.N. Pandis. Coupled Partitioning, Dilution, and Chemical Aging of Semivolatile Organics, *Environ. Sci. Technol.*, (2006). **40**: p. 2635-2643.
11. Pankow, J.F. An Absorption Model of Gas/Particle Partitioning of Organic Compounds in the Atmosphere, *Atmos. Environ.*, (1994). **28**(2): p. 185-188.
12. Odum, J.R., T. Hoffmann, F. Bowman, D. Collins, R.C. Flagan, and J.H. Seinfeld. Gas/Particle Partitioning and Secondary Organic Aerosol Yields, *Environ. Sci. Technol.*, (1996). **30**: p. 2580-2585.
13. George, I.J., J. Slowik, and J.P.D. Abbatt. Chemical aging of ambient organic aerosol from heterogeneous reaction with hydroxyl radicals, *Geophys. Res. Lett.*, (2008). **35**(13): p. L13811.
14. Pope III, C.A. and D.W. Dockery. Health Effects of Fine Particulate Air Pollution: Lines that Connect, *J. Air & Waste Manage. Assoc.*, (2006). **56**: p. 709-742.
15. Pope III, C.A., R.T. Burnett, M.J. Thun, E.E. Calle, D. Krewski, K. Ito, and G.D. Thurston. Lung Cancer, Cardiopulmonary Mortality, and Long-term Exposure to Fine Particulate Air Pollution, *JAMA*, (2002). **287**(9): p. 1132-1141.
16. Dockery, D.W., C.A. Pope, X. Xu, J.D. Spengler, J.H. Ware, M.E. Fay, B.G. Ferris, and F.E. Speizer. An Association between Air Pollution and Mortality in Six U.S. Cities, *New Engl. J. Med.*, (1993). **329**(24): p. 1753-1759.

17. Laden, F., J. Schwartz, F.E. Speizer, and D.W. Dockery. Reduction in Fine Particulate Air Pollution and Mortality Extended Follow-up of the Harvard Six Cities Study, *Am. J. Respir. Crit. Care Med.*, (2006). **173**: p. 667-672.
18. Russell, A.G. and B. Brunekreef. A Focus on Particulate Matter and Health, *Environ. Sci. Technol.*, (2009). **43**(13): p. 4620-4625.
19. Saxena, P., L.M. Hildemann, P.H. McMurry, and J.H. Seinfeld. Organics alter hygroscopic behavior of atmospheric particles, *J. Geophys. Res.*, (1995). **100**: p. 18755-18770.
20. Racherla, P.N. and P.J. Adams. Sensitivity of global tropospheric ozone and fine particulate matter concentrations to climate change, *J. Geophys. Res.*, (2006). **111**: p. 1-11.
21. Watson, J.G. Visibility: Science and Regulation, *J. Air & Waste Manage. Assoc.*, (2002). **52**: p. 628-713.
22. Bytnerowicz, A., K. Omasa, and E. Paoletti. Integrated effects of air pollution and climate change on forests: A northern hemisphere perspective, *Environ. Pollut.*, (2007). **147**(3): p. 438-445.
23. Atkinson, R. and J. Arey. Atmospheric Degradation of Volatile Organic Compounds, *Chem. Rev.*, (2003). **103**: p. 4605-4638.

24. Pandis, S.N., R.A. Harley, G.R. Cass, and J.H. Seinfeld. Secondary organic aerosol formation and transport, *Atmospheric Environment. Part A. General Topics*, (1992). **26**(13): p. 2269-2282.

25. Kroll, J.H., J.D. Smith, D.L. Che, S.H. Kessler, D.R. Worsnop, and K.R. Wilson. Measurement of fragmentation and functionalization pathways in the heterogeneous oxidation of oxidized organic aerosol, *Phys. Chem. Chem. Phys.*, (2009). **11**: p. 8005 - 8014.

26. Kalberer, M., D. Paulsen, M. Sax, M. Steinbacher, J. Dommen, A.S.H. Prevot, R. Fisseha, E. Weingartner, V. Frankevich, R. Zenobi, and U. Baltensperger. Identification of Polymers as Major Components of Atmospheric Organic Aerosols, *Science*, (2004). **303**(5664): p. 1659 - 166.

27. Kalberer, M., M. Sax, and V. Samburova. Molecular Size Evolution of Oligomers in Organic Aerosols Collected in Urban Atmospheres and Generated in a Smog Chamber, *Environ. Sci. Technol.*, (2006). **40**(19): p. 5917-5922.

28. Atkinson, R. Atmospheric chemistry of VOCs and NO_x, *Atmos. Environ.*, (2000). **34**: p. 2063-2101.

29. Ng, N.L., M.R. Canagaratna, Q. Zhang, J.L. Jimenez, J. Tian, I.M. Ulbrich, J.H. Kroll, K.S. Docherty, P.S. Chhabra, R. Bahreini, S.M. Murphy, J.H. Seinfeld, L. Hildebrandt, N.M. Donahue, P.F. DeCarlo, V.A. Lanz, A.S.H. Prévôt, E. Dinar, Y. Rudich, and D.R. Worsnop. Organic aerosol components observed in Northern Hemispheric datasets from Aerosol Mass Spectrometry, *Atmos. Chem. Phys.*, (2010). **10**: p. 4625-4641.

30. Carslaw, N. and D. Carslaw. The Gas-Phase Chemistry Of Urban Atmospheres, *Surveys in Geophysics*, (2001). **22**(1): p. 31-53.

31. Hatakeyama, S., K. Izumi, T. Fukuyama, and H.j. Akimoto. Reactions of Ozone with a-Pinene and b-Pinene in Air: Yields of Gaseous and Particulate Products, *J. Geophys. Res.*, (1989). **94**: p. 13013-13024.

32. Hatakeyama, S., K. Izumi, T. Fukuyama, H. Akimoto, and N. Washida. Reactions of OH with a-Pinene and b-Pinene in Air: Estimate of Global Co Production from the Atmospheric Oxidation of Terpenes, *J. Geophys. Res.*, (1991). **96**: p. 947-958.

33. Atkinson, R. and J. Arey. Gas-phase tropospheric chemistry of biogenic volatile organic compounds: a review, *Atmos. Environ.*, (2003). **37, Supplement 2**: p. 197-219.

34. Logan, J.A., M.J. Prather, S.C. Wofsy, and M.B. McElroy. Tropospheric Chemistry: A Global Perspective, *J. Geophys. Res.*, (1981). **86**: p. 7210-7254.

35. Lee, A., A.H. Goldstein, J.H. Kroll, N.L. Ng, V. Varutbangkul, R.C. Flagan, and J.H. Seinfeld. Gas-phase products and secondary aerosol yields from the photooxidation of 16 different terpenes, *J. Geophys. Res.*, (2006). **111**: p. D17305.

36. Larsen, B.R., D. Di Bella, M. Glasius, R. Winterhalter, N.R. Jensen, and J. Hjorth. Gas-Phase OH Oxidation of Monoterpenes: Gaseous and Particulate Products, *J. Atmos. Chem.*, (2001). **38**(3): p. 231-276.

37. Donahue, N.M., S.A. Epstein, S.N. Pandis, and A.L. Robinson. A two-dimensional volatility basis set: 1. organic-aerosol mixing thermodynamics, *Atmos. Chem. Phys.*, (2011). **10**: p. 3303-3318, doi:10.5194/acp-11-3303-2011.

38. Donahue, N.M., J.H. Kroll, S.N. Pandis, and A.L. Robinson. A two-dimensional volatility basis set – Part 2: Diagnostics of organic-aerosol evolution, *Atmos. Chem. Phys.*, (2012). **12**: p. 615–634, doi:10.5194/acp-12-615-2012.

39. Aumont, B., S. Szopa, and S. Madronich. Modelling the evolution of organic carbon during its gas-phase tropospheric oxidation: development of an explicit model based on a self generating approach, *Atmos. Chem. Phys.*, (2005). **5**: p. 2497–2517.

40. Camredon, M., B. Aumont, J. Lee-Taylor, and S. Madronich. The SOA/VOC/NO_x system: an explicit model of secondary organic aerosol formation, *Atmos. Chem. Phys.*, (2007). **7**: p. 5599-5610.

41. Valorso, R., B. Aumont, M. Camredon, T. Raventos-Duran, C. Mouchel-Vallon, N. L. Ng, J. H. Seinfeld, J. Lee-Taylor, and S. Madronich. Explicit modelling of SOA formation from α -pinene photooxidation: sensitivity to vapour pressure estimation, *Atmos. Chem. Phys.*, (2011). **11**: p. 6895-6910.

42. Kwok, E.S.C. and R. Atkinson. Estimation of Hydroxyl Radical Reaction Rate Constants for Gas-Phase Organic Compounds Using a Structure-Reactivity Relationship: An Update, *Atmos. Environ.*, (1995). **29**(14): p. 1685-1695.

43. Pankow, J.F. and W.E. Asher. SIMPOL.1: a simple group contribution method for predicting vapor pressures and enthalpies of vaporization of multifunctional organic compounds, *Atmos. Chem. Phys.*, (2008). **8**: p. 2773-2796.

44. Lipari, F., J.M. Dasch, and W.F. Scruggs. Aldehyde emissions from wood-burning fireplaces, *Environ. Sci. Technol.*, (1984). **18**: p. 326-330.

45. Schauer, J.J., M.J. Kleeman, G.R. Cass, and B.R.T. Simoneit. Measurement of Emissions from Air Pollution Sources. 2. C₁ through C₃₀ Organic Compounds from Medium Duty Diesel Trucks, *Environ. Sci. Technol.*, (1999). **33**: p. 1578-1587.

46. Schauer, J.J., M.J. Kleeman, G.R. Cass, and B.R.T. Simoneit. Measurement of Emissions from Air Pollution Sources. 1. C₁ through C₂₉ Organic Compounds from Meat Charbroiling, *Environ. Sci. Technol.*, (1999). **33**: p. 1566-1577.

47. Cicciolia, P., E. Brancaleonia, M. Frattonia, A. Cecinatoa, and A. Brachettia. Ubiquitous occurrence of semi-volatile carbonyl compounds in tropospheric samples and their possible sources *Atmos. Environ., Part A*, (1993). **27**(12): p. 1891-1901.

48. Carliera, P., H. Hannachia, and G. Mouviera. The chemistry of carbonyl compounds in the atmosphere, *Atmos. Environ.*, (1986). **20**(11): p. 2079-2099.

49. Calogirou, A., B.R. Larsen, and D. Kotzias. Gas-phase terpene oxidation products: a review, *Atmos. Environ.*, (1999). **33**(9): p. 1423-1439.

50. Vandenberk, S. and J. Peeters. The reaction of acetaldehyde and propionaldehyde with hydroxyl radicals: experimental determination of the primary H₂O yield at room temperature, *J. Photoch. Photobio. A: Chem.*, (2003). **157**: p. 269-274.

51. Cleary, P.A., P.J. Wooldridge, D.B. Millet, M. McKay, A.H. Goldstein, and R.C. Cohen. Observations of total peroxy nitrates and aldehydes: measurement interpretation and interference of OH radical concentrations, *Atmos. Chem. Phys.*, (2007). **7**: p. 1947-1960.

52. Kroll, J.H., N.L. Ng, S.M. Murphy, R.C. Flagan, and J.H. Seinfeld. Secondary organic aerosol formation from isoprene photooxidation under high-NO_x conditions *Geophys. Res. Lett.*, (2005). **32**.

53. Donahue, N.M., K.E.H. Hartz, B. Chuong, A.A. Presto, C.O. Stanier, T. Rosenhørn, A.L. Robinson, and S.N. Pandis. Critical factors determining the variation in SOA yields from terpene ozonolysis: A combined experimental and computational study, *Faraday Discuss.*, (2005). **130**: p. 295-309.

54. Kroll, J.H., J.D. Smith, D.L. Che, S.H. Kessler, D.R. Worsnop, and K.R. Wilson. Measurement of fragmentation and functionalization pathways in the heterogeneous oxidation of oxidized organic aerosol, *Phys. Chem. Chem. Phys.*, (2009). **11**: p. 8005-8014.

55. Tyndall, G.S., R.A. Cox, C. Granier, R. Lesclaux, G.K. Moortgat, M.J. Pilling, A.R. Ravishankara, and T.J. Wallington. Atmospheric chemistry of small organic peroxy radicals, *J. Geophys. Res.*, (2001). **106**(D11): p. 12157-12182.

56. Sander, S.P. *Chemical Kinetics and Photochemical Data for Use in Atmospheric Studies*. 2006 [cited; Available from: <http://jpldataeval.jpl.nasa.gov/>].

57. Arey, J., S.M. Aschmann, E.S.C. Kwok, and R. Atkinson. Alkyl Nitrate, Hydroxyalkyl Nitrate, and Hydroxycarbonyl formation from the NO_x-Air Photooxidations of C₅-C₈ *n*-Alkanes, *J. Phys. Chem.*, (2001). **105**: p. 1020-1027.

58. Cassanelli, P., D.J. Fox, and R.A. Cox. Temperature dependence of pentyl nitrate formation from the reaction of pentyl peroxy radicals with NO, *Phys. Chem. Chem. Phys.*, (2007). **9**: p. 4332-4337.

59. Lim, Y.B. and P.J. Ziemann. Products and Mechanism of Secondary Organic Aerosol Formation from Reactions of *n*-Alkanes with OH Radicals in the Presence of NO_x, *Environ. Sci. Technol.*, (2005). **39**: p. 9229-9236.

60. Lim, Y.B. and P.J. Ziemann. Effects of Molecular Structure on Aerosol Yields from OH Radical-Initiated Reactions of Linear, Branched, and Cyclic Alkanes in the Presence of NO_x, *Environ. Sci. Technol.*, (2009). **43**: p. 2328-2334.

61. Kwok, E.S.C., J. Arey, and R. Atkinson. Alkoxy Radical Isomerization in the OH Radical-Initiated Reactions of C₄-C₈ *n*-Alkanes, *J. Phys. Chem.*, (1996). **100**: p. 214-219.

62. Atkinson, R. Rate constants for the atmospheric reactions of alkoxy radicals: An updated estimation method, *Atmos. Environ.*, (2007). **41**: p. 8468-8485.

63. Jenkin, M.E., D.E. Shallcross, and J.N. Harvey. Development and application of a possible mechanism for the generation of cis-pinic acid from the ozonolysis of a- and b-pinene, *Atmos. Environ.*, (2000). **34**: p. 2837-2850.

64. Atkinson, R. Atmospheric reactions of alkoxy and B-hydroxyalkoxy radicals, *Int. J. Chem. Kinet.*, (1999). **29**(2): p. 99-111.

65. Hildebrandt, L., N.M. Donahue, and S.N. Pandis. High formation of secondary organic aerosol from the photo-oxidation of toluene, *Atmos. Chem. Phys.*, (2009). **9**: p. 2973–2986.

66. de Gouw, J.A., P.D. Goldan, C. Warneke, W.C. Kuster, J.M. Roberts, M. Marchewka, S.B. Bertman, A.A.P. Pszenny, and W.C. Keene. Validation of proton transfer reaction-mass spectrometry (PTR-MS) measurements of gas-phase organic compounds in the atmosphere during the New England Air Quality Study (NEAQS) in 2002, *J. Geophys. Res.*, (2003). **108**(D21): p. 4682.

67. Weitkamp, E.A., A.M. Sage, J.R. Pierce, N.M. Donahue, and A.L. Robinson. Organic Aerosol Formation from Photochemical Oxidation of Diesel Exhaust in a Smog Chamber, *Environ Sc. Technol.*, (2007). **41**(20): p. 6969-6975.

68. Miracolo, M.A., A.A. Presto, A.T. Lambe, C.J. Hennigan, N.M. Donahue, J.H. Kroll, D.R. Worsnop, and A.L. Robinson. Photo-Oxidation of Low-Volatility Organics Found in Motor Vehicle Emissions: Production and Chemical Evolution of Organic Aerosol Mass, *Environ. Sci. Technol.*, (2010). **44**(5): p. 1638-1643.

69. Donahue, N. Reaction Barriers: Origin and Evolution, *Chem. Rev.*, (2003). **103**: p. 4593-4604.

70. Ferenac, M.A., A.J. Davis, A.S. Holloway, and T.S. Dibble. Isomerization and Decomposition Reactions of Primary Alkoxy Radicals Derived from Oxygenated Solvents, *J. Phys. Chem. A*, (2003). **107**: p. 63-72.

71. Hein, H., A. Hoffmann, and R. Zellner. Direct investigations of reactions of 1-butoxy and 1-pentoxy radicals using laser pulse initiated oxidation: reaction with O₂ and isomerisation at 293 K and 50 mbar, *Phys. Chem. Chem. Phys.*, (1999). **1**: p. 3743-3752.

72. Presto, A.A., M.A. Miracolo, N.M. Donahue, and A.L. Robinson. Secondary Organic Aerosol Formation from High-NO_x Photo-Oxidation of Low Volatility Precursors: n-Alkanes, *Environ. Sci. Technol.*, (2010).

73. Presto, A.A., K.E.H. Hartz, and N.M. Donahue. Secondary Organic Aerosol Production from Terpene Ozonolysis. 2. Effect of NO_x Concentration, *Environ. Sci. Technol.*, (2005). **39**: p. 7046-7054.

74. Veyret, B., R. Lesclaux, M.T.R.J.C. Rayez, R.A. Cox, and G.K. Moortgat. Kinetics and mechanism of the photo-oxidation of formaldehyde. 1. Flash photolysis study, *J. Phys. Chem.*, (1989). **93**(6): p. 2368-2374.

75. Lim, Y.B. and P.J. Ziemann. Kinetics of the heterogeneous conversion of 1,4-hydroxycarbonyls to cyclic hemiacetals and dihydrofurans on organic aerosol particles, *Phys. Chem. Chem. Phys.*, (2009). **11**: p. 8029-8039.

76. Lim, Y.B. and P.J. Ziemann. Chemistry of Secondary Organic Aerosol Formation from OH Radical-Initiated Reactions of Linear, Branched, and Cyclic Alkanes in the Presence of NO_x. *Aerosol Sci.Tech.*, (2009). **43**: p. 604-619.

77. Holt, T., R. Atkinson, and J. Arey. Effect of water vapor concentration on the conversion of a series of 1,4-hydroxycarbonyls to dihydrofurans, *J. Photoch. Photobio A*, (2005). **176**: p. 231-237.

78. Jordan, C.E., P.J. Ziemann, R.J. Griffin, Y.B. Lim, R. Atkinson, and J. Arey. Modeling AOA formation from OH reactions with C₈-C₁₇ n-alkanes, *Atmos. Environ.*, (2008). **42**: p. 8015-8026.

79. Aschmann, S.M., J. Arey, and R. Atkinson. Kinetics and Products of the Gas-Phase Reaction of OH Radicals with 5-Hydroxy-2-Pentanone at 296 ± 2K, *J. Atmos. Chem.*, (2003). **45**: p. 289-299.

80. Hallquist, M., J.C. Wenger, U. Baltensperger, Y. Rudich, D. Simpson, M. Claeys, J. Dommen, N.M. Donahue, C. George, A.H. Goldstein, J.F. Hamilton, H. Herrmann, T. Hoffmann, Y. Iinuma, M. Jang, M.E. Jenkin, J.L. Jimenez, A. Kiendler-Scharr, W. Maenhaut, G. McFiggans, T.F. Mentel, A. Monod, A.S.H. Prévôt, J.H. Seinfeld, J.D. Surratt, R. Szmigielski, and J. Wildt. The formation, properties and impact of secondary organic aerosol: current and emerging issues, *Atmos. Chem. Phys.*, (2009). **9**: p. 5155-5236.

81. Atkinson, R., J. Arey, and S.M. Aschmann. Atmospheric chemistry of alkanes: Review and recent developments, *Atmos. Environ.*, (2008). **42**: p. 5859-5871.

82. Balkanski, Y.J., D.J. Jacob, G.M. Gardner, W.C. Graustein, and K.K. Turekian. Transport and Residence Times of Tropospheric Aerosols Inferred from a Global Three-Dimensional Simulation of ^{210}Pb , *J. Geophys. Res.*, (1993). **98**(11): p. 20573-20586.

83. Smith, J.D., J.H. Kroll, C.D. Cappa, D.L. Che, C.L. Liu, M. Ahmed, S.R. Leone, D.R. Worsnop, and K.R. Wilson. The heterogeneous reaction of hydroxyl radicals with sub-micron squalane particles: a model system for understanding the oxidative aging of ambient aerosols, *Atmos. Chem. Phys.*, (2009). **9**: p. 3209–3222.

84. George, I., A. Vlasenko, J. Slowik, J. Abbatt, C.D. O'Dowd, and P.E. Wagner, *Heterogeneous Oxidation of Saturated Organic Particles by OH*. Nucleation and Atmospheric Aerosols. 2007: Springer Netherlands. 736-740.

85. Rudich, Y., N.M. Donahue, and T.F. Mentel. Aging of Organic Aerosol: Bridging the Gap Between Laboratory and Field Studies, *Annu. Rev. Phys. Chem.*, (2007). **58**: p. 321-352.

86. Donahue, N.M., J.H. Kroll, S.N. Pandis, and A.L. Robinson. A two-dimensional volatility basis set – Part 2: Diagnostics of organic-aerosol evolution, *Atmos. Chem. Phys. Discuss.*, (2011). **11**: p. 24883-24931, doi:10.5194/acpd-11-24883-2011.

87. Aiken, A.C., P.F. DeCarlo, J.H. Kroll, D.R. Worsnop, J.A. Huffman, K.S. Docherty, I.M. Ulbrich, C. Mohr, J.R. Kimmel, D. Sueper, Y. Sun, Q. Zhang, A. Trimborn, M. Northway, P.J. Ziemann, M.R. Canagaratna, T.B. Onasch, M.R. Alfarra, A.S.H. Prevot, J. Dommen, J. Duplissy, A. Metzger, U. Baltensperger, and J.L. Jimenez. O/C and OM/OC Ratios of Primary, Secondary, and Ambient Organic Aerosols with High-Resolution Time-of-Flight Aerosol Mass Spectrometry, *Environ. Sci. Technol.*, (2008). **42**(12): p. 4478-4485.

88. Atkinson, R., S.M. Aschmann, and A.M. Winer. Alkyl nitrate formation from the reaction of a series of branched RO₂ radicals with NO as a function of temperature and pressure, *J. Atmos. Chem.*, (1987). **5**(1): p. 91-102.

89. Arey, J., S.M. Aschmann, E.S.C. Kwok, and R. Atkinson. Alkyl Nitrate, Hydroxyalkyl Nitrate, and Hydroxycarbonyl Formation from the NO_x-Air Photooxidations of C₅-C₈ n-Alkanes, *J Phys. Chem. A*, (2001). **105**(6): p. 1020-1027.

90. Schradera, W., J. Geigerb, and M. Godejohann. Studies of complex reactions using modern hyphenated methods: α -Pinene ozonolysis as a model reaction, *J. Chromatogr. A*, (2005). **1075**: p. 185-196.

91. Glasius, M., A. Calogirou, N.R. Jensen, J. Hjorth, and C.J. Nielsen. Kinetic Study of Gas-Phase Reactions of Pinonaldehyde and Structurally Related Compounds, *Int. J. Chem. Kinet.*, (1997). **29**: p. 527-533.

92. Chacon-Madrid, H.J., A.A. Presto, and N.M. Donahue. Functionalization vs. Fragmentation: *n*-Aldehyde Oxidation Mechanisms and Secondary Organic Aerosol Formation, *Phys. Chem. Chem. Phys.*, (2010). **12**: p. 13975-13982.

93. Jobson, B.T., M.L. Alexander, G.D. Maupin, and G.G. Muntean. On-line analysis of organic compounds in diesel exhaust using a proton transfer reaction mass spectrometer (PTR-MS), *Int. J. Mass Spectrom.*, (2005). **245**(1-3): p. 78-89.

94. McMurry, J.E. and G.K. Bosch. Synthesis of macrocyclic terpenoid hydrocarbons by intramolecular carbonyl coupling: bicyclogermacrene, lepidozene, and casbene, *J. Org. Chem.*, (1987). **52**(22): p. 4885-4893.

95. Matsunaga, A. and P.J. Ziemann. Gas-Wall Partitioning of Organic Compounds in a Teflon Film Chamber and Potential Effects on Reaction Product and Aerosol Yield Measurements, *Aerosol Sci. Tech.*, (2010). **44**(10): p. 881-892.

96. Pierce, J.R., G.J. Engelhart, L. Hildebrandt, E.A. Weitkamp, R.K. Pathak, N.M. Donahue, A.L. Robinson, P.J. Adams, and S.N. Pandis. Constraining Particle Evolution from Wall Losses, Coagulation, and Condensation-Evaporation in Smog-Chamber Experiments: Optimal Estimation Based on Size Distribution Measurements, *Aerosol Sci. Tech.*, (2008). **42**(12): p. 1001-1015.

97. Presto, A.A., K.E. Huff Hartz, and N.M. Donahue. Secondary Organic Aerosol Production from Terpene Ozonolysis. 1. Effect of UV Radiation, *Environ. Sci. Technol.*, (2005). **39**(18): p. 7036-7045.

98. Singh, H.B., L.J. Salas, and W. Viezee. Global distribution of peroxyacetyl nitrate, *Nature*, (1986). **321**(6070): p. 588-591.

99. Aschmann, S.M., J. Arey, and R. Atkinson. Atmospheric Chemistry of Three C₁₀ Alkanes, *J. Phys. Chem.*, (2001). **105**: p. 7598-7606.

100. Atkinson, R., S.M. Aschmann, W.P.L. Carter, and J.N.P. Jr. Rate Constants for the Gas-Phase Reaction of OH Radicals with a Series of Ketones at 299±2 K, *Int. J. Chem. Kinet.*, (1982). **14**(8): p. 839-847.

101. Appel, K.W., P.V. Bhave, A.B. Gilliland, G. Sarwar, and S.J. Roselle. Evaluation of the community multiscale air quality (CMAQ) model version 4.5: Sensitivities impacting model performance; Part II-particulate matter, *Atmos. Environ.*, (2008). **42**: p. 6057-6066.

102. Zhang, Y., K. Vijayaraghavan, X.-Y. Wen, H.E. Snell, and M.Z. Jacobson. Probing into regional ozone and particulate matter pollution in the United States: 1. A 1 year CMAQ simulation and evaluation using surface and satellite data, *J. Geophys. Res.*, (2009). **114**: p. 1-31.

103. Presto, A. and N.M. Donahue. Investigation of alpha-pinene + ozone secondary organic aerosol formation at low total aerosol mass., *Environ. Sci. Technol.*, (2006). **40**(11): p. 3546-43.

104. Griffin, R.J., D.R.C. III, J.H. Seinfeld, and D. Dabdub. Estimate of global atmospheric organic aerosol from oxidation of biogenic hydrocarbons, *Geophys. Res. Lett.*, (1999). **26**: p. 2721-2724.

105. Atkinson, R. and J. Arey. Atmospheric Chemistry of Biogenic Organic Compounds, *Accounts Chem. Res.*, (1998). **31**(9): p. 574-583.

106. Grosjean, D., E.L. Williams, and J.H. Seinfeld. Atmospheric oxidation of selected terpenes and related carbonyls: gas-phase carbonyl products, *Environ. Sci. Technol.*, (1992). **26**(8): p. 1526-1533.

107. Chacon-Madrid, H.J. and N.M. Donahue. Fragmentation vs. functionalization: chemical aging and organic aerosol formation, *Atmos. Chem. Phys.*, (2011). **11**: p. 10553–10563.

108. Lelieveld, J., T.M. Butler, J.N. Crowley, T.J. Dillon, H. Fischer, L. Ganzeveld, H. Harder, M.G. Lawrence, M. Martinez, D. Taraborrelli, and J. Williams. Atmospheric oxidation capacity sustained by a tropical forest, *Nature*, (2008). **452**: p. 737-740.

109. Fehsenfeld, F., J. Calvert, R. Fall, P. Goldan, A.B. Guenther, C.N. Hewitt, B. Lamb, S. Liu, M. Trainer, H. Westberg, and P. Zimmerman. Emissions of volatile organic compounds from vegetation and the implications for atmospheric chemistry, *Global Biochem. Cy.*, (1992). **6**: p. 389-430.

110. Carlton, A.G., P.V. Bhave, S.L. Napelenok, E.O. Edney, G. Sarwar, R.W. Pinder, G.A. Pouliot, and M. Houyoux. Model Representation of Secondary Organic Aerosol in CMAQv4.7, *Environ. Sci. Technol.*, (2010). **44**: p. 8553–8560.

111. Hakola, H., J. Arey, S.M. Aschmann, and R. Atkinson. Product formation from the gas-phase reactions of OH radicals and O₃ with a series of monoterpenes, *J. Atmos. Chem.*, (1994). **18**(1): p. 75-102.

112. Donahue, N.M. and R.G. Prinn. In Situ Nonmethane Hydrocarbon Measurements on SAGA 3, *J. Geophys. Res.*, (1993). **98**(D9): p. 16915-16932.

113. Docherty, K.S., W. Wu, Y.B. Lim, and P.J. Ziemann. Contributions of Organic Peroxides to Secondary Aerosol Formed from Reactions of Monoterpenes with O₃, *Environ. Sci. Technol.*, (2005). **39**(11): p. 4049-4059.

114. Maksymiuk, C.S., C. Gayahtri, R.R. Gil, and N.M. Donahue. Secondary organic aerosol formation from multiphase oxidation of limonene by ozone: mechanistic constraints via two-dimensional heteronuclear NMR spectroscopy, *Phys. Chem. Chem. Phys.*, (2009). **11**(36): p. 7810-7818.

115. Hasson, A.S., G.S. Tyndall, and J.J. Orlando. A Product Yield Study of the Reaction of HO₂ Radicals with Ethyl Peroxy (C₂H₅O₂), Acetyl Peroxy (CH₃C(O)O₂), and Acetonyl Peroxy (CH₃C(O)CH₂O₂) Radicals, *J. Phys. Chem. A*, (2004). **108**(28): p. 5979-5989.

116. Crawford, M.A., T.J. Wallington, J.J. Szente, M.M. Maricq, and J.S. Francisco. Kinetics and Mechanism of the Acetylperoxy + HO₂ Reaction, *J. Phys. Chem. A*, (1999). **103**(3): p. 365-378.

117. Moortgat, G.K., B. Veyret, and R. Lesclaux. Kinetics of the reaction of HO₂ with CH₃C(O)O₂ in the temperature range 253 - 368 K, *Chem. Phys. Lett.*, (1989). **160**(4): p. 443-447.

118. Lambe, A.T., J. Zhang, A.M. Sage, and N.M. Donahue. Controlled OH Radical Production via Ozone-Alkene Reactions for Use in Aerosol Aging Studies, *Environ. Sci. Technol.*, (2007). **41**(7): p. 2357-2363.

119. Zhang, J., K.E. Huff Hartz, S.N. Pandis, and N.M. Donahue. Secondary Organic Aerosol Formation from Limonene Ozonolysis: Homogeneous and Heterogeneous Influences as a Function of NO_x, *J. Phys. Chem. A*, (2006). **110**(38): p. 11053-11063.

120. Ng, N.L., P.S. Chhabra, A.W.H. Chan, J.D. Surratt, J.H. Kroll, A.J. Kwan, D.C. McCabe, P.O. Wennberg, A. Sorooshian, S.M. Murphy, N.F. Dalleska, R.C. Flagan, and J.H. Seinfeld. Effect of NO_x level on secondary organic aerosol (SOA) formation from the photooxidation of terpenes, *Atmos. Chem. Phys.*, (2007). **7**: p. 5159-5174.

121. Park, J., A.L. Gomez, M.L. Walser, A. Lin, and S.A. Nizkorodov. Ozonolysis and photolysis of alkene-terminated self-assembled monolayers on quartz nanoparticles: implications for photochemical aging of organic aerosol particles, *Phys. Chem. Chem. Phys.*, (2006). **8**(21): p. 2506-2512.

122. Henry, K.M. and N.M. Donahue. Photochemical Aging of α -Pinene Secondary Organic Aerosol: Effects of OH Radical Sources and Photolysis, *J. Phys. Chem. A*, (2012). **Accepted**.

123. Salo, K., M. Hallquist, A.M. Jonsson, H. Saathoff, K.-H. Naumann, C. Spindler, R. Tillmann, H. Fuchs, B. Bohn, F. Rubach, T.F. Mentel, L. Muller, M. Reinnig, T. Hoffmann, and N.M. Donahue. Volatility of secondary organic aerosol during OH radical induced ageing, *Atmos. Chem. Phys.*, (2011). **11**: p. 11055–11067.

124. Donahue, N.M., K.M. Henry, T.F. Mentel, A. Kiendler-Scharr, C. Spindler, B. Bohn, T. Brauers, H.P. Dorn, H. Fuchs, R. Tillmann, A. Wahner, H. Saathoff, K.-H. Naumann, O. Mohler, T. Leisner, L. Muller, T. Hoffmann, K. Salo, M. Hallquist, M. Frosch, M. Bilde, T.

Tritscher, P. Barmet, A.P. Praplan, P.F. DeCarlo, J. Dommen, A.S.H. Prévôt, and U. Baltensperger. Aging of Secondary Organic Aerosol via Gas-Phase OH Radical Reactions, *P. Natl. Acad. Sci.*, (2012). **Under Review**.

125. Henry, K.M., T. Lohaus, and N.M. Donahue. (2012).

126. Wagstrom, K. and S. Pandis. Determination of the age distribution of primary and secondary aerosol species using a chemical transport model, *J. Geophys. Res.*, (2009). **114**(D14): p. 1-12.

127. Murphy, B.N. and S.N. Pandis. Simulating the Formation of Semivolatile Primary and Secondary Organic Aerosol in a Regional Chemical Transport Model, *Environ. Sci. Technol.*, (2009). **43**(13): p. 4722-4728.

128. Daewon, B. and L.S. Kenneth, *Review of the Governing Equations, Computational Algorithms, and Other Components of the Models-3 Community Multiscale Air Quality (CMAQ) Modeling System*. 2006, ASME. p. 51-77.

129. Tesche, T.W., R. Morris, G. Tonnesen, D. McNally, J. Boylan, and P. Brewer. CMAQ/CAMx annual 2002 performance evaluation over the eastern US, *Atmos. Environ.*, (2006). **40**(26): p. 4906-4919.

130. Schell, B., I.J. Ackermann, H. Hass, F.S. Binkowski, and A. Ebel. Modeling the formation of secondary organic aerosol within a comprehensive air quality model system, *J. Geophys. Res.*, (2001). **106**: p. 28,275–28,293.

131. Lane, T.E., N.M. Donahue, and S.N. Pandis. Simulating secondary organic aerosol formation using the volatility basis-set approach in a chemical transport model *Atmos. Environ.*, (2008). **42**(32): p. 7439-7451

132. Murphy, B.N., N.M. Donahue, C. Fountoukis, and S.N. Pandis. Simulating the oxygen content of ambient organic aerosol with the 2D volatility basis set, *Atmos. Chem. Phys.*, (2011). **11**: p. 7859–7873.

133. Griffin, R.J., K. Nguyen, D. Dabdub, and J.H. Seinfeld. A Coupled Hydrophobic-Hydrophilic Model for Predicting Secondary Organic Aerosol Formation, *J. Atmos. Chem.*, (2003). **44**(2): p. 171-190.

134. Pankow, J.F. and K.C. Barsanti. The carbon number-polarity grid: A means to manage the complexity of the mix of organic compounds when modeling atmospheric organic particulate matter, *Atmos. Environ.*, (2009). **43**(17): p. 2829-2835.

135. Lambe, A.T., M.A. Miracolo, C.J. Hennigan, A.L. Robinson, and N.M. Donahue. Effective Rate Constants and Uptake Coefficients for the Reactions of Organic Molecular Markers (n-Alkanes, Hopanes, and Steranes) in Motor Oil and Diesel Primary Organic Aerosols with Hydroxyl Radicals, *Environ. Sci. Technol.*, (2009). **43**(23): p. 8794-8800.

136. Myrdal, P.B. and S.H. Yalkowsky. Estimating pure component vapor pressures of complex organic molecules, *Ind. Eng. Chem. Res.*, (1997). **36**: p. 2394-2499.

137. Nannoolal, Y., J. Rarey, and D. Ramjugernath. Estimation of pure component properties: Part 3. Estimation of the vapor pressure of non-electrolyte organic compounds via group contributions and group interactions, *Fluid Phase Equilibr.*, (2008). **269**(117-133).

138. Barley, M.H. and G. McFiggans. The critical assessment of vapour pressure estimation methods for use in modelling the formation of atmospheric organic aerosol, *Atmos. Chem. Phys.*, (2010). **10**: p. 749–76.

139. Chacon-Madrid, H.J., K.M. Henry, and N.M. Donahue. Photo-oxidation of pinonaldehyde at low NO_x: from chemistry to organic aerosol formation, *Submitted to Atmos. Chem. Phys.*, (2012).

140. Chacon-Madrid, H.J., K.M. Henry, and N.M. Donahue. Photo-oxidation of pinonaldehyde at low NO_x: from chemistry to organic aerosol formation, *Atmos. Chem. Phys. Discuss.*, (2012). **12**: p. 7727-7752.

141. Heald, C.L., J.H. Kroll, J.L. Jimenez, K.S. Docherty, P.F. DeCarlo, A.C. Aiken, Q. Chen, S.T. Martin, D.K. Farmer, and P. Artaxo. A simplified description of the evolution of organic aerosol composition in the atmosphere, *Geophys. Res. Lett.*, (2010). **37**(8): p. L08803.